Downloaded from orbit.dtu.dk on: Dec 17, 2017

Technical University of Denmark

Formation of Enzyme Containing Particles by Spray Drying

Sloth, Jakob; Kiil, Søren; Jensen, Anker Degn; Bach, Poul

Publication date:
2008

Document Version
Publisher's PDF, also known as Version of record

Link back to DTU Orbit

Citation (APA):
Sloth, J., Kiil, S., Jensen, A. D. (Ed.), & Bach, P. (2008). Formation of Enzyme Containing Particles by Spray Drying.

DTU Library
Technical Information Center of Denmark

General rights
Copyright and moral rights for the publications made accessible in the public portal are retained by the authors and/or other copyright owners and it is a condition of accessing publications that users recognise and abide by the legal requirements associated with these rights.

- Users may download and print one copy of any publication from the public portal for the purpose of private study or research.
- You may not further distribute the material or use it for any profit-making activity or commercial gain
- You may freely distribute the URL identifying the publication in the public portal

If you believe that this document breaches copyright please contact us providing details, and we will remove access to the work immediately and investigate your claim.

Formation of Enzyme Containing Particles by Spray Drying

Ph.D. Thesis

Jakob Sloth

August 29, 2007

Novozymes Bioprocess Academy

CHEC Research Centre
Department of Chemical Engineering
Technical University of Denmark

Preface

This thesis is submitted as partial fulfilment of the requirements for the Ph.D. degree at the Technical University of Denmark.

The work was carried out in the period from September 2004 to August 2007 and was supervised by Associate Professor Søren Kiil, Professor Anker D. Jensen at the Technical University of Denmark and Senior Science Manager Poul Bach at Novozymes A/S. The research work was performed partly at the Department of Chemical Engineering, Technical University of Denmark and partly at Novozymes A/S in Bagsværd, Denmark. The project was funded by the Novozymes Bioprocess Academy and also supported by the CHEC Research Centre and Novozymes A/S.

First, I would like to thank my supervisors Poul, Anker and Søren for their great belief in me and my project. Each supervisor has, in his own way, been a tremendous source of inspiration and given me invaluable advice throughout my three years of Ph.D. study. All three supervisors have always taken time to discuss questions – big or small – whenever I needed help. For this I wish to express my unbounded gratitude.

A special thanks goes to Kåre Jørgensen with whom I have had many interesting discussions on both practical and theoretical matters. I am grateful that he has taken the time for this even after finalizing his own Ph.D. study.

I appreciate the help of CHEC as well as Novozymes technicians during the experimental part of my work. Especially, I want to thank Eva Marianne Langhoff for her advice at the Novozymes laboratories.

Also, great thanks goes to M.Sc. student Jesper Jensen with whom I faced numerous practical problems.

It has been a pleasure to work both at Solid Products Development (Novozymes A/S) and at the Department of Chemical Engineering. I want to thank my colleagues in both places for making the past three years very rewarding.

Most importantly, I am grateful beyond words for the unceasing support of my family and friends during my Ph.D. study.

Kgs. Lyngby, August 2007

Jakob Sloth

Summary

Spray drying is often used in the manufacture of biotechnological and pharmaceutical products. In spray drying a suspension or solution is fed to an atomizer and the droplets formed are mixed with a hot gas. This causes the solvent of the droplets to evaporate, leaving dry particles. Industrial enzyme containing formulations are often subjected to spray drying because product handling is easier and the enzyme storage stability is better in a dry product than in a liquid formulation. Furthermore, it is important that the enzyme products are produced with a constant high quality and consequently, the choices of process conditions and formulation ingredients become critical and preferably rely on a detailed insight into the various processes occurring during product drying.

The objective of this thesis is to contribute to the fundamental understanding of the single droplet drying process taking place inside a spray dryer. Specifically, the drying of enzyme containing formulations is treated with focus on the drying rate, temperature development and particle morphology formation during drying of a single droplet. Further, one of the main topics of the thesis is to investigate means of reducing enzyme degradation during spray drying.

A model for the drying of a single solution droplet into a solid, dense particle is developed. The model describes heat and mass transfer to the surface and inside the droplet. Model predictions of the drying behavior of aqueous solutions of maltodextrin and trehalose are in good agreement with data obtained from experiments using an ultrasonic levitator.

In accordance with the literature, the model shows that the course of drying proceeds in two rather distinct successive drying periods usually referred to as the constant rate period and the falling rate period. Also, in agreement with the literature drying is rapid during the constant rate period and the droplet temperature is close to the wet bulb temperature. In the falling rate period, the drying rate is significantly lower and the temperature quickly approaches the temperature of the surroundings. The model shows that even though the Biot number is slightly above the critical value of 0.1 a uniform temperature in the radial direction inside the droplet may be assumed. Most importantly, it is concluded that the drying rate during the constant rate period is limited by mass and heat transfer between the surroundings and the droplet surface. In

the falling rate period, the drying rate is limited by internal mass transport.

The kinetics for single droplet drying are further investigated by conducting a series of experiments, using the so-called Droplet Dryer. The Droplet Dryer is a pilot scale spray dryer which is designed for in situ drying experiments where droplets are dried under well-defined temperature and flow conditions. The experiments have focus on the influence on the drying rate and particle morphology formation of formulation ingredients often used in the biotechnological and pharmaceutical industries.

Based on the experimental results, it is concluded that adding water activity reducing compounds (maltodextrin, dextrin, Na_2SO_4 or NaCl) to a suspension consisting of water and insoluble rice starch particles increases the droplet temperature rather than reducing the drying rate. On the contrary, adding insoluble TiO_2 primary particles to the water/rice starch suspension does not influence the droplet temperature nor the drying rate. The explanation of this is that TiO_2 does not reduce the water activity. These conclusions should be considered when designing formulations which contain heat sensitive compounds such as enzymes.

Sequences for formation of the observed particle morphologies are given and explained in detail. This includes sequences for the drying of a material (rice starch) which may gelatinize during drying. The most important conclusion is that even small changes in the feed formulation may drastically change the final morphology.

Furthermore, a method is presented for fast and cheap evaluation of the performance of enzyme containing formulations in terms of preserving the highest enzyme activity during spray drying. The method is based on differential scanning calorimeter experiments using samples in the milligramme range followed by modeling the kinetics of the thermal inactivation reaction which occurs during the drying process. Relevant kinetic parameters are determined from the differential scanning calorimeter experiments and the model is used to simulate the severity of the inactivation reaction for temperatures and moisture levels relevant for spray drying. After conducting experiments and subsequent simulations for a number of different formulations it may be deduced which formulation performs best. This is illustrated by a formulation design study where four different enzyme containing formulations are evaluated. The method is validated by comparison to pilot scale spray dryer experiments.

It is concluded that simple formulation changes may significantly improve the activity preservation during spray drying. Thus, using the method for evaluating different enzyme containing formulations may be valuable in the industry. Also, it is important that a model which calculates the rate of inactivation during drying is developed.

The model for inactivation is used in the final part of the work where it is

combined with a model which simulates the droplet moisture content and temperature during drying. The combined model is set up for the drying of a droplet which consists of water, insolubles and solubles, including enzymes. The model divides the course of drying into the constant rate period and the falling rate period. In the former, water evaporates from the droplet surface whereas the evaporation occurs from a shrinking wet core during the falling rate period. The water vapor evaporated from the wet core diffuses through a porous crust which surrounds the core.

Simulations of the drying behavior using the combined model show that the enzyme suffers most inactivation during the falling rate period. This is explained by the fact that a higher temperature prevails in this part of the drying. Also, it is concluded that the enzyme experiences more inactivation in the wet core compared to the crust because of unfortunate combinations of moisture concentration and temperature in the core.

Moreover, based on the model simulations the following advice is given for limiting the activity loss when spray drying an enzyme containing formulation on an industrial scale. The initial droplet size should be as small as possible and the relative humidity in the drying air should be kept at a minimum. Also, the temperature inside the spray dryer should be kept low because an elevated temperature has a more substantial negative effect on the activity preservation than a prolonged drying. Finally, it is suggested to carefully investigate the impact of spray drying on the enzyme activity. The simulations have verified that a simple formulation change may lead to significantly improved activity preservation. However, the choices of process parameters and formulation design are trade-offs between activity loss and other product requirements.

Resumé

Spraytørring anvendes ofte som et led i produktionen af bioteknologiske og farmaceutiske produkter. Ved spraytørring forstøves en suspension eller en opløsning, og de dannede dråber bringes i kontakt med en opvarmet gasstrøm. Herved fordamper opløsningsmidlet i dråberne, og partikler dannes. Formuleringer indeholdende industrielle enzymer spraytørres ofte, da håndteringen af det endelige produkt lettes, og enzymernes lagerstabilitet er betydeligt bedre end i en flydende formulering. Det er afgørende, at enzymholdige produkter fremstilles med en konstant, høj kvalitet. Derfor bliver valgene af procesbetingelser og formuleringsingredienser vigtige og træffes i denne forbindelse mest hensigtsmæssigt på baggrund af en detaljeret indsigt i de forskellige processer, der forekommer under tørringen.

Formålet med denne afhandling er at bidrage til den grundlæggende forståelse af den dråbetørringsproces, der finder sted i et spraytørringsanlæg. Konkret omhandler nærværende arbejde tørring af enzymholdige formuleringer, idet fokus er på tørrehastighed, temperaturudvikling og morfologidannelse under tørring af enkeltdråber. Yderligere er et af hovedemnerne for afhandlingen at undersøge metoder til at reducere den termiske enzymnedbrydning, der sker ved spraytørring.

Der er udviklet en matematisk model til simulering af forløbet, hvor en dråbe, der består af en opløsning, tørres til en kompakt og massiv partikel. Modellen beskriver masse- og varmetransport fra omgivelserne til dråbeoverfladen såvel som internt i dråben. Modellens forudsigelser af tørringsforløb for vandige opløsninger af maltodextrin og trehalose udviser god overensstemmelse med eksperimentelle resultater fra en ultralydslevitator.

I lighed med den eksisterende litteratur viser modellen, at tørringsforløbet kan inddeles i to adskilte tørringsfaser, der normalt omtales som perioden med konstant tørrehastighed og perioden med aftagende tørrehastighed. Modellen viser, at tørringen er hurtig i perioden med konstant tørrehastighed, mens temperaturen er tilnærmelsesvis lig den våde termometertemperatur, hvilket ligeledes er i overensstemmelse med den eksisterende litteratur. I perioden med aftagende tørrehastighed forløber tørringen langsomt, og temperaturen nærmer sig hurtigt omgivelsernes temperatur. Modellen viser, at på trods af, at Biot-tallet for

dråben er en smule højere end den kritiske værdi på 0.1, kan en ensartet temperaturfordeling i dråben antages med god rimelighed. De vigtigste konklusioner, der kan drages på baggrund af modelberegningerne, er, at tørringen i perioden med konstant tørrehastighed begrænses af masse- og varmetransport mellem dråbeoverfladen og omgivelserne. I perioden med aftagende tørrehastighed begrænses tørringen af intern massetransport.

Kinetikken for tørring af enkeltdråber er yderligere undersøgt, idet der er udført en række eksperimenter på den såkaldte Droplet Dryer. Droplet Dryeren er en spraytørrer i pilot størrelse, som er designet med henblik på at undersøge dråbetørringen under veldefinerede temperatur- og strømningsforhold. Eksperimenterne har til formål at kortlægge indflydelsen af forskellige formuleringsingredienser på tørringshastigheden og morfologidannelsen, idet fokus lægges på formuleringsingredienser, der ofte anvendes i den bioteknologiske og farmaceutiske industri.

Baseret på de eksperimentelle resultater konkluderes det, at tilsætning af ingredienser, som reducerer vandaktiviteten (maltodextrin, dextrin, Na_2SO_4 eller NaCl), til en suspension bestående af uopløseligt risstivelse og vand medfører en forøgelse af dråbetemperaturen under tørring snarere end at reducere tørrehastigheden. Modsat viser forsøgene at tilsætning af uopløseligt TiO_2 til vand/risstivelsessuspensionen, hverken har en effekt på temperaturen eller tørrehastigheden. Forklaringen på dette er, at TiO_2 ikke påvirker vandaktiviteten. Disse konklusioner er af stor vigtighed for design af formuleringer, der indeholder varmefølsomme materialer såsom enzymer.

Forskellige forløb for dannelse af de partikelmorfologier, der er observeret under forsøgene, er givet og forklaret i detaljer. Dette indbefatter morfologidannelsesforløb for et stof (risstivelse), der kan gelatinere under tørring. Den vigtigste konklusion omkring morfologidannelse er, at selv små ændringer i formuleringen kan have stor indflydelse på den endelige partikelmorfologi.

Yderligere præsenteres en billig og hurtig metode til vurdering af enzymholdige formuleringers evne til at bevare enzymaktiviteten under spraytørring. Metoden er baseret på eksperimenter med et differential scanning calorimeter, hvor der blot bruges få milligram af enzymformuleringen. Dette efterfølges af modellering af den termiske inaktiveringsreaktion, der forløber under tørringsprocessen. De kinetikparametre, der indgår i modellen, estimeres fra eksperimenterne, og under anvendelse af modellen simuleres omfanget af inaktiveringen ved temperaturer og fugtindhold, som er relevante ved spraytørring. Når der er udført eksperimenter og simuleringer for en række forskellige formuleringer kan det udledes, hvilken formulering der bedst bevarer enzymaktiviteten. Dette er eksemplificeret ved et designstudie, hvor fire forskellige enzymholdige formuleringer evalueres. Endeligt valideres metoden ved sammenligning med data fra et pilot spraytørringsanlæg.

Det konkluderes, at selv meget simple formuleringsændringer kan medføre en

væsentlig reducering i aktivitetstabet ved spraytørring. Således kan den udviklede metode til evaluering af enzymholdige formuleringer være værdifuld i industrien. Yderligere er det af stor vigtighed, at der er opstillet en model, der kan bestemme inaktiveringshastigheden under tørring.

Denne model for inaktiveringen anvendes i den sidste del af nærværende arbejde, hvor modellen kobles til en model, som beregner vandindholdet såvel som temperaturen i en tørrende dråbe. Den samlede model er opstillet for tørring af en enkelt dråbe, der består af vand, uopløselige samt opløselige komponenter, hvilket inkluderer enzymer. Modellen opdeler tørringsforløbet i de to tidligere nævnte perioder – perioden med konstant tørringshastighed og perioden med aftagende tørringshastighed. Den førstnævnte modelleres således, at fordampningen sker fra dråbeoverfladen, hvorimod fordampningen sker fra en skrumpende kerne i perioden med aftagende tørrehastighed. Det fordampede vand diffunderer gennem en porøs skorpe, der omslutter den skrumpende kerne.

Simuleringer af tørringsforløbet viser, at enzymet udsættes for den mest omfattende inaktivering i perioden med aftagende tørrehastighed. Dette kan forklares ved, at der opnås en høj temperatur i dråben i denne del af tørringen. Ligeledes konkluderes det, at enzymet oplever mere inaktivering i den skrumpende kerne end i skorpen, fordi der opstår uheldige kombinationer af temperatur og vandindhold i kernen.

Baseret på modelsimuleringerne gives afslutningsvis følgende anbefalinger til begrænsning af aktivitetstabet ved spraytørring af enzymholdige formuleringer i industriel skala. Startdråbestørrelsen bør være så lille som muligt og den relative fugtighed i tørreluften skal holdes lavt. Yderligere anbefales det at bruge en lav temperatur i spraytørreren, da en høj temperatur har en væsentlig mere negativ effekt på aktivitetsbevarelsen end den forlængede tørretid. Endelig foreslås det at undersøge indflydelsen af formuleringen på enzyminaktiveringen nøje, da simuleringerne har verificeret, at en simpel ændring i formuleringen kan forbedre restaktiviteten betydeligt. Det noteres dog, at valget af procesparametre såvel som valget af formuleringsingredienser er en afvejning mellem acceptabelt aktivitetstab og andre produktspecifikationer.

Contents

Chapter 1

Introduction

This chapter contains a general introduction to the PhD thesis. The background of the work is presented and the specific objectives are given. The chapter ends with an explanation of the structure of the thesis.

The focal point of this project is on the formation of enzyme containing particles by spray drying. In spray drying a liquid feed is sprayed into a hot drying medium (usually air). Consequently, the solvent of the droplets formed evaporates and the feed is transformed from the fluid state into a particulate form. The greatest advantage of spray drying is that drying and particle formation are carried out in a one step process. Furthermore, the process facilitates some control of final powder properties such as particle size, bulk density, flowability, mechanical strength and solubility.

Numerous enzyme containing formulations are subjected to a dehydration process because the enzyme storage stability is better if the enzyme is in the dry state rather than in a liquid formulation. Often spray drying is the preferred method of dehydration because of the advantages mentioned above.

However, the complex enzyme molecules may lose their structure and thereby their catalytic activity when exposed to the high temperatures inside a spray dryer. Both the final product properties and the enzyme activity loss are highly dependent on the choice of process conditions (e.g. drying gas temperature and initial droplet size) and feed composition (i.e. formulation).

Hence, extensive knowledge of the influence of process parameters and formulation design on the drying process is desirable for improving the final enzyme containing powder product. Contributing to the obtainment of this knowledge is the primary motivation for the initiation of this PhD project.

1.1 Objectives

The objective of this thesis is to contribute to the fundamental understanding of the single droplet drying process taking place inside a spray dryer. The focus is on drying of enzyme containing formulations and the main topics of the work are

- Drying rate and temperature development of a drying droplet.
- Enzyme activity loss during spray drying.
- Particle morphology formation.

Especially, the influence of feed formulation ingredients and spray dryer process parameters on the three topics listed are investigated. A combined experimental and theoretical approach to the investigations is taken and emphasis is put on attaining results which may be used for improving enzyme containing powders produced by spray drying.

1.2 About the Thesis

The thesis consists of three consecutive parts. First a literature survey of the main topics is given. This includes explanations of different concepts in spray drying and enzymology, providing a basis for the remaining parts of the thesis.

Next, the research work conducted is described in details in chapters 3-6. Chapter 3 is a published journal paper whereas chapters 4 and 5 are papers currently in the publication process. Obviously, each of the journal papers must be understandable when standing alone. Consequently, a few details needed for the chapters 3-5 to be self-explanatory are repeated in the present thesis. The three papers are simply referred to as Paper I-III.

The thesis ends with a conclusion which summarizes the most important findings of the investigations and gives suggestions for further work.

Chapter 2

Literature Survey

The existing literature on the various topics of spray drying of enzymes treated in this thesis is reviewed in the present chapter. The purpose of this literature survey is to introduce and explain the relevant concepts in the field of enzyme spray drying. Further, the purpose is to describe the various approaches taken to the subject in previous studies.

First, a general description of the spray drying process is given as the process is the focal point of the thesis. Next, the course of drying for a single droplet inside a spray dryer is given in details which includes developments in drying rate, droplet temperature and morphology formation. Finally, the impact of the spray drying process on the enzyme activity is treated.

Additional references of interest are discussed in the beginning of Papers I-III in chapters 3-5

2.1 Spray Drying

Spray drying is one of the most suitable methods for conversion of a solution or suspension into particles. This unit operation is of great importance in the manufacture of powder products and is widely used within e.g. the food stuff, chemical, pharmaceutical and biotechnological industries. Spray drying is a part of the production line for numerous products – among the most well-known are instant coffee, laundry detergents and powdered milk.

The most evident advantage of spray drying is that the process allows for simultaneous drying and particle formation. Also, operation may be continuous and automatic process control is readily implemented. The throughput capacity is large and numerous different process layouts exist, enabling production of many different products with specific properties. The latter is often the decisive factor when spray drying is chosen over cheaper drying methods such as drum drying.

However, spray drying is a cheap method of production compared to e.g. freeze drying where the solution or suspension is frozen and the solvent is removed by sublimation under vacuum.

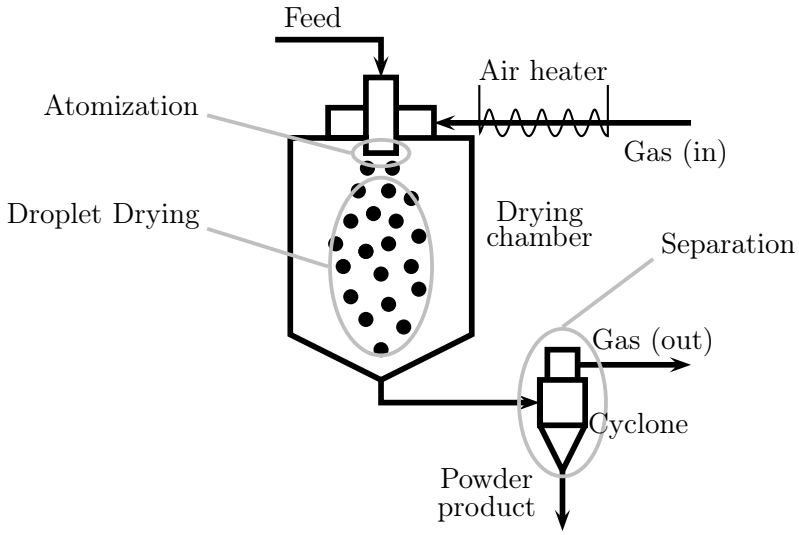

Figure 2.1: Basic spray dryer diagram including the three process stages. The layout shown is an open loop unit operating with a cocurrent flow field.

The spray drying process is elaborately described by Masters [42] and this section is therefore primarily based on this reference. A simple spray dryer plant layout is shown in figure 2.1, illustrating the three process stages which characterize spray drying [6].

1. Feed atomization
2. Droplet drying by mixing of drying gas and spray
3. Separation of dry powder and drying gas

Each of the process stages above are – along with the physical and chemical properties of the feed – critical for the final product characteristics. Thus, each process stage must be designed with the aim of attaining the desired product specifications while considering economical aspects.

2.1.1 Feed Atomization

The design as well as the operation of the atomizing device is most important both for the final product properties and the overall process economy. An

optimal evaporation from the formed droplets in the drying chamber is highly dependent on the spray characteristics. E.g. the droplets must have a large surface area compared to their mass but it is equally important that the droplets have a narrow size distribution [60]. A broad size distribution leads to the formation of large droplets which compared to smaller droplets require a prolonged residence time inside the drying chamber. The smaller droplets, however, remain too long in the drying chamber which is particularly unfortunate when drying temperature-sensitive materials. Furthermore, the manufacture of a homogeneous product demands a narrow droplet size distribution.

Numerous different atomizing devices have been developed but according to Masters [43] rotary atomizers and two-fluid nozzles are the two types most widely used in industry.

Rotary Atomizers

A rotary atomizer consists of a rotating disc or cylinder (figure 2.2a) which is located horizontally at the top of the drying chamber. The liquid feed is supplied to the center of the device and flows due to a centrifugal force at an increasing velocity towards the disc edge. At the edge the feed is broken down into droplets.

In most cases, the feed flows inside the disc in channels which may be designed differently to obtain specific droplet properties. The channel design, the disc angular velocity and the feed flow rate control the mean droplet size. The disc diameter is usually $15 - 20\,\mathrm{cm}$ and a rotary atomizer is normally used when the desired droplet size falls within the range $20 - 150\,\mu\mathrm{m}$ which requires disc edge velocities of 180 and $75\,{}^{\mathrm{m}}/_{\mathrm{s}}$, respectively [42]. However, the exact velocity necessary also depends on e.g. the flow rate, composition and viscosity of the feed. Rotary atomizers can generate droplets from fluctuating feed flows at rates up to $200\,{}^{\mathrm{ton}}/_{\mathrm{h}}$ [42]. A rotary atomizer rarely blocks, enabling spray generation from very different solutions and suspensions. Thus, rotary atomizers have a large number of advantages and are used in many high throughput industries. Examples are production of dairy, colored pigment and food stuffs products as well as inorganic chemicals. The most important disadvantage of the rotary atomizer is that it is mechanically complex and requires regular maintenance of the moving parts.

A special design of a rotary atomizer is the so-called *LAMROT*. The principle of the LAMROT is to spray the feed into the channels using a nozzle. In the channels the liquid flow is kept in laminar mode until it exits the channel and is broken down into droplets. This droplet generation principle leads to formation of droplets with a narrow size distribution and is discussed in detail by Schröder and Walzel [54] and by Walzel et al. [63].

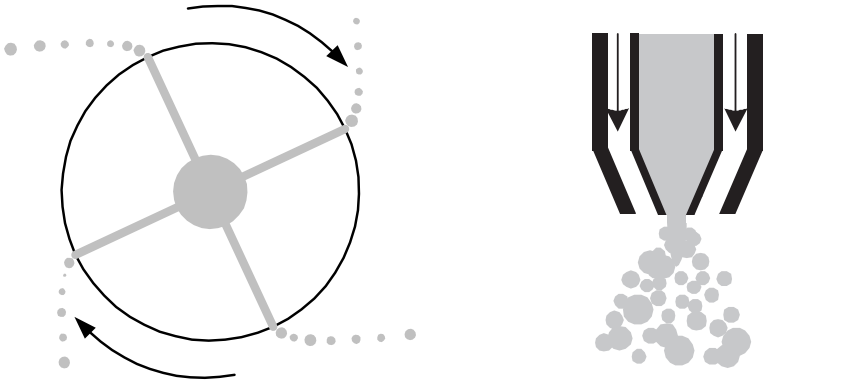

(a) Horizontal cross-sectional view of a rotary atomizer.

(b) Vertical cross-sectional view of a two-fluid nozzle.

Figure 2.2: Simplified sketches of atomizing devices.

Two-fluid Nozzles

Droplet generation using a two-fluid nozzle is based on contacting a liquid jet with a high velocity gas. An example is shown in figure 2.2b where cocurrent flows of gas and a liquid are contacted at the rim of a nozzle head. The high frictional forces between the gas and the liquid jet cause disintegration of the liquid jet into droplets .

The size of the droplets generated by a two-fluid nozzle is obviously dependent on the specific nozzle design but the mean droplet size also depend on liquid properties, in particular surface tension, density and viscosity. Further, gaseous flow properties such as velocity and density influence the droplet size [26]. Numerous different nozzle designs exist, enabling production of droplets with a diameter in the range of a few microns up to about 300 µm.

2.1.2 Droplet Drying by Mixing of Drying Gas and Spray

Subsequent to the spray formation the droplets are dried which is the next important stage of the spray drying process. The droplet drying takes place inside the drying chamber (figure 2.1) where liquid evaporates from the droplets and is transferred to the drying gas. The course of drying for a single droplet is described in detail in section 2.2. However, the choice of flow mode is a design parameter which characterizes a given spray dryer unit. Further, the flow mode influences the course of droplet drying and thereby the drying kinetics, morphology formation and enzyme inactivation when drying enzyme containing formulations. That is, the drying chamber flow field determines how a droplet "experiences" the stay in the drying chamber [60]. Spray dryers are usually

operated in cocurrent, counter current or mixed flow mode. Figure 2.3 outlines the three flow modes.

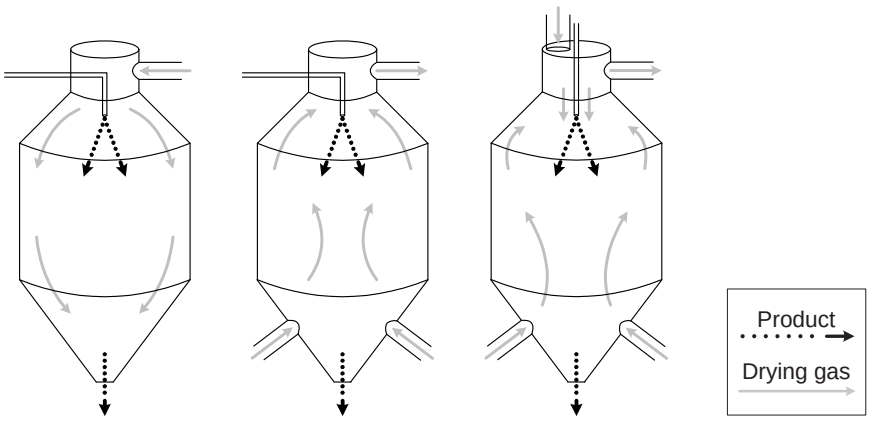

(a) Cocurrent. (b) Counter current. (c) Mixed flow.

Figure 2.3: The three flow modes usually used in spray dryers.

In cocurrent mode, the spray and the drying gas are fed in the same direction. The drying gas is hottest in the uppermost part of the drying chamber and evaporation from the newly formed droplets is fast. During evaporation, the drying gas is cooled while it is mixed well in the drying chamber. Thus, there is a low temperature with a somewhat uniform distribution in most of the drying chamber. Therefore, cocurrent flow is particularly well-suited for the drying of temperature-sensitive materials such as enzymes.

Alternatively, a spray dryer may be operated in counter current mode where the atomization takes place in the top of the dryer while the drying gas enters in the bottom of the dryer. This usually results in improved heat utilization but the almost dried powder is subjected to a very high temperature at the bottom of the dryer. Therefore, counter current mode is often used when drying thermo stable materials which require elevated temperatures in the later part of the drying process [60]. Also, it may be expedient to combine counter current mode with nozzle atomization because the drying gas flow reduces the downward velocity of the droplets.

Likewise, mixed flow is often combined with a nozzle but it is avoided that nearly dried particles are subjected to intense heat. Mixed flow also includes *fountain mode* (not shown in figure 2.3) where the atomizer is placed at the bottom of the drying chamber and sprays upward. This mode is well-suited for production of large particles and coarse powders.

2.1.3 Separation of Dried powder and Drying Gas

The final stage of the spray drying process is to separate the dried powder from the drying gas. This may be done using a cyclone as shown in figure 2.1 but alternatives include bag filters and electrostatic filters. The choice of separation unit depends on e.g., the gas and particle flow rates and the level of product loss accepted. Finally, the drying gas may be passed through a wet scrubber before it is released to the surroundings to prevent emission of harmful particles.

2.1.4 Spray Dryer Layouts

A great advantage of the spray drying process is that numerous different products with specific properties may be produced. This is possible because a large number of different process layouts have been designed. In the following different process layouts are given to illustrate the variety of spray dryers.

Figure 2.1 shows a spray dryer operating in open loop which is the most common process layout. The principle of open loop is that the drying gas passes only once through the drying chamber before it is emitted to the surroundings.

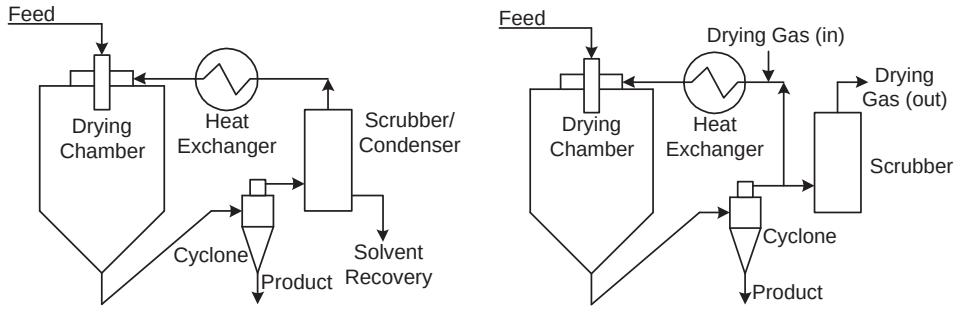

(a) Closed loop. (b) Semi-closed loop.

Figure 2.4: Common spray dryer layouts.

Opposite to this is the closed loop layout where the drying gas is recirculated – figure 2.4a. Often nitrogen is used as the drying gas and closed loop thereby allows for drying of many products which cannot by produced in a conventional open loop process. It is possible to manufacture products which degrade in contact with oxygen, dust explosions are avoided and release of hazardous compounds is prevented, allowing drying of solutions based on organic solvents.

Semi-closed loop is – as the term implies – a combination of open and closed loop. A number of different semi-closed loop process layouts exist but the one shown in figure 2.4b is designed to achieve high thermal efficiency. The off-gas

is divided into two flows where one is recycled and mixed with air from the atmosphere. Less energy is required to heat this gas stream but the humidity is increased. Consequently, a higher temperature is necessary for sufficient product drying. However, Masters [42] states that an energy utilization reduction of 20% is attainable by using a semi-closed loop setup.

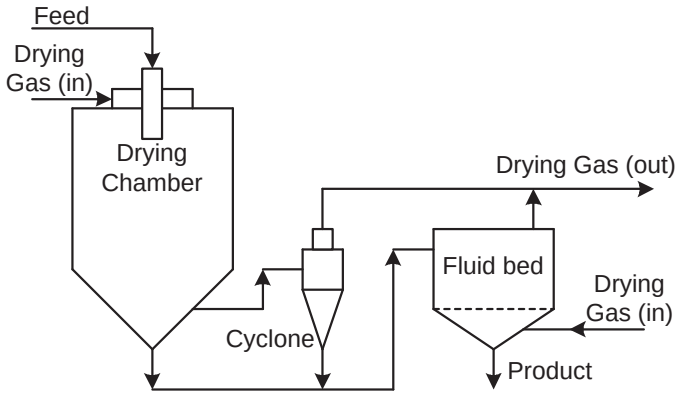

Figure 2.5: Open loop spray dryer equipped with an external stationary fluid bed.

For the production of agglomerated products a fluid bed is often introduced in the process layout. Also, a fluid bed may help reduce the residual moisture content of the powder or improve the overall heat efficiency. The fluid bed may be implemented externally or internally in the spray dryer and may be either vibrating or stationary. The latter is shown in figure 2.5.

Further, spray dryers may be equipped with additional cooling units which is used for the drying of highly temperature-sensitive materials.

Disadvantages of Spray Drying

It is evident from the above that spray drying is a very suitable method for conversion of a solution or suspension into a dry powder product. However, spray drying is not always the preferred method. When the process is excluded from consideration it is most often because the process cannot meet the product requirements or if the feed has certain characteristics, e.g. is difficult to atomize. Also, the costs of designing, constructing and commissioning a new plant are considerable. The units are often very large, necessitating establishment of equivalently large supporting structures.

Also, despite innovations like semi-closed loops and implementation of fluid beds the energy efficiency of spray dryers remains low.

Finally, during dryer operation particle depositing in the drying chamber and

separation equipment is a substantial problem. Deposits often form if the powder is not sufficiently dry or if the powder consists of a sticky material.

2.2 Single Droplet Drying

Spray drying is characterized by the atomization of the feed and subsequent drying of the formed droplets as elaborated above. Insight into the droplet drying process is critical in the investigations of the drying kinetics, morphology formation and enzyme deactivation which are the focal points of this thesis. For that reason, knowledge about single droplet drying is deduced from the literature in this section. This includes a discussion of previous studies of particle morphology formation.

2.2.1 Stages of Drying

When a droplet consisting of a solution or a suspension is drying inside a drying chamber it undergoes continuous changes in temperature, mass and appearance. The course of drying may be divided into several stages (figure 2.6) which are described in literature by e.g. Farid [20].

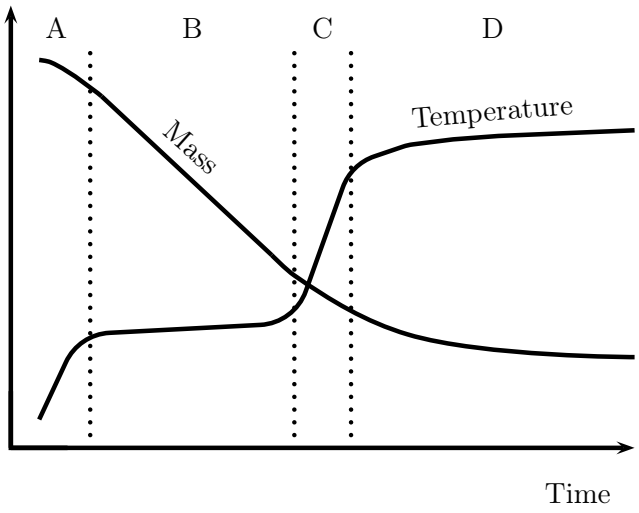

Figure 2.6: Development in mass and temperature for the drying of a single droplet inside a spray dryer.

Stage A After being formed at the atomizing device a droplet experiences initial heating and evaporation occurs. The temperature increases until it is very close to the so-called wet bulb temperature of the solvent [28].

During stage A evaporation is slow because most of the heat transferred to the droplet from the surroundings is used for droplet heating.

Note, that the wet bulb temperature is the specific temperature which is attained by a droplet with a velocity relative to the surrounding gas. The wet bulb temperature is lower than the temperature of the gas and is dependent on the relative humidity and temperature of the gas phase.

Stage B During stage B of drying solvent is readily available at the droplet surface, giving rise to fast evaporation. Most of the heat transferred to the droplet is used for this evaporation and the temperature remains close to the wet bulb temperature.

The droplet diameter decreases due to the evaporation and solute or primary particle concentration builds up inside the droplet. Thus, the droplet temperature may increase slightly because of minor evaporation hindrance [48].

Stage C If a solution is being dried, precipitation occurs at a certain point in time because of the concentration build-up. This marks the beginning of stage C. Most often the precipitation occurs at the droplet surface and a solid phase forms around a wet core because the droplet diameter decreases faster than the solute can diffuse into the droplet center.

Similarly, if a suspension is being dried, a solid phase forms around the wet core of the droplet when the primary particles have packed as closely as possible at the droplet surface.

Stage D The crust formed thickens towards the droplet center until a particle has formed. This is referred to as stage D of drying. During this stage the rate of evaporation falls because the thickening crust is a significant resistance to water transport from the center to the surface. The decrease in evaporation rate induces an increase in droplet temperature because less energy is needed for evaporation.

By the end of stage D complex bound water may evaporate as the particle temperature approaches the dry bulb temperature (i.e. the temperature of the surroundings.)

The process of single droplet drying may differ significantly. Particularly in stages C and D where the specific materials dried and the particle morphology formation influence the course of drying. Particle morphology is discussed in section 2.2.2.

In the literature, the single droplet drying process has also been divided into other stages than those given above. Sometimes stage B is referred to as the *constant rate period* [4] because the drying displays approximately zero order

kinetics during this period. Indeed, zero order kinetics mean constant evaporation rate. Similarly, stages C and D are called the *declining* or *falling rate period* [4]. Also, the two periods mentioned may be referred to as the *low* and the *high temperature periods*.

Nesic and Vodnik [48] divide the course of droplet drying into stages equivalent to the above. However, Nesic and Vodnik [48] include an additional stage during stage D. This stage is labeled the *boiling stage* and might occur if the temperature of the surroundings is above the boiling point of the solvent. As mentioned the boiling stage starts during stage D but does not end until all water has evaporated because the droplet cannot be cooled below the temperature of the surroundings.

2.2.2 Particle Morphology

The development in droplet mass and temperature during drying outlined above is merely qualitative but valid for most formulations. To understand the drying process for a specific formulation it is important to take the particle morphology formation into account. The final morphology reflects the course of drying and thus, morphology analyses may lead to a better understanding of the single droplet drying process in terms of drying kinetics and also in terms of the ability to preserve enzyme activity. The latter is a parameter of the final product quality but the morphology determines other quality parameters as well. These include mechanical strength, flowability, dissolution rate and retention of e.g. flavor and color. In the following, the formation of different particle morphologies during drying is discussed. Based on the literature spray dried particles are classified according to morphology and examples of particle structures are given. Further, the influence of spray dryer process variables on the final morphology is given.

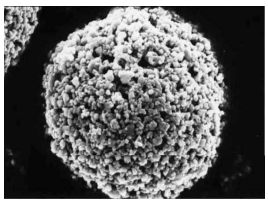

(a) Agglomerate (ferrite).

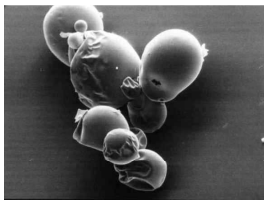

(b) Skin-forming (coffee).

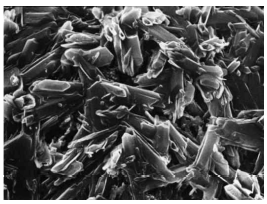

(c) Crystalline (trisodiumorthophosphate).

Figure 2.7: Examples of different morphology classes [61].

Classification

The diameter of a spray dried particle is usually in the range $0.1 - 350\,\mu m$. There are, however, exceptions from this, e.g. sticky particles may conglutinate to form sizes above 1 mm. Thus, the particle size may vary greatly and classification based on morphology rather than size seems most reasonable. Walton [60] has analyzed numerous spray dried particles and gives three basic morphology classes.

Agglomerate A particle which is made of primary particles that have a size of upto $10\,\mu m$ (figure 2.7a).

Skin-forming A particle which consists of a continuous non-liquid phase. This solid phase may consist of a polymer, submicron primary particles or crystals and appears polymeric but is difficult to define (figure 2.7b).

Crystalline A particle which consists of large individual crystal nuclei bound together by a continuous micro crystalline phase (figure 2.7c).

Generally, inorganic materials form agglomerates or crystalline structures [60] while drying of organic compounds normally form particles with a skin-forming structure. Yet, it is noted that specific organic and inorganic compounds may form particles in either of the three classes.

Many spray dried particles are spherical or nearly spherical with a solid or hollow interior. However, variations in the spherical form is often observed as a number of quite different morphology characteristics exist. As shown in figure 2.8 particles may have collapsed or contracted while others have blowholes or craters. Likewise, some particles have cavities, fractures, cracks or expand during drying. Exceptional morphologies include mushroom-head shape particles or large particles holding smaller particles [60, 23].

Effect of Drying Air Temperature

As mentioned above, the spray drying process variables greatly influence the course of drying and thereby the final particle morphology. The first process variable to be considered is the drying air temperature.

Figures 2.9 and 2.10 show the appearance of droplets drying at low and high air temperatures, respectively. The specific values are of minor importance as they just represent a low and a high temperature but it is noted that they are below and above the boiling point of the solvent.

Figures 2.9 and 2.10 are based on experiments where different materials have been dried [4] but the experiments showed that the course is identical for all materials during drying stages A and B (see section 2.2.1). Only when a solid

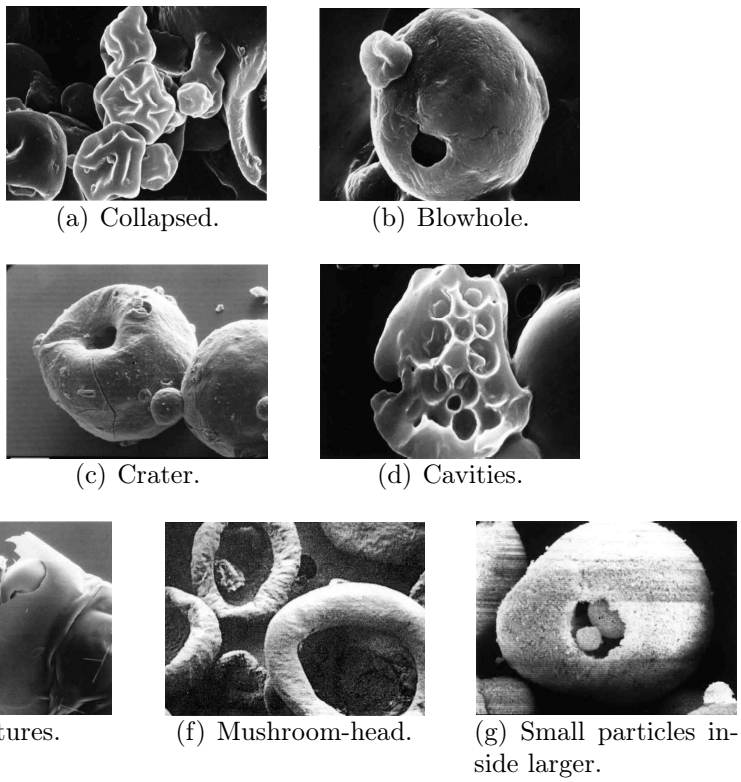

(a) Collapsed. (b) Blowhole.

(c) Crater. (d) Cavities.

(e) Fractures. (f) Mushroom-head. (g) Small particles inside larger.

Figure 2.8: Different morphology characteristics. The particles consist of a mixture of eggs and milk (a), powder yoghurt (b), dyestuff (c), powdered milk (d), coffee (e), sodium silicate (f) and lead chromate (g) [61, 62].

phase has formed around the wet core of the droplets, the process of morphology formation varies.

Depending on the nature of the formulation being dried several different drying sequences may occur when the air temperature is low (figure 2.9). If the solid phase formed during stage C is rigid and porous (sequence 1) which is the case for agglomerates and crystalline structures, the particle surface does not change during the remaining part of the drying. Water/vapor is easily transported to the surface through the pores as the wet core recedes into the particle interior. According to Lijn [34] the particle may become hollow if an air bubble is formed inside the droplet during atomization. Otherwise, the particle becomes solid. Jayanthi et al. [27] and Ford [21] believe that the final internal structure depends on the diffusion coefficient of the solute in the solvent. If the solute diffuses slowly, a hollow particle is formed because the concentration in the droplet center remains low. Formation of hollow versus formation of solid particles is discussed below. Materials that follow drying sequence 1 are e.g. potassium sulphate, ammonium chloride and sodium chloride [4, 35].

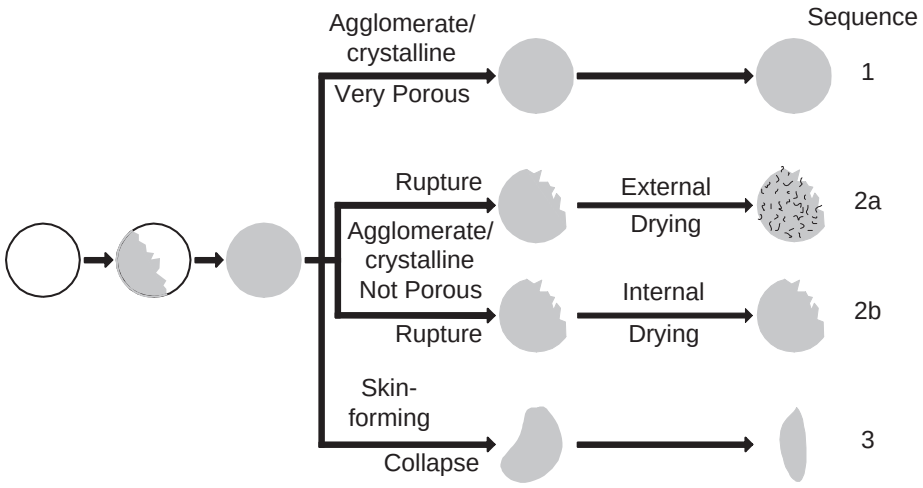

Figure 2.9: Sequences for morphology formation using a low drying air temperature. After [4].

If an agglomerate or a particle with a crystalline structure has a low porosity, the crust fractures and the drying air enters the particle interior. This may force the remaining liquid out of the interior onto the particle surface where it dries, leaving an irregular and rough surface (sequence 2a). Alternatively, the liquid may stay inside the particle and simply evaporate (sequence 2b). Compounds which follow sequence 2a or 2b include ammonium sulphate, cupric sulphate and ammonium nitrate [4].

Drying of skin-forming materials at low temperatures generally progresses according to sequence 3. The skin-forming structure prevents evaporated liquid from escaping the particle interior. As drying advances a positive pressure may built up inside the particle which ultimately ruptures and collapses. E.g. coffee extract exhibits this drying sequence [4].

In connection to drying sequences for low drying air temperatures it is noted that Crosby and Marshall [5] have conducted experiments which show that the particle density decreases with increasing air temperature.

When a droplet is dried at a temperature above the boiling point of the solvent (representing a high drying air temperature), the liquid in the droplet might begin boiling, causing a substantial pressure increase in the droplet center (figure 2.10). The influence on the morphology formation of this pressure increase depend on the structure of the initial crust. If the crust is very porous which is often the case for agglomerates and crystalline structures vapor easily escapes the particle and no changes to the surface morphology occur (sequence 4). However, agglomerates and crystalline structures may have low porosity and the pressure increase forces liquid from the droplet center out onto the surface

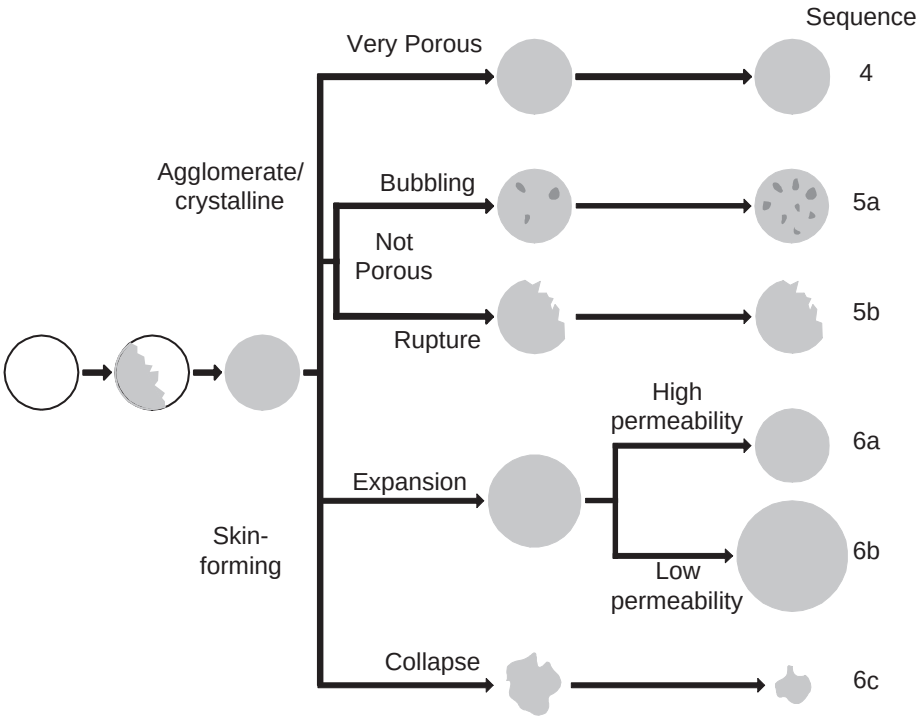

Figure 2.10: Sequences for morphology formation using a high drying air temperature. After [4].

where bubbles are created (sequence 5a). Alternatively, the positive pressure causes particle rupture (sequence 5b) [16]. Particles dried from ammonium sulphate solutions are known to have desiccated bubbles covering the surface while lithium hypochlorite particles suffer rupture [4].

Likewise, a positive pressure may develop inside a particle with skin-forming morphology when drying at a high air temperature. The pressure increase might stretch the particle skin through particle volume expansion until the skin permeability is increased sufficiently and the vapor escapes (sequence 6a). Subsequent to the pressure equalization the particle shrinks, the permeability of the skin decreases and volume expansion reoccurs. A particle might pass through this cycle several times before drying completely [15, 24, 25]. If the permeability remains low despite the stretching, the particle size simply continues to increase (sequence 6b) or the particle explodes (sequence 6c). The course of drying for skin-forming materials at high air temperatures is also discussed by Adhikari et al. [1] and Alamilla-Beltrán et al. [2].

A few examples of skin-forming materials which display the drying sequences explained are sucrose, maltodextrin (sequence 6a), polyvinyl acetate (sequence 6b) and coffee extract (sequence 6c) [4, 15, 35, 59].

Effect of Initial Concentration

Like the drying air temperature, the feed solid or solute concentration has influence on the final particle morphology. At very low initial concentrations (i.e. less than 1 wt%) the major part of the drying progresses as evaporation from a pure liquid droplet. The particles formed have difficult determinable morphologies [60].

At initial concentrations above 15 wt% the drying process proceeds as described above [60]. The final particle volume increases approximately proportional to an increase in the initial concentration [15] and as the initial concentration is increased hollow particles become thick-walled [18]. This, obviously, means that a higher initial concentration leads to a higher particle density.

However, surprising results were attained by Crosby and Marshall [5] according to whom a lower initial concentration leads to a higher particle density. At an elevated initial concentration solid precipitation occurs earlier in the drying process. The particle becomes very compact and liquid trapped inside the particle cannot escape. For agglomerates and crystalline structures this favors sequences 2 and 5. The probability of particle rupture is increased which may explain the lower particle density at a higher initial concentration observed by Crosby and Marshall [5].

Effect of other Process Variables

Crosby and Marshall [5] have investigated the influence of the feed temperature on the properties of the particles produced. The results showed a trend of an increased particle density but a smaller particle diameter as the feed temperature was increased. The variations were, however, insignificant.

Lin and Gentry [35] have investigated the influence of solute properties on the course of drying. Specifically, the influence of solubility and heat of crystallization were investigated but the extent of the investigations were limited and the conclusions thus poorly supported. Nevertheless, the results indicate that a higher solubility leads to smaller particles while a high heat of crystallization favors positive pressure build-up in the particle. As described above this gives preference to drying sequences 2 and 5.

Drying of Suspensions

As yet, the discussion of morphology formation has been somewhat general for both solutions and suspensions. However, when a droplet consisting of a suspension is being dried, the motion of the primary particles inside the droplet may determine the final particle morphology.

First, if the size of the primary particles is in the submicron range, the crust formed at the droplet surface has a skin-forming structure [62]. Due to strong van der Waals forces between the small primary particles the surface structure is locked, rendering rearrangement of the primary particles impossible. Thus, a hollow particle is formed which may be inflated or deformed (non-spherical).

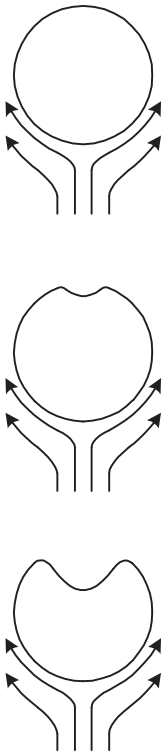

Figure 2.11: Formation of an indentation [After 3].

Normally, agglomerates form at particle sizes above 1 µm. Large pores in the particle allow for a considerable liquid flow from the particle center to the surface through capillary action. The surface remains wet, enabling rearrangement of the large primary particles as the drying progresses. Consequently, a solid, dense particle is formed [62]. This is supported by Liang et al. [30] who showed that increasing the primary particle size gives preference to formation of solid rather than hollow particles.

The particles produced by spray drying of suspensions are not always spherical but in fact often exhibit surface indentations. The formation of indentations is discussed in detail in Paper III (chapter 5) but a generally accepted theory is summarized here. During drying after the initial crust formation capillary forces draw liquid from the particle center toward the surface. If the primary particles at the surface are unable to rearrange, the transport of liquid from the center leaves an internal void. A significant pressure difference between the partial vacuum of the void and the atmospheric pressure around the particles arises. This may lead to particle collapse if the crust is not strong enough to withstand the pressure difference. The theory is discussed by Büttiker [3], Crosby and Marshall [5], Lukasiewicz [39], Walker Jr. and Reed [58] and Minoshima et al. [46].

Further to this is the theory discussed by Büttiker [3], Duffie and Marshall [13, 14] and Shaw [56]. The theory is sketched in figure 2.11 and assumes that the droplet does not rotate during drying. The front of the droplet is subjected to a very substantial drag, increasing the transfer of heat to the droplet and the transfer of mass (i.e. evaporated liquid) from the droplet. The evaporation from the rear surface is slow, drawing liquid to the front where evaporation is quicker. The flow of liquid carries along primary particles and the rear surface is drawn inward, forming an indentation.

Undoubtedly the process of morphology formation is complex. The outline given above illustrates that both the spray drying process parameters and the feed composition and properties influence the final particle morphology. The process of morphology is among other things explored in chapter 5.

2.3 Enzyme Structure and Thermal Inactivation

The particle morpholology has a great impact on the final product properties. This includes particle mechanical strength, friability, flowability, density etc. However, when spray drying temperature-sensitive materials the most important requirement of the process is often to avoid degradation of the material. This includes spray drying of enzymes where any activity loss represents a reduction in the final product value. In the literature several authors consider the subject. The following is a short survey of the literature including a description of enzymes and how the enzyme inactivation rate during spray drying may be investigated.

2.3.1 Enzymes

Enzymes are proteins that may work as catalysts of chemical reactions. They temporarily bind a number (or in some cases just one) of the reactants of the reactions which they catalyze. The activation energy needed for the reaction is thereby lowered and the reaction rate increases. To understand the effect of spray drying on the catalytic activity of the enzymes it is important to first understand the structure of the enzymes and how the enzymes work.

Enzyme Structure

Enzymes are proteins which again are polymers. These polymers are formed by the linkage of α-amino acids by a peptide bond. An α-amino acid consists of an α-carbon atom to which four parts are attached: A hydrogen atom, an amino group, a carboxylic acid group and finally one of 20 different side chains called R-groups. The specific properties of different enzymes are determined by the sequence of α-amino acids. The amino acids may be divided into two groups – hydrophobic and hydrophilic depending on the nature of the R-group. The hydrophilic amino acids are usually located at the exterior of the enzyme because they form hydrogen bonds with the surrounding aqueous medium. On the contrary, the hydrophobic amino acids are located in the interior of the enzyme.

Primary Structure

Proteins have multiple levels of structure. The most basic is the primary structure which simply is the order of the amino acids (see figure 2.12). It is noted that some disulfide bridges may exist, these are also a part of the primary structure.

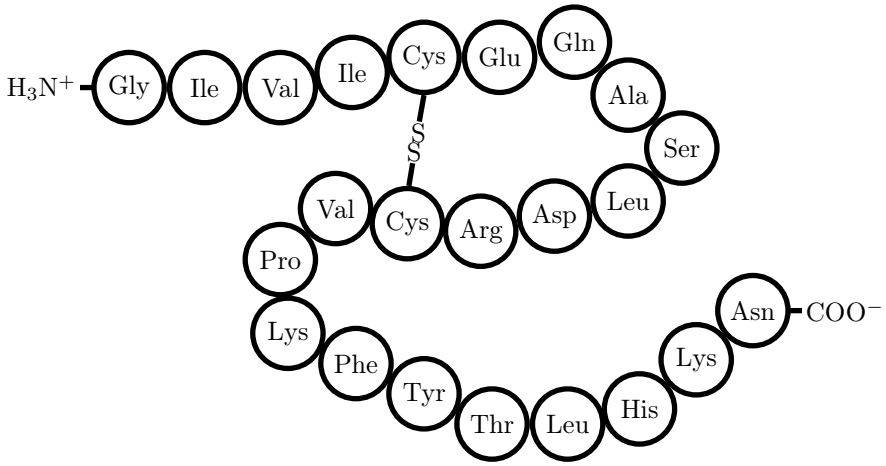

Figure 2.12: Example of protein primary structure. Different amino acids are shown using the standard abbreviations.

Secondary Structure

The common repeating structures found in proteins constitute the secondary structure. There are two types of secondary structure, one being the α-helix (see figure 2.13), the other being the β-sheet.

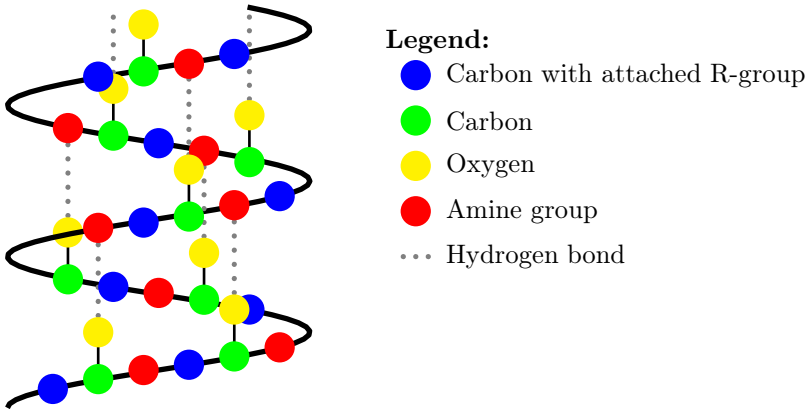

Figure 2.13: Secondary protein structure illustrated by an α-helix.

As shown in figure 2.13, the α-helix twists in a clockwise direction and makes a complete turn every 3.6 amino acids. Also, the carbonyl groups of the peptide bonds form hydrogen bonds with amine groups which also are a part of the peptide bonds. These hydrogen bonds are always formed by amine and carbonyl groups which are four amino acids apart in the helix. The hydrogen bonds are

parallel to the axis of the helix and strengthen the structure quite significantly.

Unlike the α-helix the β-sheet consists of pairs of amino acid chains lying side-by-side. The structure is like a pleated sheet held together by hydrogen bonds between the carbonyl group on one chain and the amine group on the adjacent chain. Thus, like for the α-helix the existence of the hydrogen bonds is crucial to maintain the β-sheet structure.

Tertiary Structure

The three dimensional structure of the polypeptide chain is called the tertiary structure. Thus, the structure describes the folding of the secondary elements, including α-helices, β-sheets and more undefined elements called random coils. Stabilization of the tertiary structure involves different interactions. First, weak forces such as hydrogen bonds and van der Waals forces. But also stronger forces such as ionic and disulfide bonds. Finally, hydrophobic and electrostatic interactions are important in the tertiary structure.

Quaternary Structure

Some proteins contain multiple polypeptide chains and the quaternary structure is their interconnections and organization. The individual polypeptide chains are held together by non-covalent forces (ionic interactions, hydrophobic interactions or hydrogen bonds).

Enzyme Action

In addition to the elements mentioned above many enzymes require the presence of a non-protein component called a cofactor to have catalytic activity. These may be metal ions such as Zn^{2+}, Cu^{2+}, Mn^{2+}, K^{+} or Na^{+}. The additional compound may also be a small organic molecule in which case it is termed a coenzyme. Coenzymes may be covalently bonded to the enzymes but some coenzymes are bonded more loosely and may in fact bind only transiently to the enzyme as it performs the catalytic act.

The reactants in an enzyme catalyzed reaction are called substrates. In order to work the enzyme must unite with at least one of the reactants. In most cases the forces which hold the enzyme and the substrate are non-covalent and rather weak (e.g. hydrogen bonds, ionic interactions, or hydrophobic interactions). This means that the two molecules cannot be very far apart and successful binding depend on the two molecules being able to approach each other closely over a broad surface. An analogy often used is that a substrate molecule binds the enzyme like a key in a lock (see figure 2.14) – the substrate fits into the

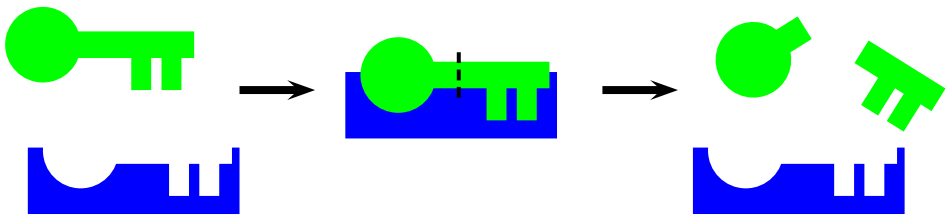

Figure 2.14: The lock-and-key model for enzyme and substrate interaction.

complementary site on the enzyme like a key in a lock [49]. According to this lock-and-key model all structures remain fixed throughout the binding process.

Opposed to the above, the induced-fit theory has been put forward [49]. In this hypothesis it is stated that the enzyme undertakes conformational changes to bind to the substrate. This suggests that at least some parts of the enzyme are flexible.

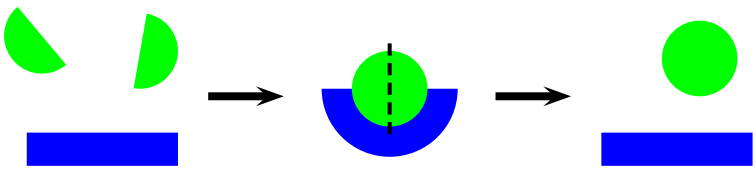

Figure 2.15: The induced fit hypothesis for enzyme and substrate interaction.

According to both hypotheses there is an important requirement for complementarity in the configuration of the substrate and the enzyme. Thus, even very small conformational changes to an enzyme might lead to loss of catalytic activity. It also explains the remarkable specificity of most enzymes – generally an enzyme is only able to catalyze a single reaction.

2.3.2 Structure and Inactivation

During spray drying the rapid changes in droplet temperature and moisture content influence the enzyme directly but also the environment around the enzyme. This section treats different aspects of the dehydration process which cause enzyme inactivation.

Temperature

An enzyme functions best at a certain temperature. The activity of the enzyme is reduced below and especially above this temperature. The former trend reflects the general effect of decreasing the temperature in a chemical reaction, the latter trend reflects the loss of catalytic activity as the enzyme becomes denaturated. The term "denaturation" is explained below but it basically means that the enzyme loses activity due to a structural change.

As elaborated in section 2.3.1 the enzyme is dependent on hydrogen bonds to maintain the secondary, tertiary and quaternary structures. It is well-known that increasing the temperature reduces the strength of hydrogen bonds.

The obvious solution to the above would be to operate the spray dryer at a lower temperature. This, however, often represents an undesirable manufacturing condition which reduces the production rate. Furthermore, it deteriorates the final product because the residual moisture content is high, leading to poor storage stability [41, 51].

Dehydration

Removal of the aqueous medium surrounding the enzyme may also lead to breakage of the hydrogen bonds. Further, the interactions between the hydrophilic groups may change [45]. These factors lead to enzyme denaturation and inactivation as mentioned above.

The enzyme suspension which is subjected to spray drying may contain additional materials such as salts, organic compounds and buffers. The dehydration causes changes in e.g. salt concentrations [65]. A significant increase in salt concentration will alter the electrostatic interaction between charged amino acids. The alteration might give rise to enzyme denaturation. This also applies to changes in pH which can occur because one buffer compound precipitates before the other during the dehydration process [65].

In the above the term "denaturation" is used several times. The function of a protein is absolutely dependent on the three dimensional structure. As mentioned changes in temperature, salt concentration and pH but also the presence of reducing agents (breaks the disulfide bridges between amino acids) may cause denaturation. However, none of these breaks the peptide bond between the amino acids and thus, this part of the primary structure remains intact [49].

The denaturation process is not necessarily irreversible. If an enzyme has been denaturated it might spontaneously resume the native three dimensional shape when it is returned to the normal conditions (e.g. upon rehydration) [12]. Thereby the catalytic activity is regained. The process is shown in figure 2.16.

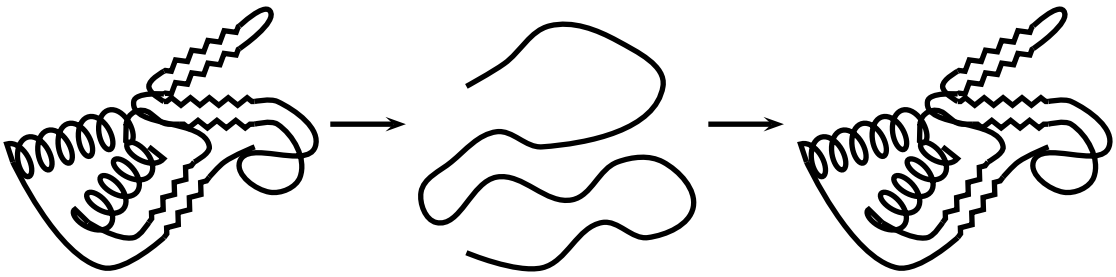

Figure 2.16: Enzyme dehydration which causes denaturation. Upon rehydration the enzyme spontaneously resumes the native structure.

Surface Adsorption

Millqvist-Fureby et al. [45] have investigated the amount of trypsin on the surface of spray dried particles. The study revealed that the trypsin was strongly overrepresented at the surface. In fact, it covered up to 65 % of the surface area although it only made up about 5 % of the total amount of solids in the particles. The results suggest that proteins are adsorbed at the droplet surface during the drying process.

According to Landström et al. [29] there may be several reasons for the adsorption of proteins on the surface. The adsorption to an interface is commonly assumed to be controlled by the diffusion rate and the surface activity of the protein, making the adsorption a three step process. First, diffusion of the protein to the subsurface region followed by adsorption to the air-liquid interface. The final step is rearrangement of the adsorbed molecule at the surface. The diffusion plays an important role in this but Landström et al. [29] have studied competitive adsorption between bovine serum albumin and β-lactoglobulin which have significantly different diffusion coefficients ($6.7 \cdot 10^{-11}\mathrm{m}^2/\mathrm{s}$ and $9.7 \cdot 10^{-11}\mathrm{m}^2/\mathrm{s}$, respectively). The study showed that the fraction of each protein adsorbed at the surface was nearly the same as the protein fraction in the solution, although the protein with the higher diffusion coefficient is expected to be overrepresented at the surface. Therefore, the protein adsorption during spray drying may not be explained with the diffusion rate and surface activity alone. Other factors may be involved, e.g. temperature and pressure gradients and internal forces from droplet formation.

Millqvist-Fureby et al. [45] explain that adsorption of trypsin to the droplet surface drying may lead to two kinds of inactivation. First, the thermal inactivation is increased because the droplet temperature, according to Millqvist-Fureby et al. [45], is highest at the surface. Secondly, interactions between the

surface and the trypsin account for some of the inactivation.

Combined Millqvist-Fureby et al. [45] and Landström et al. [29] have studied a number of different proteins which all adsorbed to the surface. This suggests that adsorption is a problem during spray drying regardless of the protein chosen. However, in actual production spray drying of a commercial enzyme product the enzyme is usually not highly purified. This means that numerous compounds from upstream processes remain in the spray dryer feed, inhibiting enzyme surface adsorption. Thus, adsorption might only be a substantial problem for drying of pure enzymes.

Other Factors

Other factors than those mentioned above may contribute to the inactivation of enzymes during spray drying. Elversson and Millqvist-Fureby [17] mention that shear forces during droplet formation in a nozzle or rotary atomizer is a source of loss of protein structure.

Also, Mumenthaler et al. [47] have investigated spray drying of solutions of recombinant methionyl humane growth hormone and tissue-type plasminogen activator. The study showed that insoluble aggregates are formed during the drying process. This, obviously, leads to loss of activity.

2.3.3 Effects of Excipients

Any inactivation during the spray drying process represents a loss of valuable enzyme and a reduction in the quality of the final product. Thus, a number of measures are usually taken to avoid this inactivation. Process conditions may be altered but also, different additives (usually called excipients) are added to the enzyme containing formulation prior to dehydration. This section describes the excipients in terms of function.

Carbohydrates

In the literature there are several studies of adding carbohydrates to protein containing formulations. For example Selivanov [55] examines the effects of glucose, cellobiose and carboxymethylcellulose upon the activity of cellulase after spray drying. Also Millqvist-Fureby et al. [45] study trypsin mixed with lactose, sucrose, mannitol, α-cyclodextrin and dextrin. Further, Maa et al. [41] use mannitol and trehalose to stabilize recombinant human deoxyribonuclease and recombinant human anti-IgE monoclonal antibody.

The authors mentioned above report better activity preservation by adding the carbohydrates before spray drying the formulations. The degree of improvement

is very dependent on the nature of the protein and the carbohydrate. Also, the concentrations of the compounds and the specific drying conditions play important roles. Selivanov [55] reports a very significant decrease in activity loss from 54% to 18% when adding maltodextrin to a cultural cellulase liquid.

Millqvist-Fureby et al. [45] go through two hypotheses that may explain the stabilizing effects of the carbohydrates. The first hypothesis is the "water replacement hypothesis" which states that in order to preserve the native structure of a protein the hydrogen bonds formed between the protein and the surrounding aqueous medium must be replaced by new hydrogen bonds in the dry state. The carbohydrates will, according to the hypothesis, form these hydrogen bonds with proteins upon dehydration.

The second hypothesis is the so-called "vitrification hypothesis" which states that it is essential to maintain the carbohydrate in an amorphous (vitreous) state that prevents the protein from changing shape. More specifically, the rigidity of the matrix fully immobilizes the protein and thus, denaturation is avoided because this generally involves conformational changes of the protein. From the above it is clear that the carbohydrate chosen for a specific formulation must have a high glass transition temperature.

It is not straight forward to point out which of the mechanisms of the two hypotheses predominates the protein stabilization during spray drying. However, the answer is most likely formulation specific and DePaz et al. [12] mention that for the stabilization of subtilisin, trehalose and sucrose both help maintain protein via hydrogen bonding and formation of an amorphous phase. Dextran and maltodextrin are large polymers and because of steric hindrance they cannot form hydrogen bonds with the subtilisin but they do form an amorphous phase. It is noted that DePaz et al. [12] work with a spray coating drying process rather than spray drying. The two processes are, however, very closely related.

An additional advantage of adding carbohydrates is the "dilution effect" [45]. The addition of the carbohydrates may reduce the possibility of a given protein to interact with other proteins. The risk of aggregate formation therefore decreases (more on aggregates below).

Adsorption

As described in section 2.3.2 some authors believe that adsorption of proteins on the droplet surface during spray drying is a significant problem both because of thermal degradation and because of conformational changes of the protein at the air-liquid interface.

The literature describes a number of different studies where it is attempted to alter protein containing formulations so that adsorption is avoided. The method which by far is the simplest is suggested by Landström et al. [29]. The

authors have measured the apparent surface load of bovine serum albumin as a function of the protein concentration in the starting solution. The results show that the apparent surface load increases with concentration sharply but after a certain point the increase in the amount of protein is less pronounced and does in fact become insignificant. The experiment was repeated for β-lactoglubin and qualitatively the same results were obtained.

The findings of Landström et al. [29] suggest that there exists a rather well-defined limit to the amount of protein which can accumulate at a droplet surface. Therefore, it might be possible to reduce the fraction of protein being denaturated during the drying process by using a high initial concentration because in this case most of the protein resides in the droplet interior.

The method above has the disadvantage that some protein undoubtedly will denaturate. Instead of increasing the initial concentration the denaturation might be kept at a minimum by altering the protein formulation in a different manner. An attempt to do this was made by Elversson and Millqvist-Fureby [17] who tested spray drying of bovine serum albumin in a two phase system consisting of polyvinyl alcohol and a dextran solution.

The bovine serum albumin preferentially partitioned in the dextran phase and was almost absent in the polymer. Furthermore, the polymer encapsulated the dextran phase thus providing protection of the protein from adsorption. Therefore the two phase concept can be said to be successful in terms of minimizing the exposure of protein to the air-liquid interface. However, a large amount of the protein suffered from extensive aggregation, according to Elversson and Millqvist-Fureby [17] because of interaction with the polyvinyl alcohol. This polymer can therefore not be considered appropriate for the purpose of encapsulation during spray drying.

Millqvist-Fureby et al. [45] have investigated the effects of adding a surfactant to the protein formulation. The idea with this is that the surfactant preferentially adsorbs at the droplet surface, expelling the proteins from the air-liquid interface. The surfactant used was Tween 80 which was added to a solution of trypsin. The experimental results of Millqvist-Fureby et al. [45] showed that the addition of Tween 80 improved the residual activity of trypsin regardless of the initial concentration of trypsin.

As mentioned on page 41 Millqvist-Fureby et al. [45] have added carbohydrates to the formulation to form hydrogen bonds and an amorphous matrix. The authors believe that addition of the carbohydrates also has an effect on the amount of protein which adsorbs at the droplet surface. The long chained carbohydrates are viscosity enhancing and therefore they retard the transportation of the protein from the droplet interior to the surface.

Aggregates

The work of Mumenthaler et al. [47] focuses on the number of insoluble aggregates formed when spray drying formulations containing recombinant methionyl human growth hormone. Addition of polysorbate 20 to the formulation reduced the formation of insoluble aggregates by approximately 85 %. Polysorbate 20 is a surfactant and is thus expected to greatly inhibit access of the protein to the droplet surface as discussed above. The results led the authors to hypothesize that the aggregates are formed at the air-liquid interface. If this is true then the addition of a surfactant is very important in the formulation design process because it both (partly) solves the problems mentioned in the previous section and reduces the number of aggregates formed.

2.3.4 Previous Investigations of Inactivation Kinetics

Several researchers have attempted to find ways to minimize the enzyme degradation during drying by taking a theoretical approach. Usually, the approach is to formulate a mathematical model for the inactivation reaction and combine the model with an additional model for the single droplet drying process. The aim is to simulate the inactivation during drying for a given enzyme for different process conditions or feed formulations. If successful, this may be used for process and formulation optimization.

Most studies have been devoted to map the inactivation of alkaline phosphatase, an enzyme found in skimmed milk. Wijlhuizen et al. [66] base the setup of a theoretical model on the assumption that inactivation of the alkaline phosphatase inside a drying droplet may be described by first order reaction kinetics. That is, the rate constant k_r of inactivation is

$$k_r = \exp\left(A - {}^{B}/_{T}\right) \tag{2.1}$$

where A and B are water concentration dependent parameters. The two parameters are fitted to experimental data by Daemen [7][1] (described later in this section). The inactivation kinetics are coupled with a drying kinetics model for a single droplet which may form a solid or a hollow sphere.

Although Wijlhuizen et al. [66] fail to give comparisons to experimental data their model simulations give rise to some interesting conclusions. The simulations show that enzyme inactivation is strongly dependent on both droplet temperature and liquid content in such a way that the inactivation occurs primarily in the falling rate period. This conclusion is supported by many authors, including Turner and Vulfson [57] who recently studied how temperature and water activity affect denaturation of candida antarctica lipase.

[1] This is not a chronological error, in 1979 Wijlhuizen et al. [66] cite Daemen [7] prior to the publication of his work in 1981

Table 2.1: Literature references containing relevant experiments and modelling on enzyme inactivation during drying. See chapter 5 or references for details on the experimental methods.

Author	Enzyme	Inactivation experiment	Inactivation model	Drying model	Validation experiment
Daemen and coworkers [7, 8, 9, 10, 11]	Alkaline phosphatase, rennin and α-amylase	Aluminum box	First order reaction kinetics	From Lijn [34]	Medium sized spray dryer
Etzel et al. [19]	Alkaline phosphatase	None	From Liou [36]	From Sano and Keey [53], solid or hollow particle	Mini spray dryer
Fu et al. [22]	Lactococcus Lactis (bacteria) and alkaline phosphatase	None	From Liou [36]	From Sano and Keey [53], solid particle	Spray dryer
Lievense et al. [31, 32, 33]	Lactobacillus plantarum (bacteria)	Fluidized bed	First order reaction kinetics for thermal inactivation. Linear decay for dehydration inactivation	Cylinder geometry. From Liou and Bruin [37, 38]	Fluidized-bed

continued on next page

continued from previous page

Author	Enzyme	Inactivation experiment	Inactivation model	Drying model	Validation experiment
Liou [36]	Lipoxygenase	Aluminum box	First order reaction kinetics	Ideal drying. Slab, cylinder or sphere	Suspended spherical gel with enzyme
Luyben et al. [40]	Catalase, lipase and alkaline phosphatase	From literature	First order reaction kinetics	Ideal drying. Slab, cylinder or sphere	None
Meerdink [44]	Maxymyl and Fungamyl (both α-amylases)	Aluminum box	First order reaction kinetics	Ideal shrinkage, solid sphere	Suspended droplet, free falling
Sadykov et al. [50]	Ten different, including α-amylase	Differential thermal analysis	First order reaction kinetics	Ideal shrinkage, slab geometry	Differential thermal analysis
Samborska et al. [52]	Fungamyl (α-amylase)	None - experimental investigations of influence of spray dryer process conditions on Fungamyl inactivation			Mini spray dryer
Wijlhuizen et al. [66]	Alkaline phosphatase	From Daemen [7]	First order reaction kinetics	Single droplet, bubble forming	None
Yamamoto et al. [68]	Glucose oxidase, alkaline phosphatase and alcohol dehydrogenase	Water bath	First order reaction kinetics	Single droplet, solid sphere	Suspended droplet

The inactivation of alkaline phosphatase is further analyzed in the very elaborate paper series by Daemen and coworkers [7, 8, 9, 10, 11]. Though the work focuses on alkaline phosphatase, two other enzymes (rennin and α-amylase) and two types of bacteria (Serratia marcescens and Straphyloccus C 131) are included in some parts of the investigations.

Like Wijlhuizen et al. [66] it is believed by Daemen [7] that the enzyme inactivation during drying may be described by a first order reaction kinetic expression where the rate constant is dependent on the temperature and moisture content of the drying droplet. Consequently, Daemen [7] uses the well-known Arrhenius form of equation (2.1)

$$k_r = A \exp\left(-{}^{E_a}/_{RT}\right) \tag{2.2}$$

where the parameter A is not the same as in equation (2.1) but it is still a reaction rate parameter which is water concentration dependent like the activation energy E_a. Experiments to find expressions for these parameters are conducted, using a small air- and watertight cylindrical aluminum box (figure 2.17). The box is filled with a moistened enzyme powder sample and kept for a specific period of time at a constant temperature. Carrying out multiple experiments, changing either time period, temperature or moisture content and subsequently measuring the residual enzyme activity yields data to which the parameters of equations (2.2) may be fitted.

The parameters are, however, somewhat inexactly determined because the experimental results are scattered. The main problem with the experiments is that they are very time consuming to conduct. Further, thermal lag occurs in the aluminum box, both when the box is heated in the beginning of an experiment and when it is cooled prior to the activity assay. Therefore, the specific sample temperature varies during the experiment and the time interval in which the sample is exposed to a certain temperature is inaccurately measured.

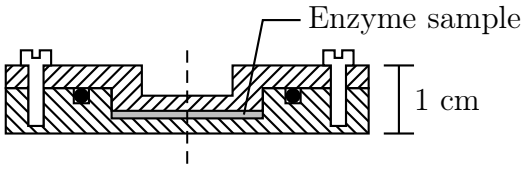

Figure 2.17: Aluminium box used by several authors for measuring enzyme inactivation (after [44]).

Nevertheless, the inactivation kinetics are coupled to a drying kinetics model setup by Lijn [34]. The model predictions are compared to experimental results for the residual activity upon drying in a medium sized spray dryer (a liquid evaporation rate of approximately 25 $^{kg}/_{h}$) [9]. From a qualitative point of view the model responds correctly to changes in the spray dryer outlet temperature. Also, inactivation with different initial droplet sizes and initial solid contents

are simulated but the comparison to the spray dryer experiments lack. Daemen [9] points out the influence of the formation of particle vacuoles on the enzyme inactivation. The model is extended to account for the fact that hollow particles formed during experiments. Generally, the presence of a centrally located vacuole leads to lower inactivation because of faster drying.

The effect of geometry is also explored by Luyben et al. [40] who developed a model that calculates the kinetics of ideal shrinkage drying. The geometry may be varied to be either a sphere, cylinder or slab by setting a model parameter. Considering catalase, lipase and alkaline phosphatase enzymes, Luyben et al. [40] include the inactivation through equation (2.2). However, shortcoming of other model parameters (e.g. water activities and diffusivities) lead Luyben et al. [40] to make educated guesses at values and thereby construct a fictitious system. With that, experimental validation of model simulations makes next to no sense and is omitted.

Based on simulations Luyben et al. [40] show that the degree of inactivation is very different for the three enzymes as lipase appear to be very thermo stable opposed to catalase and alkaline phosphatase. Furthermore, the role of the geometry is somewhat peculiar because slab geometry preserves enzyme activity best at high bulk phase temperatures (i.e. 100 °C) whereas spherical geometry leads to the most significant inactivation. At a lower bulk phase temperature (i.e. 60 °C) the opposite is the case. This observation holds true for all three enzymes considered.

Like all the authors mentioned above Yamamoto et al. [68] use first order reaction kinetics to describe the enzyme inactivation process during drying. However, in their study of the drying of glucose oxidase, alkaline phosphatase and alcohol dehydrogenase they use a different experimental approach to obtain data for fitting the parameters of the reaction rate expression. A sample is incubated in a constant temperature bath. At different points in time samples are taken and the remaining activity of the enzymes is assayed. In this way the inactivation kinetics at different moisture contents and temperatures are measured, enabling determination of the parameters mentioned. Thus, considering that some authors use the aluminum box method (figure 2.17), simple methods seem to be prevalent. One exception is the differential thermal analysis method used by Sadykov et al. [50].

Though using a rather simple method to measure the inactivation kinetics, Yamamoto et al. [68] reach interesting conclusions when combining inactivation kinetics with a drying model. That is, model simulations are generally in good agreement with experimental data obtained by drying a drop suspended from a glass filament (the experimental method is described in chapter 5). The study shows that the enzyme inactivation takes place in the falling rate period as it was already stated by Wijlhuizen et al. [66].

The work is continued by Yamamoto and Sano [67] where the effect of adding

high and low molecular weight sugars to the enzymes prior to drying is investigated. Experiments using a glass filament apparatus show that the inactivation is most prevalent when high molecular weight sugars are added. Yamamoto and Sano [67] explain this by noting that the diffusion of a high molecular weight sugar is significantly slower than that of a low molecular weight sugar. As a droplet dries the sugar concentration at the droplet surface increases because of the evaporation water loss. However, the high molecular weight sugar diffuses only slowly toward the droplet center and the point of sugar saturation is reached rather quickly. Consequently, the falling rate period is prolonged compared to that of drying a low molecular weight sugar – therefore, inactivation is more significant.

Meerdink [44] also reaches the conclusion that enzyme inactivation primarily occurs in the falling rate period. The conclusion is brought forward after very elaborate experimental and modeling work on Maxamyl and Fungamyl, both α-amylases. The work includes enzyme inactivation measurements which are analogous to those of Daemen [7], again fitting a temperature and liquid content dependent first order reactions kinetics model to the data obtained. As described above the inactivation model is coupled to a drying kinetics model which is set up for the formation of a solid sphere through ideal shrinkage. Sensitivity analysis and experimental validation are done in detail, comparing the simulations to both drying of suspended and free falling droplets (see chapter 5 for details on these experimental methods). Although the model generally underestimates the drying and inactivation rates for the latter experiments, the reference is rather interesting as it is unique in the literature because it includes enzyme inactivation measurements during free fall experiments. Also, the simulations predict the course of drying well for a suspended droplet.

Combining the results from the two experimental methods and the simulation results, Meerdink [44] arrives at the conclusion that the rate of inactivation is fastest in the falling rate period as mentioned. Moreover, it is concluded that inactivation is more significant in the droplet center than at the surface. Meerdink [44] believes that the explanation for this is that the moisture content in the droplet center is still very high when the temperature rises drastically in the falling rate period, leaving unfortunate temperature/moisture combinations in that part of the droplet. According to Samborska et al. [52] this may partly be avoided by using a low temperature in the spray dryer.

Etzel et al. [19] quantify the above partly by claiming that most alkaline phosphatase inactivation occur in a critical region of $20 - 30\%$ moisture, wherein the temperature is sufficiently elevated. This statement is based on simulations only, using literature drying modeling and inactivation kinetics. Experiments are conducted using a mini spray dryer but the model validation is rather limited. Analogous investigations are done by Fu et al. [22] who also conclude that a critical inactivation region around $15 - 30\%$ moisture exists.

All of the work mentioned above treat the enzyme inactivation as a consequence of a thermal influence only. Lievense et al. [31, 32, 33] discuss the validity of this. Their investigations are on destruction of a bacteria during drying which they cannot model solely through thermal inactivation. They reason out that there must be a second mechanism – inactivation due to the dehydration. They successfully model this and show that the dehydration mechanism prevails at low temperatures (i.e. drying below 50 °C). However, Lievense et al. [32] argue that enzyme inactivation in fact can be described with thermal inactivation as the only mechanism while the significant damage of dehydration on some bacteria remains an uncertainty. Destruction of the cell membrane is a probable explanation, especially considering that different microorganisms have differences of cell membrane sturdiness which could give them different dehydration resistance as experimentally observed [32]. Bacteria have complex structures compared to enzymes and drying of the two materials may not always be compared.

2.4 Recapitulation

In this literature review the spray drying process has been introduced and basic concepts have been explained. Also, the process of single droplet drying is described which includes an outline of morphology formation. Morphology formation is complex and both the spray drying process parameters and the feed properties influence the final particle morphology. However, some general guidelines of morphology formation exist in the literature and these have been presented.

Further, the survey has introduced the enzyme structure and explained how essential the structure is to the catalytic activity of the enzyme. However, maintaining this structure during drying depends on weak bonds (e.g. hydrogen bonds, ionic interaction, or hydrophobic interaction) which are easily broken by the high temperatures prevailing in a spray dryer.

Also, the literature review in this chapter shows that most authors believe the rate of enzyme inactivation during spray drying may be described by first order reaction kinetics. Often, simple experiments are conducted to find relevant constants in liquid concentration dependent correlations for parameters in Arrhenius type kinetics expressions. Unfortunately, the parameters are not accurately determined because the experiments generate scattered results. However, the Arrhenius expression is coupled to a drying kinetics model, usually for a single spherical droplet drying ideally. Generally, the model predictions for inactivation lack comparisons to experimentally obtained validation data.

In the literature there appears to be a general agreement that most enzyme inactivation occurs at certain unfortunate combinations of temperature and residual liquid content. Specific values depend on the enzyme regarded, however, the

greater part of the inactivation is believed to take place in the falling rate period.

It is noted that most literature on the subject of enzyme inactivation during spray drying has been written in the period from the early 1980's until the middle 1990's. Later literature focuses on the challenges in the formulation design of pharmaceutical proteins. Although numerous publications exist in this area, they are of little relevance because they concentrate on e.g. structural changes of a particular protein due to drying or the specific effects of an excipient. The review papers of Wang [64, 65] elaborately describe the formulation design process of pharmaceutical proteins.

2.5 References

[1] B. Adhikari, T. Howes, B. R. Bhandari, and V. Truong. Experimental studies and kinetics of single drop drying and their relevance in drying of sugar-rich foods: A review. *International Journal of Food Properties*, 3(3): 323–351, 2000.

[2] L. Alamilla-Beltrán, J. J. Chanona-Pézez, A. R. Jiménez-Aparicio, and G. F. Gutiérrez-Lopéz. Description of morphological changes of particles along spray drying. *Journal of Food Engineering*, 67:179–184, 2005.

[3] R. Büttiker. *Erzeugung von Gleich Grossen Tropfen mit Suspendiertem und Gelöstem Feststoff und Deren Trocknung im Freien Fall.* PhD thesis, Eidgenössische Technische Hochschule Zürich, Switzerland, 1978.

[4] D. H. Charlesworth and W. R. Marshall. Evaporation from drops containing dissolved solids. *AIChE Journal*, 6(1):9–23, 1960.

[5] E. J. Crosby and W. R. Marshall. Effects of drying conditions on the properties of spray-dried particles. *Chemical Engineering Progress*, 54(7): 56–63, 1958.

[6] C. T. Crowe. Modeling spray-air contact in spray-drying systems. In A. S. Mujumdar, editor, *Advances in Drying*, volume 1, chapter 3, pages 63–99. Hemisphere Publishing Corporation, 1980.

[7] A. L. H. Daemen. The destruction of enzymes and bacteria during the spray-drying of milk and whey. 1. The thermoresistance of some enzymes and bacteria in milk and whey with various total solids contents. *Netherlands Milk and Dairy Journal*, 35:133–144, 1981.

[8] A. L. H. Daemen. The estimation of the mean particle density, the vacuole volume and porosity of spray-dried porous powders. *Netherlands Milk and Dairy Journal*, 36:53–64, 1982.

[9] A. L. H. Daemen. The destruction of enzymes and bacteria during the spray-drying of milk and whey. 4. A comparison of theoretical computed results concerning the destruction of phosphatase with those obtained experimentally. *Netherlands Milk and Dairy Journal*, 38:55–70, 1984.

[10] A. L. H. Daemen and H. J. V. der Stege. The destruction of enzymes and bacteria during the spray-drying of milk and whey. 2. The effect of the drying conditions. *Netherlands Milk and Dairy Journal*, 36:211–229, 1982.

[11] A. L. H. Daemen, A. Kruk, and H. J. V. der Stege. The destruction of enzymes and bacteria during the spray-drying of milk and whey. 3. Analysis of the drying process according to the stages in which the destruction occurs. *Netherlands Milk and Dairy Journal*, 37:213–228, 1983.

[12] R. A. DePaz, D. A. Dale, C. C. Barnett, J. F. Carpenter, A. L. Gaertner, and T. W. Randolph. Effects of drying methods and additives on the structure, function, and storage stability of subtilisin: Role of protein conformation and molecular mobility. *Enzyme and Microbial Technology*, 31: 765–774, 2002.

[13] J. A. Duffie and W. R. Marshall. Factors influencing the propeties of spray-dried materials. *Chemical Engineering Progress*, 49(8):417–423, 1953.

[14] J. A. Duffie and W. R. Marshall. Factors influencing the propeties of spray-dried materials. 2. Drying studies. *Chemical Engineering Progress*, 49(9): 480–486, 1953.

[15] T. M. El-Sayed, D. A. Wallack, and C. J. King. Changes in particle morphology during drying of drops of carbohydrate solutions and food liquids - part 1: Effects of composition and drying conditions. *Industrial and Engineering Chemistry Research*, 29(10):2346–2354, 1990.

[16] T. Elperin and B. Krasovitov. Evaporation of liquid droplets containing small solid particles. *International Journal of Heat and Mass Transfer*, 38 (12):2259–2267, 1995.

[17] J. Elversson and A. Millqvist-Fureby. Aqueous two-phase systems as a formulation concept for spray-dried protein. *International Journal of Pharmaceutics*, 294:73–87, 2005.

[18] M. Eslamian and N. Ashgriz. Effect of atomization method on the morphology of spray-generated particles. *Transactions of the ASME*, 129:130–142, 2007.

[19] M. R. Etzel, S.-Y. Suen, S. L. Halverson, and S. Budijono. Enzyme inactivation in a droplet forming a bubble during drying. *Journal of Food Engineering*, 27:17–34, 1996.

[20] M. Farid. A new approach to modelling of single droplet drying. *Chemical Engineering Science*, 58:2985–2993, 2003.

[21] I. J. Ford. Models of crystallisation in evaporating droplets. *Materials Research Society Symposium Proceedings*, 398:637–642, 1996.

[22] W.-Y. Fu, S.-Y. Suen, and M. R. Etzel. Inactivation of lactococcus lectis ssp lactis c2 and alkaline phosphatase during spray drying. *Drying Technology*, 13(5-7):1463–1476, 1995.

[23] C. G. Greenwald and C. J. King. The effects of design and operating conditions on particle morphology for spray-dried foods. *Journal of Food Process Engineering*, 4:171–187, 1981.

[24] J. P. Hecht and C. J. King. Spray drying: Influence of developing drop morphology on drying rates and retention of volatile substances. 2. Modeling. *Industrial and Engineering Chemistry Research*, 39:1766–1774, 2000.

[25] J. P. Hecht and J. King. Spray drying: Influence of developing drop morphology on drying rates and retention of volatile substances. 1. Single-drop experiments. *Industrial and Engineering Chemistry Research*, 39(6):1756–1765, 2000.

[26] M. Jacob. Granulation equipment. In A. D. Salman, M. J. Hounslow, and J. P. K. Seville, editors, *Granulation - Handbook of Powder Technology (Volume 11)*. Elsevier, Amsterdam, The Netherlands, 2007.

[27] G. V. Jayanthi, S. C. Zhang, and L. Messing. Modeling of solid particle formation during solution aerosol thermolysis. *Aerosol Science Technology*, 19:478–490, 1993.

[28] P. S. Kuts, C. Strumillo, and I. Zbicinski. Evaporation kinetics of single droplets containing dissolved biomass. *Drying Technology*, 14:2041–2060, 1996.

[29] K. Landström, J. Alsins, and B. Bergenståhl. Competitive protein adsorption between bovine serum albumin and β-lactoglobulin during spray-drying. *Food Hydrocolloids*, 14:75–82, 2000.

[30] H. Liang, K. Shinohara, H. Minoshima, and K. Matsushima. Analysis of constant rate period of spray drying of slurry. *Chemical Engineering Science*, 56:2205–2213, 2001.

[31] L. C. Lievense, M. A. M. Verbeek, G. Meerdink, and K. V. Riet. Inactivation of lactobacillus plantarum during drying. i. measurement and modelling of the drying process. *Bioseparation*, 1(2):149–159, 1990.

[32] L. C. Lievense, M. A. M. Verbeek, G. Meerdink, and K. V. Riet. Inactivation of lactobacillus plantarum during drying. II. measurement and modelling of the thermal inactivation. *Bioseparation*, 1(2):161–170, 1990.

[33] L. C. Lievense, M. A. M. Verbeek, T. Taekema, G. Meerdink, and K. V. Riet. Modelling the inactivation of lactobacillus plantarum during a drying process. *Chemical Engineering Science*, 47(1):87–97, 1992.

[34] J. v. d. Lijn. *Simulation of heat and mass transfer in spray drying*. PhD thesis, Landbouwhogeschool te Wageningen, The Netherlands, 1976.

[35] J.-C. Lin and J. W. Gentry. Spray drying drop morphology: Experimental study. *Aerosol Science and Technology*, 37:15–32, 2003.

[36] J. K. Liou. *An Approximate Method for Nonlinear Diffusion Applied to Enzyme Inactivation During Drying*. PhD thesis, Agricultural University of Wageningen, The Netherlands, 1982.

[37] J. K. Liou and S. Bruin. An approximate method for the nonlinear diffusion problem with a power relation between diffusion coefficient and concentration - I. Computation of desorption times. *International Journal of Heat and Mass Transfer*, 25(8):1209–1220, 1982.

[38] J. K. Liou and S. Bruin. An approximate method for the nonlinear diffusion problem with a power relation between diffusion coefficient and concentration - II. Computation of concentration profiles. *International Journal of Heat and Mass Transfer*, 25(8):1221–1229, 1982.

[39] S. J. Lukasiewicz. Spray-drying ceramic powders. *Journal of the American Ceramic Society*, 72(4):617–624, 1989.

[40] K. C. A. M. Luyben, J. K. Liou, and S. Bruin. Enzyme degradation during drying. *Biotechnology and Bioengineering*, 24:533–552, 1982.

[41] Y.-F. Maa, P.-A. Nguyen, J. D. Andya, N. Dasovich, , T. D. Sweeney, S. J. Shire, and C. C. Hsu. Effect of spray drying and subsequent processing conditions on residual moisture content and physical/biochemical stability of portein inhalation powders. *Pharmaceutical Research*, 15(5):768–775, 1998.

[42] K. Masters. *Spray Drying Handbook*. Longman Scientific and Technical, 5th edition, 1991.

[43] K. Masters. *Spray Drying in Practice*. Gershof Grafisk ApS, 2002.

[44] G. Meerdink. *Drying of Liquid Food Droplets - Enzyme Inactivation and Multicomponent Diffusion*. PhD thesis, Landbouwuniversiteit te Wageningen, The Netherlands, 1993.

[45] A. Millqvist-Fureby, M. Malmsten, and B. Bergenståhl. Spray drying of trypsin - surface characterisation and activity preservation. *International Journal of Pharmaceutics*, 188:243–253, 1999.

[46] H. Minoshima, K. Matsushima, H. Liang, and K. Shinohara. Basic model of spray drying granulation. *Journal of Chemical Engineering of Japan*, 34 (4):472–478, 2001.

[47] M. Mumenthaler, C. C. Hsu, and R. Pearlman. Feasibility study on spray-drying protein pharmaceuticals: Recombinant human growth hormone and tissue-type plasminogen activator. *Pharmaceutical Research*, 11(1):12–20, 1994.

[48] S. Nesic and J. Vodnik. Kinetics of droplet evaporation. *Chemical Engeering Science*, 46:527–537, 1991.

[49] T. Palmer. *Understanding Enzymes*. Ellis Horwood, 3rd edition, 1991.

[50] R. Sadykov, D. G. Pobedimsky, and F. R. Bakhtiyarov. Drying of bioactive products: Inactivation kinetics. *Drying Technology*, 15(10):2401–2420, 1997.

[51] K. Samborska and D. Witrowa-Rajchert. Enzyme spray drying. The influence of water content on α-amylase activity. *Inzynieria Chemiczna I Procesowa*, 27:559–565, 2006.

[52] K. Samborska, D. Witrowa-Rajchert, and A. Goncalves. Spray-drying of α-amylase - the effect of process variables on enzyme inactivation. *Drying Technology*, 23:941–953, 2005.

[53] Y. Sano and R. B. Keey. The drying of a spherical particle containing colloidal material into a hollow sphere. *Chemical Engineering Science*, 37 (6):881–889, 1982.

[54] T. Schröder and P. Walzel. Design of laminar operating rotary atomizers under consideration of the detachment geometry. *Chemical Engineering Technology*, 21(4):349–354, 1998.

[55] A. S. Selivanov. Stabilization of cellulases using spray drying. *Engineering in Life Sciences*, 5(1):78–80, 2005.

[56] F. V. Shaw. Spray drying: A traditional process for advanced applications. *Ceramic Bulletin*, 69(9):1484–1489, 1990.

[57] N. A. Turner and E. N. Vulfson. At what temperature can enzymes maintain their catalytic activity? *Enzyme and Microbial Technolgy*, 27:108–113, 2000.

[58] W. J. Walker Jr. and J. S. Reed. Influence of slurry parameters on the characteristics of spray-dried granules. *Journal of the American Ceramic Society*, 82(7):1711–1719, 1999.

[59] D. A. Wallack, T. M. El-Sayed, and C. J. King. Changes in particle morphology during drying of drops of carbohydrate solutions and food liquids - part 2: Effects on drying rate. *Industrial and Engineering Chemistry Research*, 29(10):2354–2357, 1990.

[60] D. E. Walton. The morphology of spray-dried particles - a qualitative view. *Drying Technology*, 18(9):1943–1986, 2000.

[61] D. E. Walton and C. J. Mumford. Spray dried products - characterization of particle morphology. *Transactions of the Institute of Chemical Engineers*, 77:21–38, 1999.

[62] D. E. Walton and C. J. Mumford. The morphology of spray-dried particles: The effect of process variables upon the morphology of spray-dried particles. *Transactions of the Institute of Chemical Engineers*, 77:442–460, 1999.

[63] P. Walzel, C. R. Funder, S. B. Flyger, and P. Bach. Process and a device for atomizing liquids. United States Patent US006098895A, 2000.

[64] W. Wang. Instability, stabilization, and formulation of liquid protein pharmaceuticals. *International Journal of Pharmaceutics*, 185:129–188, 1999.

[65] W. Wang. Lyophilization and development of solid protein pharmaceuticals. *International Journal of Pharmaceutics*, 203:1–60, 2000.

[66] A. E. Wijlhuizen, P. J. A. M. Kerkhof, and S. Bruin. Theoretical study of the inactivation of phosphatase during spray drying of skim-milk. *Chemical Engineering Science*, 34:651–660, 1979.

[67] S. Yamamoto and Y. Sano. Drying of carbohydrate and protein solutions. *Drying Technology*, 13(1):29–41, 1995.

[68] S. Yamamoto, M. Agawa, H. Nakano, and Y. Sano. Enzyme inactivation during drying of a single droplet. In R. Toei and A. S. Mujumdar, editors, *Proceedings of the Fourth International Drying Symposium, Kyoto, Japan*, pages 328–335, July 1984.

Chapter 3

Model Based Analysis of the Drying of a Single Solution Droplet in an Ultrasonic Levitator

In this chapter, the course of drying for a single droplet is investigated based on theoretical considerations. The focus is on the drying kinetics and development in droplet temperature during drying. Further, it is analyzed which transport phenomena have greatest influence on the drying process.

The present chapter is published as a peer-reviewed article in the journal *Chemical Engineering Science*, volume 61, pages 2701-2709 in 2006. The article is authored by Jakob Sloth (Technical University of Denmark), Søren Kiil (Technical University of Denmark), Anker D. Jensen (Technical University of Denmark), Sune K. Andersen (GEA – Niro A/S), Kåre Jørgensen (Technical University of Denmark), Heiko Schiffter (University of Erlangen-Nürnberg) and Geoffrey Lee (University of Erlangen-Nürnberg). The following is an exact reproduction of the article but the formatting is adapted to that of this thesis. The chapter is referred to as *Paper I* throughout the other chapters.

Abstract

A model for the drying of a single solution droplet into a solid, dense particle is presented and simulations are made to achieve a more fundamental understanding of the single droplet drying process relevant in connection with spray drying processes. Model predictions of drying behaviour are compared to data for the drying of aqueous solutions of maltodextrin DE 15 and trehalose from experiments conducted using an ultrasonic levitator. Model predictions are in good agreement with the experimental data, indicating that the model describes

the most important physical phenomena of the process.

3.1 Introduction

Spray drying is widely used in industry for conversion of a slurry or solution into a dry powder product. Applications of the process include production of different compounds such as inorganic salts, foodstuffs, enzymes and pharmaceuticals. In spray drying the liquid feed is atomized to droplets and contacted with a hot gas which causes the solvent of the droplets to evaporate, leaving dried particles. The process is very flexible and allows good control over various powders properties such as a well-defined particle size, particle morphology and residual solvent content.

3.1.1 Mechanisms of Drying

Mechanisms of droplet drying are complex, typically involving a period where the rate of evaporation is almost constant, followed by a time period where the rate of evaporation falls. During the constant rate period the solvent is readily available at the droplet surface but as the size of the droplet decreases, due to evaporation, the concentration of solute reaches saturation (i.e. precipitation occurs). A solid phase with a significant resistance to evaporation forms around the wet core of the droplet and throughout the remaining part of the drying process the rate of evaporation falls. During the constant rate period the temperature of the droplet is close to the wet bulb temperature of the solvent but it increases slightly because of a build-up in solute concentration [14]. In the falling rate period the temperature approaches the dry bulb temperature.

3.1.2 Previous Models

Due to the complexity of the droplet drying process the drying kinetics remain difficult to predict even though a large number of experimental investigations and mathematical modelling studies have been devoted to map the phenomena involved. The most frequently used approach to modelling is to set up a model consisting of two or more submodels, each valid for a specific period in the drying process, e.g. initial heating, constant rate period and falling rate period. Models of this kind were developed by Nesic and Vodnik [14] and more recently by Farid [7]. A different approach is to regard the drying process as continuous which was done by Wijlhuizen et al. [24] and Sano and Keey [20] who developed models for drying of droplets which may form hollow or solid particles.

In the literature, some disagreement exists on whether the droplet internal tem-

perature profile needs to be calculated. Sano and Keey [20], Nesic and Vodnik [14], Wijlhuizen et al. [24] all assume a uniform droplet temperature while Cheong et al. [4] assumes a linear profile between the droplet surface and centre. Farid [7] argues, based on a calculation of the Biot number, that determination of the internal temperature profile is necessary. The authors mentioned above have investigated different systems and the necessity of calculating the temperature profile most likely depends on the nature of the droplet and the drying conditions as indicated by calculating the Biot number ($= {}^{(h\, r_d)}/_{k}$). Therefore, a model capable of predicting the drying kinetics for many different droplet compositions and sizes over a broad range of drying conditions should calculate the temperature profile. In this context it is also noted that in the literature there is agreement that the droplet surface temperature during the constant rate period is close to the wet bulb temperature. In fact, some authors [10, 7] use the wet bulb temperature as a model input parameter to describe the droplet temperature during the constant rate period. It is therefore clear that a model which does not use the wet bulb temperature as an input parameter must be able to predict this if it describes the physical phenomena involved in the drying process well.

Mathematical models are often compared to experimental data for validation purposes. The drying kinetics experiments may be divided into two categories, free fall and single droplet. Previously, the latter was conducted using a filament from which a droplet was suspended, enabling observations of the course of drying. However, the filament affected the drying which is not the case for the more recently developed ultrasonic levitation technique [1].

3.1.3 Objective

In this work a model for drying of a single solution droplet is given while drying experiments for aqueous solutions of maltodextrin and trehalose in an ultrasonic levitator provide the experimental basis for model validation. The purpose of this is to investigate the physical phenomena involved in single droplet drying and thereby contribute to the general understanding of the drying process.

Like models published in the literature by Wijlhuizen et al. [24] and Sano and Keey [20] the model developed here is continuous but calculations of the droplet temperature profile are included, enabling predictions of drying kinetics over a broad range of formulations and process conditions. Also, the droplet temperature during the constant rate period (which is close to the wet bulb temperature) is calculated by the model rather than being an input parameter. Further, this model is based on fundamental physical phenomena and all model parameters are related to these phenomena. The model is valid for drying of solutions which form solid, dense particles as shown in figure 3.1.

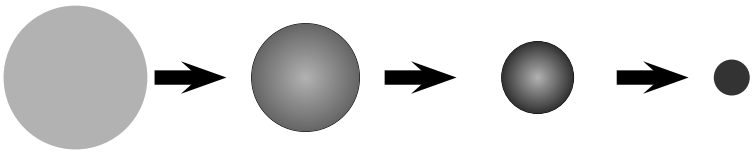

Figure 3.1: Illustration of the course of drying for which the model is valid. Darker color indicates higher solute concentration.

3.2 Experimental

The experimental setup used (figure 3.2) consists of an ultrasonic levitator similar to that described by Toei and Furuta [22], Groenewold et al. [8], Yarin et al. [25] and others. The levitator operates at a frequency of 58 kHz and is enclosed by an acrylic glass housing which allows experiments to be performed under constant drying conditions. Temperature and relative humidity may be set in ranges between 25 °C – 80 °C and 0 % – 80 %, respectively. To avoid changes, these two parameters are continuously checked using a hygrometer and a thermometer placed inside the housing. The setup includes a camera equipped with a macrolens for recordings of the droplet drying process which can be subject to subsequent image analysis.

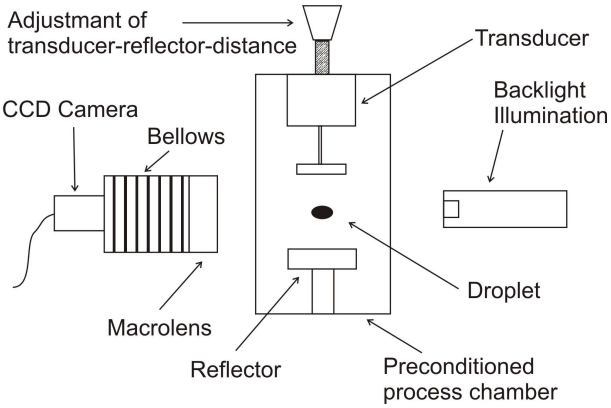

Figure 3.2: Experimental setup for study of single droplet drying.

It is noted that the droplets in the levitator are slightly elliptical due to the pressure from the ultrasonic waves. Further, the ultrasonic field induces acoustic streaming (figure 3.3) around the drying droplet which significantly increases heat and mass transfer to the bulk phase. This phenomenon is described in detail by Yarin et al. [25] and is addressed several times in the present work.

Experiments were conducted using pure water droplets and aqueous solutions of maltodextrin DE 15 (i.e. with 15 dextrose equivalents in the chain) and

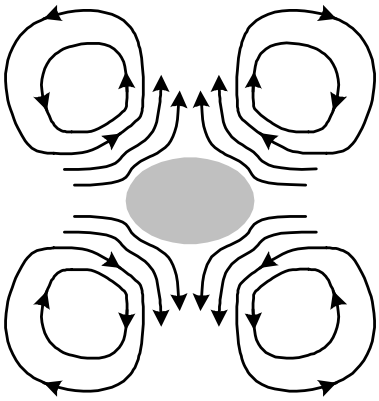

Figure 3.3: Acoustic streaming around the drying droplet induced by the ultrasonic field [After 25].

trehalose. Maltodextrin is often added when spray drying sugar containing compounds such as fruit juices to reduce stickiness [2]. Trehalose stabilizes biological material during dehydration and is therefore used as a carrier when spray drying pharmaceutics, cells and proteins [12].

3.3 Mathematical Model

This section describes a model capable of predicting the drying kinetics for droplets in the ultrasonic levitator. The model is valid for droplets that form a particular morphology observed during experiments and takes into account heat and mass transfer to the surface and inside the droplet. The model is based on the following assumptions

1. Droplets form solid, dense particles and drying progresses as shown in figure 3.1.

2. Mass loss caused by evaporation gives rise to a change in droplet radius.

3. Droplets are spherical.

4. Internal circulation in the droplets is negligible.

5. The diffusion rate inside the droplet may be calculated as a continuous Fick's law solvent concentration dependent diffusion coefficient.

6. Maltodextrin and trehalose solutions are ideal.

It seems reasonable to make assumptions (1)-(3) if the particles formed are spherical, solid and dense as the course of drying then is likely to be that shown in figure 3.1. Experimental investigations have shown that trehalose particles have the assumed morphology (figure 3.4) while maltodextrin particles are less spherical when spray dried under conditions similar to those in the levitator.

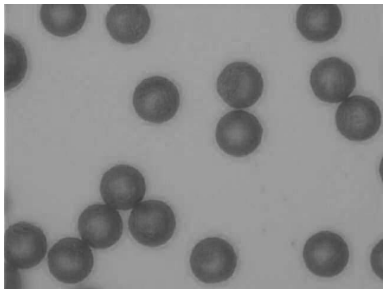

Figure 3.4: Spray dried trehalose particles of size approximately 50 μm.

The validity of assumption (4) has been checked by calculating the Peclet number using the method suggested by Mugeninstein et al. [13]. The Peclet number for drying trehalose droplets in the levitator is approximately 62 and internal circulation may be neglected when this number is lower than 100 [13].

Assumption (5) states that the rate of solvent diffusion is described by a concentration dependent diffusion coefficient in a Fick's law formulation. Thus, we regard the solvent (water) solute system as an ideal mixture independent of the mixture composition. This is valid for a number of compounds (e.g. sugars and other polymers) but might not be valid for coumpounds which crystallize or if the drying occurs in a porous media. Also, the diffusion coefficient in the model presented here is assumed to be valid throughout the course of drying, therefore it is highly dependent on the concentration of water and decreases dramatically at low water concentration. The diffusion coefficient function is presented in a later section.

3.3.1 Mass Transfer Inside Droplet

Fick's law of diffusion is used to describe the mass transfer rate inside the droplet because internal circulation is insignificant. Choosing the water mass fraction as the independent variable enables development of a model which is continuous as discussed above. The diffusion equation with a concentration dependent diffusion coefficient yields

$$\frac{\partial w_\mathrm{l}}{\partial t} = \frac{1}{r^2}\frac{\partial}{\partial r}\left(r^2 \mathcal{D}_\mathrm{l}\frac{\partial w_\mathrm{l}}{\partial r}\right) \tag{3.1}$$
$$0 \leq t < \infty \quad 0 \leq r \leq r_\mathrm{d}$$

with the initial condition

$$w_\mathrm{l}(0, r) = w_{\mathrm{l},0} \quad 0 \leq r \leq r_\mathrm{d} \tag{3.2}$$

The boundary conditions are given by

$$\frac{\partial w_\mathrm{l}(t, 0)}{\partial r} = 0 \tag{3.3}$$

$$\mathcal{D}_\mathrm{l}\frac{\partial w_\mathrm{l}(t, r_\mathrm{d})}{\partial r} = (1 - w_\mathrm{l})_{r_\mathrm{d}}\frac{\mathrm{d}r_\mathrm{d}}{\mathrm{d}t} \tag{3.4}$$

The outer boundary condition (3.4) may be obtained by considering that the solute content of the droplet is constant throughout the drying period

$$\frac{\mathrm{d}}{\mathrm{d}t}\int_0^{r_\mathrm{d}} r^2 w_\mathrm{a}\mathrm{d}r = 0 \tag{3.5}$$

or, applying the Leibnitz rule

$$\int_0^{r_\mathrm{d}} r^2\frac{\mathrm{d}w_\mathrm{a}}{\mathrm{d}t}\mathrm{d}r + r^2 w_\mathrm{a}\frac{\mathrm{d}r_\mathrm{d}}{\mathrm{d}t} = 0 \tag{3.6}$$

Using that $w_\mathrm{a} = 1 - w_\mathrm{l}$ and the diffusion equation (3.1)

$$\int_0^{r_\mathrm{d}} -\frac{\partial}{\partial r}\left(r^2 \mathcal{D}_\mathrm{l}\frac{\partial w_\mathrm{l}}{\partial r}\right)\mathrm{d}r + r^2 w_\mathrm{a}\frac{\mathrm{d}r_\mathrm{d}}{\mathrm{d}t} = 0 \tag{3.7}$$

integration of this expression and evaluation at the outer boundary yields (3.4).

3.3.2 Mass Transfer to Bulk Phase

The boundary layer between the droplet surface and the surroundings is a resistance to both mass and heat transfer. Recalling that the droplet radius decreases throughout the entire drying period, the mass transfer to the bulk phase may be calculated using the difference in vapor pressure between the droplet surface and the bulk phase

$$\frac{\mathrm{d}r_\mathrm{d}}{\mathrm{d}t} = -\frac{k_m M_\mathrm{l}}{R\rho_\mathrm{l} T_\mathrm{av}} \left(p_\mathrm{v,s} - p_\mathrm{v,\infty}\right) \qquad 0 \leq t < \infty \tag{3.8}$$

The temperature difference between the surface and the surroundings (T_av) is determined as the arithmetic mean which is possible because the boundary layer is much smaller than the droplet radius. The initial condition is

$$r_\mathrm{d} = r_\mathrm{d,0} \tag{3.9}$$

Raoult's law is applied in the model to link the solvent mass fraction at the surface to the vapor pressure. As shown in section 3.5 satisfactory results were obtained but more complex thermodynamic models such as the Flory-Huggins theory may be implemented if required for other solutions or drying conditions than those considered in this work.

3.3.3 Droplet Temperature

As elaborated in a later section several parameters in the above equations are temperature dependent, necessitating calculations of the droplet temperature. The temperature profile across the droplet follows from a heat balance

$$\frac{\partial T}{\partial t} = \frac{1}{C_p^* r^2} \frac{\partial}{\partial r} \left(r^2 k^* \frac{\partial T}{\partial r} \right) \qquad 0 \leq t < \infty \quad 0 \leq r \leq r_\mathrm{d} \tag{3.10}$$

where

$$C_p^* = w_\mathrm{l} \rho_\mathrm{l} C_{p,\mathrm{l}} + w_\mathrm{a} \rho_\mathrm{a} C_{p,\mathrm{a}} \tag{3.11}$$

Likewise k^* is the total heat conductivity of the solution calculated as discussed by Räderer [16].

The initial condition is

$$T(0, r) = T_0 \qquad 0 \leq r \leq r_\mathrm{d} \tag{3.12}$$

Also, the heat balance is subject to two boundary conditions

$$\frac{\partial T(t,0)}{\partial r} = 0 \tag{3.13}$$

$$\frac{\partial T(t,r_\mathrm{d})}{\partial r} = \frac{1}{k^*}\left(h(T_\infty - T_\mathrm{s}) + \lambda\rho_\mathrm{l}\frac{\mathrm{d}r_\mathrm{d}}{\mathrm{d}t}\right) \tag{3.14}$$

The latter boundary condition states that heat transfered from the surroundings to the droplet surface is used for either evaporation or droplet heating.

3.3.4 Strategy for Solving the Model

Because of droplet shrinkage the model poses a moving boundary problem. The outer boundary was immobilized by introduction of a simple coordinate transformation

$$x(t) = \frac{r}{r_\mathrm{d}(t)} \tag{3.15}$$

The model was solved by implementation in MATLAB using the Method of Lines [9]. However, numerical difficulties were encounted due to steep gradients in the diffusion coefficient at the droplet surface. To ensure convergence the domain was divided into two parts at $x = 0.90$ chosen to capture the steep gradient in the narrow zone. Half of the discretization points were placed in the zone toward the droplet surface. Convergence was assured by increasing the number of discretization points by 20% giving a change of less than 1% in the final droplet radius.

3.4 Model Parameters

The model described in the previous section contains a large number of physical and chemical parameters. Many of these parameters cannot be assumed constant through the drying process but depend on temperature or droplet moisture content if precise drying kinetic predictions are to be achieved. The majority of the model parameters have been found in various literature sources and table 3.1 lists the references of interest along with variable dependencies and short remarks. Correlations for key parameters (k_m, h and $\mathcal{D}_\mathrm{l}$) are given below.

Mass and heat transport coefficients were determined using correlations for Sherwood and Nusselts number [3].

$$k_\mathrm{m} = \frac{Sh\,\mathcal{D}_\mathrm{g}}{2r_\mathrm{d}} \tag{3.16}$$

Table 3.1: Model parameters for water, maltodextrin and trehalose – correlations for key parameters are given in the main text. Note, that C_p^* and k^* are assumed to be equal for maltodextrin and trehalose solutions. Molar mass for maltodextrin (M_m) is estimated – see reference for details.

Parameter	Dependence	Remarks	Reference
$p_{\mathrm{v,s}}^{\mathrm{sat}}$	T, w_l	Using the Antoine equation	[6]
C_p^*	T, w_l	General correlation for foodstuffs used	[5]
λ	T		[21]
k^*	T, w_l	General correlation for foodstuffs used	[5]
M_m		Estimated	[16]
M_t			[23]
ρ_l	T		[23]
ρ_m	T	General correlation for foodstuffs used	[5]
ρ_t			[23]

$$h = \frac{Nu\, k_\mathrm{g}}{2r_\mathrm{d}} \tag{3.17}$$

The temperature dependent vapor diffusion coefficient for equimolar counter diffusion ($\mathcal{D}_\mathrm{g}$) was taken from Pruppacher et al. [15] and modified to be valid for one way diffusion. Further, data for the drying gas (air) heat conductivity was found in Raznjevic [19] and a polynomial expression was fitted to the data to account for the temperature dependence.

When drying droplets in stagnant air Sherwoods and Nusselts numbers equal 2 but as shown in section 3.5 higher values for these numbers must be set to account for the acoustic streaming in the levitator. However, Sherwoods and Nusselts numbers will change throughout the course of drying because of a change in droplet radius, e.g. for Sherwoods number [18]

$$Sh = 2 + 0.6Sc^{1/3}Re^{1/2} \tag{3.18}$$

Using this correlation and assuming that all relevant parameters are constant during drying, the Sherwood number can be written as a function of the droplet radius with the initial Sherwood number Sh_0 and the initial droplet radius $r_{\mathrm{d},0}$ as parameters.

$$Sh = 2 + (Sh_0 - 2)\left(\frac{r_\mathrm{d}}{r_{\mathrm{d},0}}\right)^{1/2} \tag{3.19}$$

which is particularly important to include when using the model for a pure liquid droplet, where the dimensionless droplet radius decreases from 1 to 0. Equivalent calculations were done for the Nusselt number. Initial values for the Sherwoods and Nusselts numbers are discussed in the following section.

Based on experimental results from Rampp et al. [17] an exponential expression for the diffusivity of water in trehalose ($\mathcal{D}_{\mathrm{l,t}}$) at 298 K was found by a least square fit.

$$\mathcal{D}_{\mathrm{l,t}} = 3.27 \cdot 10^{-11} \exp\left(5.97 w_\mathrm{l}\right) \tag{3.20}$$

The expression for the diffusion coefficient varies greatly when the solvent mass fraction changes. That is, the expression gives a large diffusion rate when the water concentration is high and a small diffusion rate when the water concentration is low. This is in agreement with the discussion of the diffusion rate function in section 3.3.

Experimental data for maltodextrin DE 15 equivalent to those of trehalose are not available. Instead, an expression is found by fitting the model to a single set of experimental data from the ultrasonic levitator. This is done in section 3.5.

3.5 Results and Discussion

Before the model performance can be evaluated by comparison to experimental data, the issue of acoustic streaming is addressed again. As discussed earlier the ultrasonic waves in the levitator induce acoustic streaming around the droplet, giving rise to significant increase in heat and mass transfer to and from the bulk phase. To account for this increase proper values for Sherwood and Nusselt numbers must be set as stated earlier. Figures 3.5 and 3.6 both show simulations for $Sh_0 = Nu_0 = 2$ which is to be expected when drying pure liquid droplets in stagnant air and simulations where Sh_0 and Nu_0 have been set higher than 2 to account for the acoustic streaming. It is noted that the axes properties on the figures are chosen as given by Sano and Keey [20] to account for variation in initial radii between the individual experiments. The effect of the acoustic streaming seems to vary slightly in the individual experiments. On figure 3.5 the best result is obtained by setting $Sh_0 = Nu_0 = 4$ while $Sh_0 = Nu_0 = 4.5$ is used for figure 3.6. Other experiments than those shown on figures 3.5 and 3.6 have been conducted using pure water droplets but no correlation between process variables and the acoustic streaming was found. However, $Sh_0 = Nu_0 = 4$

appears to be a suitable value for most combinations of process variables and is thus used throughout the remaining parts of this work. According to Yarin et al. [25] this value is very reasonable for drying of water droplets in an ultrasonic levitator.

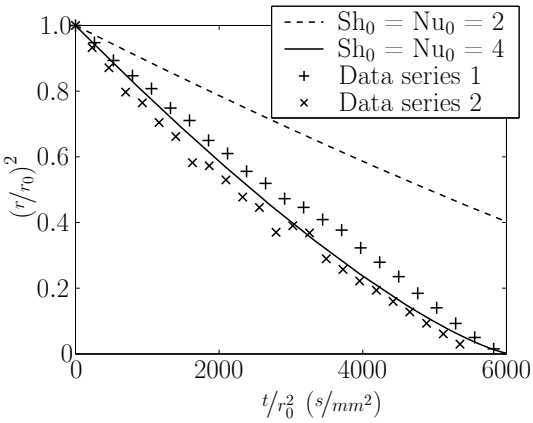

Figure 3.5: The effect of acoustic streaming on drying kinetics of a pure water droplet. Drying conditions: $r_{\mathrm{d},0} = 0.75$mm, $T_\infty = 60°$C and $RH = 80\%$. Symbols are experiments and lines represent simulations.

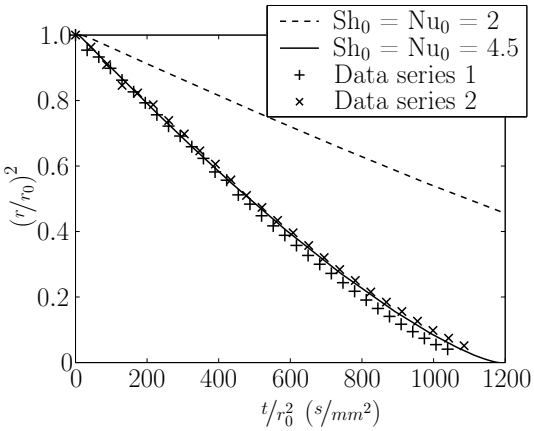

Figure 3.6: The effect of acoustic streaming on drying kinetics of a pure water droplet. Drying conditions: $r_{\mathrm{d},0} = 0.75$mm, $T_\infty = 50°$C and $RH = 20\%$. Symbols are experiments and the lines represent simulations.

3.5.1 Water–maltodextrin Diffusion Coefficient

Unlike the diffusion coefficient for water in trehalose no literature data for the diffusion coefficient of water in maltodextrin have been available. The absence

of an independently estimated diffusion coefficient of water in maltodextrin DE 15 ($\mathcal{D}_{\mathrm{l,m}}$) calls for a fit of the model to experimental data from the ultrasonic levitator. The result of this is shown in figure 3.7 where the calculated surface temperature throughout the drying also is included. Initial conditions are $r_{\mathrm{d},0} = 0.75\,\mathrm{mm}$, $T_0 = 10\,°C$ and $w_{\mathrm{m},0} = 0.20$ while the bulk phase conditions are $T_\infty = 40°C$ and $RH = 0\%$. The diffusion coefficient giving the best fit is

$$\mathcal{D}_{\mathrm{l,m}} = 1.78 \cdot 10^{-13} \exp\left(13.12 w_{\mathrm{l}}\right) \tag{3.21}$$

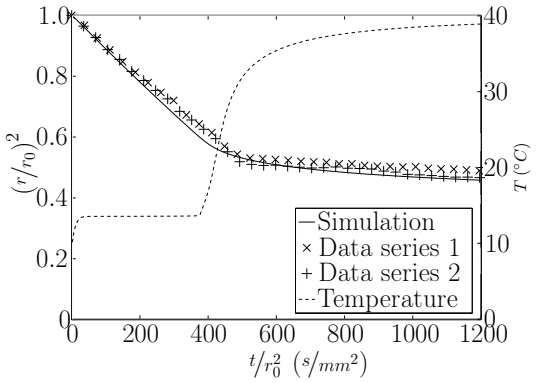

Figure 3.7: Model simulation for determination of water-maltodextrin diffusion coefficient by comparison to two sets of experimental data. Drying conditions are $r_{\mathrm{d},0} = 0.75\,\mathrm{mm}$, $T_0 = 10°C$, $w_{\mathrm{m},0} = 0.20$, $T_\infty = 40°C$ and $RH = 0\%$. The final calculated droplet radius is $r_{\mathrm{d,f}} = 0.51\,\mathrm{mm}$. Droplet surface temperature is also shown whereas the droplet center temperature is not shown because it varies only 0.39 $°C$ from the surface temperature.

Figure 3.7 displays the developments in radius and temperature during drying. Although the model is continuous it predicts what appears to be two rather distinct periods of drying – a constant rate period and a falling rate period. As discussed in section 3.3 the function for the diffusion rate gives fast water transport when the water concentration is high and vice versa. Consequently, mass transport is fast in the beginning of the drying process but it decreases significantly as the water concentration falls. The two periods of drying are simulated because the function for the diffusion rate is chosen to be exponential. This results in a quite sudden decrease in mass transport and thereby evaporation rate. A quantitative investigation of the model's ability to predict drying kinetics and temperature is given below.

3.5.2 Temperature

Simulated average temperature during the constant rate period for different drying conditions and wet bulb temperatures calculated as suggested by Mc-

Cabe et al. [11] have been compared. It was concluded that the model predicts the temperature in the constant rate period accurately.

Investigations of the radial droplet temperature profiles shows that these are only slightly curved (the maximum temperature difference between the center and the surface is $0.39\,°C$) even though the Biot number throughout the drying period is about 0.13 which is higher that 0.1 where internal heat transfer becomes significant. However, the value of 0.1 does not distinctly define the transition between insignificant and significant internal heat transfer but it is expected that a droplet temperature profile must be calculated if the Biot number increases slightly. The Biot number could increase if the initial droplet size is chosen to be larger or if the gas phase heat transfer coefficient increases (e.g. by an increase in the relative velocity between the droplet and the gas phase). This shows that a model which is valid over a broad range of drying conditions must include calculations of a droplet temperature profile.

3.5.3 Drying Kinetics

Figures 3.8 and 3.9 show simulations of maltodextrin droplet drying kinetics for two different bulk temperatures – all other conditions were kept identical at $r_{\mathrm{d},0} = 0.75\,\mathrm{mm}$, $T_0 = 20\,°C$, $w_{\mathrm{m},0} = 0.20$ and $RH = 0\,\%$. Further, two different initial concentrations of maltodextrin were tested (figures 3.10 and 3.11) while the bulk temperature remained at $T_\infty = 40°C$ along with the parameters stated above.

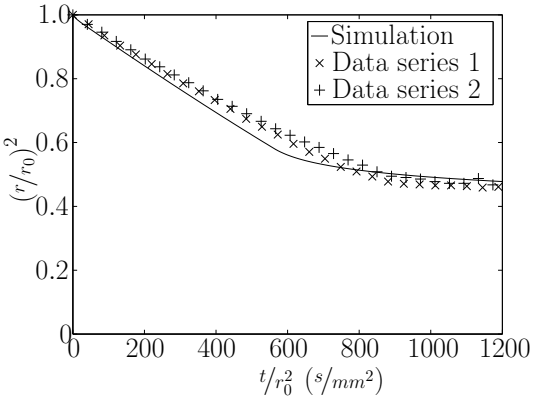

Figure 3.8: Drying of maltodextrin solution droplets: $r_{\mathrm{d},0} = 0.75\,\mathrm{mm}$, $T_0 = 20°C$, $w_{\mathrm{m},0} = 0.20$, $T_\infty = 27°C$ and $RH = 0\%$. The final calculated droplet radius is $r_{\mathrm{d,f}} = 0.52\,\mathrm{mm}$.

Figures 3.8 to 3.11 show that the model describes the drying kinetics accurately. The fact that the diffusion coefficient was fitted to experimental data from the

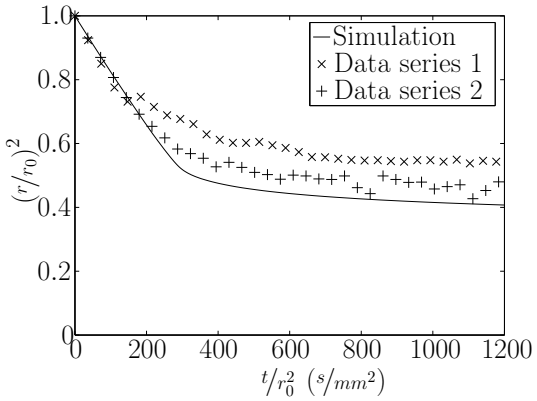

Figure 3.9: Drying of maltodextrin solution droplets: $r_{\mathrm{d},0} = 0.75\,\mathrm{mm}$, $T_0 = 20°C$, $w_{\mathrm{m},0} = 0.20$, $T_\infty = 60°C$ and $RH = 0\%$. The final calculated droplet radius is $r_{\mathrm{d,f}} = 0.48\,\mathrm{mm}$.

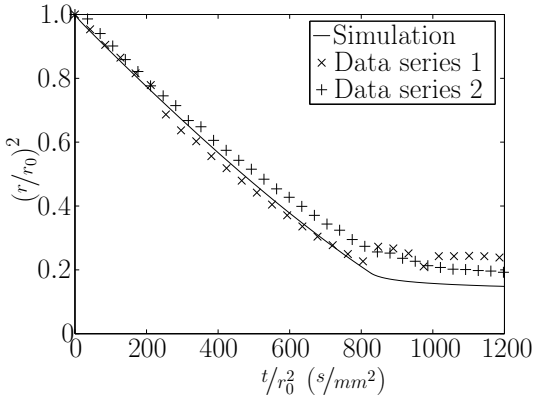

Figure 3.10: Drying of maltodextrin solution droplets: $r_{\mathrm{d},0} = 0.75\,\mathrm{mm}$, $T_0 = 20°C$, $w_{\mathrm{m},0} = 0.05$, $T_\infty = 40°C$ and $RH = 0\%$. The final calculated droplet radius is $r_{\mathrm{d,f}} = 0.29\,\mathrm{mm}$.

ultrasonic levitator might account for the very good agreement between simulations and experiments. However, the model responds quantitatively correct to changes in drying conditions.

Equivalent to the simulations above, two simulations for drying of trehalose droplets with different initial concentrations are presented in figures 3.12 and 3.13. The figures also include simulations of the development in total water mass fraction of the drying droplet. An important feature of the model is the ability to calculate this, providing information about the drying kinetics. Initially, the evaporation is fast but the mass fraction of water changes only little because the water content is very high – on figure 3.12 evaporation of half the amount of the initial water content only changes the water mass fraction from 95 % to

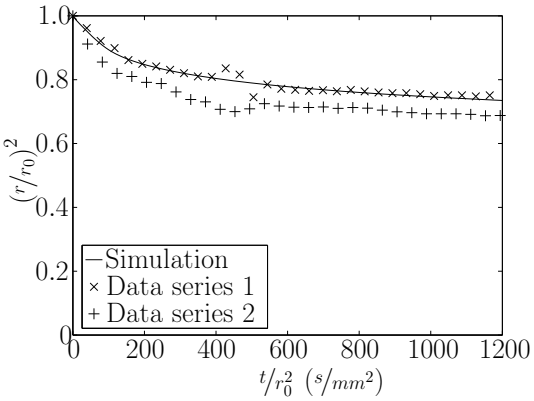

Figure 3.11: Drying of maltodextrin solution droplets: $r_{\mathrm{d},0} = 0.75\,\mathrm{mm}$, $T_0 = 20°C$, $w_{\mathrm{m},0} = 0.40$, $T_\infty = 40°C$ and $RH = 0\%$. The final calculated droplet radius is $r_{\mathrm{d,f}} = 0.64\,\mathrm{mm}$.

approximately 90 %. In the falling rate period the water mass fraction decreases slowly.

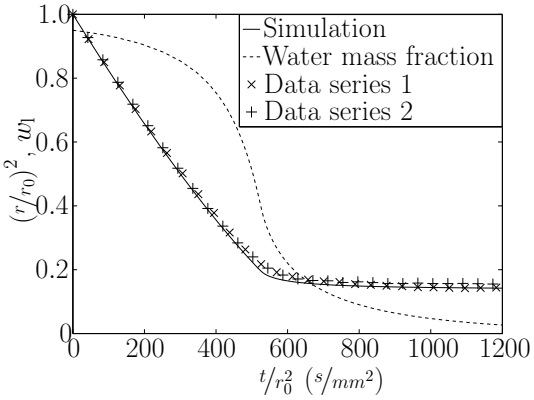

Figure 3.12: Drying of trehalose solution droplets: $r_{\mathrm{d},0} = 0.75\,\mathrm{mm}$, $T_0 = 20°C$, $w_{\mathrm{t},0} = 0.05$, $T_\infty = 60°C$ and $RH = 0\%$. The final calculated droplet radius is $r_{\mathrm{d,f}} = 0.28\,\mathrm{mm}$. Simulated development of the water mass fraction is also shown.

The final particle radius is only indirectly shown because of the axes properties chosen. However, a comparison between the simulated and measured final particle radii may be used to partly check the validity of assumption 6 on page 61 that trehalose and maltodextrin solutions are ideal. If this is true, volume addition is possible and the final particle radius may be obtained from the initial droplet radius, the initial mass fraction of solute, and the density of the solid material. The model basically calculates the final droplet radius in this

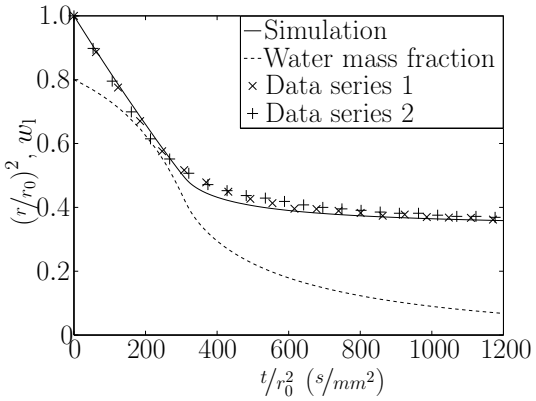

Figure 3.13: Drying of trehalose solution droplets: $r_{\mathrm{d},0} = 0.75\,\mathrm{mm}$, $T_0 = 20°C$, $w_{\mathrm{t},0} = 0.20$, $T_\infty = 60°C$ and $RH = 0\%$. The final calculated droplet radius is $r_{\mathrm{d,f}} = 0.45\,\mathrm{mm}$. Simulated development of the water mass fraction is also shown.

way. Comparisons between the simulated and measured final particle radii from figures 3.12 and 3.13 show that the difference is around 3 %. This is acceptable but implemtentation of an advanced thermodynamic model for the mixing of the relevant compounds might give better results.

All simulations for trehalose and maltodextrin droplets were carried out using the diffusion coefficients given by (3.20) and (3.21), respectively. It has been possible to achieve good agreement between simulations and experimental data without implementation of a temperature dependency into these coefficients e.g. by an Arrhenius type expression. The explanation for this is probably that the differences in bulk phase temperatures (between $27°C$ and $60°C$) used in this work are not large enough to reveal any temperature dependence of the diffusion coefficients.

Model simulations can be used to achieve better understanding of the droplet drying process. For instance, simulations with different heat and mass transfer coefficients indicate which transport phenomena govern the various periods of the droplet drying process. Figure 3.14 shows three simulations with $Nu = Sh = 3$, $Nu = Sh = 4$ and $Nu = Sh = 5$, respectively. The simulations are for droplets with an initial diameter, temperature and, maltodextrin concentration of $r_{\mathrm{d},0} = 0.75\,\mathrm{mm}$, $T_0 = 20°C$, $w_{\mathrm{m},0} = 0.20$ while the drying conditions are $T_\infty = 60°C$ and $RH = 0\%$. The figure shows that a difference in mass and heat transport around the droplet influences the drying rate during the constant rate period whereas the drying rates are approximately equal in the falling rate period. This indicates that external heat and mass transport are rate limiting during the constant rate period followed by internal mass transport in the falling rate period.

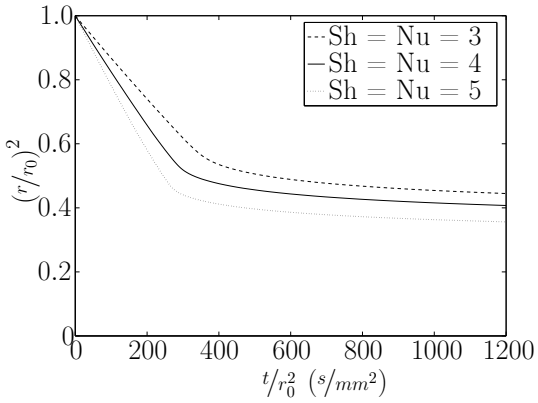

Figure 3.14: Simulations with different heat and mass transport coefficients. Drying of maltodextrin containing droplets were simulated using the following process parameters $r_{\mathrm{d},0} = 0.75\,\mathrm{mm}$, $T_0 = 20°C$, $w_{\mathrm{m},0} = 0.20$, $T_\infty = 60°C$ and $RH = 0\%$. The time until complete drying is not shown but in all three cases the final particle radius comes to 0.378 mm.

The model also provides useful information about the moisture content inside the droplet during the course of drying. Figure 3.15 shows concentration profiles for the trehalose containing droplet for which the drying kinetics are shown on figure 3.13. The profiles remain only slightly curved in the final part of the drying because of a relatively high diffusivity of water in trehalose. It is noted that the droplet radius decreases throughout the course of drying, however, this is not visible on figure 3.15 because the range of the dimensionless variable x does not vary.

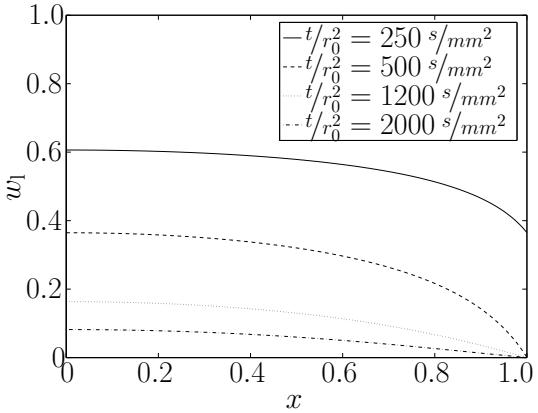

Figure 3.15: Simulated concentration profiles inside a trehalose containing droplet at different times during the course of drying. $r_{\mathrm{d},0} = 0.75\,\mathrm{mm}$, $T_0 = 20°C$, $w_{\mathrm{t},0} = 0.20$, $T_\infty = 60°C$ and $RH = 0\%$.

3.6 Conclusion

The model for drying kinetics given in this paper describes heat and mass transfer to the surface and inside a solution droplet. Further, it includes heat and mass transfer coefficients which are a function of the droplet radius. Experiments were conducted as single droplet drying experiments using an ultrasonic levitator which proved very useful for observations of the droplet drying process. Using data for pure water droplets it was possible to map the influence of acoustic streaming on the drying process for solutions containing this solvent. Subsequently, the model was validated using experimental data for the drying of aqueous solutions of maltodextrin and trehalose over a broad range of operating conditions. The model is rather general and is capable of predicting drying kinetics for other solutes and solvents than those treated in this work. Further work is to include modelling of droplets forming other morphologies than solid dense particles and drying of more complex formulations e.g. droplets containing several different solutes and different kinds of suspended particles.

Notation

C_p	Heat capacity $\mathrm{J\,kg^{-1}\,K^{-1}}$
C_p^*	See equation (3.11)
$\mathcal{D}$	Diffusion coefficient $\mathrm{m^2\,s^{-1}}$
k	Heat conductivity $\mathrm{J\,s^{-1}\,m^{-1}\,K^{-1}}$
k^*	Heat conductivity of a solution $\mathrm{J\,s^{-1}\,m^{-1}\,K^{-1}}$
h	Heat transfer coefficient $\mathrm{J\,s^{-1}\,m^{-2}\,K^{-1}}$
k_m	Mass transfer coefficient $\mathrm{m\,s^{-1}}$
M	Molar mass $\mathrm{kg\,mole^{-1}}$
Nu	Nusselts number $(= {}^{2\,h\,r_\mathrm{d}}/_{k})$
p	Pressure Pa
r	Radial coordinate m
R	Gas constant $\mathrm{J\,mole^{-1}\,K^{-1}}$
Re	Reynolds number $(= {}^{2\,r_\mathrm{d}\,v\,\rho}/_{\mu})$
RH	Relative humidity %
Sc	Schmidts number $(= {}^{\mu}/_{\rho\,\mathcal{D}})$
Sh	Sherwoods number $(= {}^{2\,r_\mathrm{d}\,k_m}/_{\mathcal{D}})$
T	Temperature K
t	Time s
v	Velocity $^{\mathrm{m}}/_{\mathrm{s}}$
w	Mass fraction
x	Dimensionless radial coordinate
λ	Heat of evaporation $\mathrm{J\,kg^{-1}}$

ρ Density $\mathrm{kg\,m^{-3}}$

Subscripts

∞	Bulk phase
0	Initial
a	Solute
av	Average
d	Droplet
f	final
g	Gas phase
l	Liquid
m	Maltodextrin
s	Surface
t	Trehalose
v	Vapor
wb	Wet bulb

3.7 References

[1] B. Adhikari, T. Howes, B. R. Bhandari, and V. Truong. Experimental studies and kinetics of single drop drying and their relevance in drying of sugar-rich foods: A review. *International Journal of Food Properties*, 3(3): 323–351, 2000.

[2] B. Adhikari, T. Howes, B. R. Bhandari, and V. Troung. Effect of addition of maltodextrin on drying kinetics and stickiness of sugar and acid-rich foods during convection drying. *Journal of Food Engineering*, 62:53–68, 2004.

[3] R. B. Bird, W. E. Stewart, and E. N. Lightfoot. *Transport Phenomena*. John Wiley & Sons Inc., 2 edition, 2002.

[4] H. W. Cheong, G. V. Jeffreys, and C. J. Mumford. A receding interface model for the drying of slurry droplets. *AIChE Journal*, 32(8):1334–1346, 1986.

[5] Y. Choi and M. R. Okos. Effects of temperature and composition on the thermal properties of foods. In M. L. Maguer and P. Jelen, editors, *Food Engineering and Process Applications - Vol 1: Transport Phenomena*, pages 93–101. Elsevier Science Publishers, 1986.

[6] J. A. Dean. *Lange's Handbook of Chemistry*. McGraw-Hill, 15th edition, 1999.

[7] M. Farid. A new approach to modelling of single droplet drying. *Chemical Engineering Science*, 58:2985–2993, 2003.

[8] C. Groenewold, C. Möser, H. Groenewold, and E. Tsotsas. Determination of single-particle drying kinetics in an acoustic levitator. *Chemical Engineering Journal*, 86:217–222, 2002.

[9] A. Iserles. *Numerical Analysis of Differential Equations*. Cambridge University Press, 4 edition, 2002.

[10] P. S. Kuts, C. Strumillo, and I. Zbicinski. Evaporation kinetics of single droplets containing dissolved biomass. *Drying Technology*, 14:2041–2060, 1996.

[11] W. L. McCabe, J. C. Smith, and P. Harriott. *Unit Operations of Chemical Engineering*. McGraw-Hill, 6th edition, 2001.

[12] D. P. Miller, J. J. de Pablo, and H. Corti. Thermophysical properties of trehalose and its concentrated aqueous solutions. *Pharmaceutical Research*, 14(5):578–590, 1997.

[13] A. Mugeninstein, M. Fichaman, and C. Gutfinger. Gas absorption in a moving drop containing suspended solids. *International Journal of Multiphase Flow*, 27:1079–1094, 2001.

[14] S. Nesic and J. Vodnik. Kinetics of droplet evaporation. *Chemical Engeering Science*, 46:527–537, 1991.

[15] H. R. Pruppacher, J. D. Klett, and D. E. Haman. *Microphysics of clouds and precipitation*. Kluwer Academic Publishers, 2 edition, 1996.

[16] M. Räderer. *Drying of viscous, shrinking products: Modelling and experimental validation*. PhD thesis, Technical University of Munich, Germany, 2001.

[17] M. Rampp, C. Buttersack, and H.-D. Lüdemann. C,T-dependence of the viscosity and the self-diffusion coefficients in some aqueous solutions. *Carbohydrate Research*, 328:561–572, 2000.

[18] W. E. Ranz and W. R. Marshall. Evaporation from drops - part 1. *Chemical Engineering Progress*, 48:141–146, 1952.

[19] K. Raznjevic. *Handbook of Thermodynamic Tables and Charts*. Hemisphere Publishing Corporation, 1st edition, 1976.

[20] Y. Sano and R. B. Keey. The drying of a spherical particle containing colloidal material into a hollow sphere. *Chemical Engineering Science*, 37 (6):881–889, 1982.

[21] J. M. Smith, H. C. van Ness, and M. M. Abbott. *Chemical Engineering Thermodynamics*. McGrawHill, 6 edition, 2001.

[22] R. Toei and T. Furuta. Drying of a droplet in a non-supported state. *AIChE Symposium Series*, 78:111–117, 1982.

[23] R. C. Weast. *CRC Handbook of Chemistry and Physics*. CRC Press, 62nd edition, 1981.

[24] A. E. Wijlhuizen, P. J. A. M. Kerkhof, and S. Bruin. Theoretical study of the inactivation of phosphatase during spray drying of skim-milk. *Chemical Engineering Science*, 34:651–660, 1979.

[25] A. L. Yarin, G. Brenn, O. Kastner, D. Rensink, and C. Tropea. Evaporation of acoustically levitated droplets. *Journal of Fluid Mechanics*, 339:151–204, 1999.

Chapter 4

Evaluation Method for the Drying Performance of Enzyme Containing Formulations

In this chapter, the focus is on enzyme inactivation during spray drying. Specifically, the ability of enzyme containing formulations to preserve the enzyme activity during drying is investigated.

The present chapter is is published as a peer-reviewed article in the journal *Biochemical Engineering Journal*, volume 40, issue 1, pages 121-129, 2008. The article is authored by Jakob Sloth (Technical University of Denmark), Poul Bach (Novozymes A/S), Anker D. Jensen (Technical University of Denmark) and Søren Kiil (Technical University of Denmark). The following is an exact reproduction of the article but the formatting is adapted to that of this thesis. The article is referred to as *Paper II* throughout the present work.

Abstract

A method is presented for fast and cheap evaluation of the performance of enzyme containing formulations in terms of preserving the highest enzyme activity during spray drying. The method is based on modeling the kinetics of the thermal inactivation reaction which occurs during the drying process. Relevant kinetic parameters are determined from differential scanning calorimeter experiments and the model is used to simulate the severity of the inactivation reaction for temperatures and moisture levels relevant for spray drying. After conducting experiments and subsequent simulations for a number of different formulations it may be deduced which formulation performs best. This is illustrated by a formulation design study where 4 different enzyme containing

formulations are evaluated. The method is validated by comparison to pilot scale spray dryer experiments.

4.1 Introduction

Spray drying is a very important unit operation used for numerous industrial applications such as waste treatment, production of inorganic salts, pharmaceuticals and food stuffs. In spray drying, a solution or suspension is fed to an atomizer and the droplets formed are mixed with a hot gas. This causes the solvent of the droplets to evaporate, leaving a dry powder product. Industrial enzymes are often subject to spray drying because product handling is easier and the enzyme storage stability is better in a powder product than in a liquid formulation.

Enzymes are widely used biocatalysts and these complex proteins are highly dependent on their structure to perform the catalytic act [21]. However, the enzymes may unfold and thereby lose the native structure during the drying process due to the high temperatures prevailing in the spray dryer. This thermal inactivation is of primary concern to enzyme producers as any activity loss evidently deteriorates the final product value.

Obviously, measures are taken to avoid the thermal inactivation during spray drying. This includes altering process parameters such as feed rate, initial droplet size and drying chamber temperature (see e.g. [23]). Also, the inactivation may be reduced by mixing the enzyme containing feed with different compounds (e.g. carbohydrates and surfactants [25, 18]) prior to drying, i.e. design activity preserving formulations.

In this work, a method for evaluating the performance of activity preserving formulations is presented, allowing fast formulation screening.

4.2 Previous Studies

The enzyme inactivation during spray drying occurs at a certain rate depending on the nature of the enzyme, formulation ingredients and process operating parameters. In the literature a number of studies are devoted to quantify the rate of the inactivation reaction and simulate the progress of the reaction during drying. In theory, such simulations allow for determination of the optimal operating conditions and the best formulation.

An approach used commonly in the literature to quantify the reaction rate is to assume that the inactivation occurs as an irreversible first order reaction

$$N \rightarrow D \tag{4.1}$$

where N and D are the native and the inactivated enzyme, respectively.

The reaction rate is described by the following (or a similar) expression

$$\frac{dX}{dt} = k(1 - X) \tag{4.2}$$

where X is the degree of conversion of the reaction given by (4.1). That is, $X = 0$ corresponds to all enzyme being in the native state while $X = 1$ when all enzyme is inactivated. Thus, X represents the fraction of enzyme which has been degraded and is therefore simply referred to as *activity loss* throughout the text.

The rate constant k is determined by an Arrhenius type expression

$$k = A \exp\left(\frac{-E_a}{RT}\right) \tag{4.3}$$

The preexponential factor A as well as the activation energy E_a may, according to the studies, depend on the water concentration of the medium surrounding the enzyme. Specific values or water concentration dependent functions for A and E_a are usually determined experimentally.

A study following the outline above is among others undertaken in the series of papers by Daemen and coworkers [2, 3, 4, 5] and by Liou [13], Meerdink [17] and Yamamoto et al. [30].

Except Yamamoto et al. [30] all of the authors mentioned use the same approach to measure the rate of inactivation as a function of sample moisture content and temperature. An enzyme powder sample moistened with a predetermined amount of water is filled into a small special designed air- and water-tight aluminum box and kept for a specific period of time at a constant temperature in an oven. Carrying out multiple experiments changing either time interval, temperature or moisture content and subsequently measure the residual enzyme activity yields data to which water concentration dependent parameters (A and E_a) may be fitted.

The experiments conducted by Yamamoto et al. [30] are quite similar but a sample incubated in a constant temperature bath is used.

Generally, the parameters determined by either of the experimental methods are not well-defined because the data obtained are limited. The main problem with the experiments is that they are difficult and time consuming to conduct [17].

Nevertheless, applying the parameters found the equations for the rate of inactivation, equations (4.2) and (4.3), may be used quantitatively in droplet drying simulations.

Simulations of this kind are conducted by calculating droplet moisture content and temperature during the course of drying using a drying kinetics model. The

results obtained are readily combined with equations (4.2) and (4.3) to estimate the residual enzyme activity subsequent to drying.

To evaluate the performance of the simulations the results are often compared to data obtained from various drying experiments. These include spray driers [3], single droplet suspended from a glass filament [13, 17, 30] or sampling of free falling droplets [17] – see references for detailed descriptions of experimental setups.

Qualitatively, simulations generally respond correctly to changes in e.g. spray dryer outlet temperature [3] or formulation [30].

Additional to the work discussed above, a number of authors perform quite similar experiments or simulations [15, 7, 8, 29]. It is, however, noted that most literature on this subject has been written in the period from the early 1980s to the middle 1990s. Later literature focuses on the challenges in the formulation design of pharmaceutical proteins. Although numerous publications exist in this area, they are of little relevance in terms of formulation screening because the methods used are quite time consuming as they focus on e.g. structural alterations of a particular protein due to drying or the specific effects of a formulation change. Readers with interests in that area are encouraged to consult the very elaborate review paper of Wang [28].

4.3 Objectives

The objective of this paper is to present a fast method for comparing the drying performances of different enzyme containing formulations in terms of maintaining the highest residual enzyme activity. The method may help reduce the number of expensive pilot and full scale spray drying experiments when designing new or improving existing formulations.

4.3.1 Method Outline

The basis of the method mentioned above is to find the kinetics of the inactivation reaction, as given by (4.1), for each formulation. This is used to calculate the enzyme activity loss in the formulation at temperatures and moisture contents relevant for spray drying. Finally, it may be deduced which formulation performs best by comparing the activity losses in all considered formulations.

The reaction kinetics are estimated from experiments using a differential scanning calorimeter (DSC). In DSC a sample of a formulation is heated using a constant temperature gradient (or another predetermined temperature profile) and the heat input required to maintain this gradient is continuously recorded. As the unfolding of the enzyme (i.e. the inactivation reaction) progresses a

small amount of heat is produced, resulting in a change in required heat input. Consequently, transient data of the full inactivation reaction is obtained.

When determining the reaction kinetics this is a great advantage over methods which only provide the progress of the reaction at a single point in time (see section 4.2). Other advantages of the DSC include that only very small samples (i.e. in the magnitude of milligrammes) are needed. Also, most DSC equipment may be combined with an auto sampler and is thus capable of testing a high number of samples automatically, greatly reducing the cost of experiments in terms of man-hours.

4.4 Experiments

All DSC experiments in this work are conducted using a purified concentrate of a model enzyme. The specific choice is kept secret for commercial reasons. However, the model enzyme is often subjected to spray drying and is temperature-sensitive.

It has been found by other researchers that the enzyme inactivation kinetics depend on the sample moisture concentration (see section 4.2). To account for this dependency, samples with different moisture contents must be prepared which is done using two different approaches – called *Method 1* and *Method 2*. The former is used to prepare samples with $w < 20\%$ by freeze drying the enzyme concentrate and placing the formed powder over water/glycerol mixtures in sealed containers. This ensures a well-defined air humidity and the samples are kept in the containers until equilibrium between the air humidity and the powder moisture content is attained (checked by weighing). Varying the water/glycerol ratio in each container entails different air humidities [11], thus producing samples of various moisture contents.

In Method 2 ($w > 20\%$) small amounts of concentrate is vacuum dried in a desiccator. Samples with different moisture content are obtained simply by varying the drying time.

To ensure that no enzyme activity is lost during sample preparation, a second set of samples has been subjected to an activity assay. It is concluded that neither Method 1 nor Method 2 cause significant inactivation.

4.4.1 DSC – Equipment and Analysis

The apparatus used for the DSC experiments is a Perkin Elmer Pyris 1 equipped with a Lauda RM 6 cooling system and an auto sampler.

The samples are prepared in 60 µL steel capsules which are sealed prior to the experiment, thus preventing any evaporation during heating. In a DSC run the

sample is cooled to 20°C and maintained at this temperature for about 4 minutes and, subsequently, the required heat input is measured as the sample is heated at a constant gradient. Three samples of identical moisture contents are analyzed using different temperature gradients, i.e. $10, 20, 30\ ^{\circ\mathrm{C}}/_{\mathrm{min}}$. Throughout the entire experiment a nitrogen flow of $20\ ^{\mathrm{mL}}/_{\mathrm{min}}$ is imposed inside the apparatus.

Also, a number of pilot scale spray dryer experiments are conducted in connection with the present work. These experiments are, however, not part of the method for evaluation of enzyme containing formulations presented but serve as validation of the method. Therefore, they are described separately in section 4.7.

4.5 Determination of Reaction Kinetics

All DSC measurements reveal distinct peaks from the inactivation reaction as illustrated in figure 4.1. (Note that temperature is used on the abscissa as this is customary practice in the literature – the temperature is, however, easily converted to time because a constant temperature gradient is used).

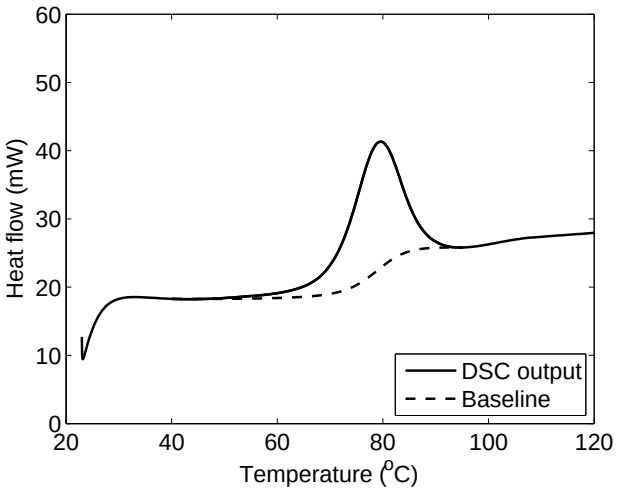

Figure 4.1: DSC output exemplified by a $20\ ^{\circ\mathrm{C}}/_{\mathrm{min}}$ heating of a sample with $w = 0.68$. The calculated baseline is included.

The enzyme activity loss – reaction (4.1) – may be calculated at any temperature as the accumulated area between the DSC output line and the baseline divided by the total area between the two lines.

The baseline connects the pre- and posttransitional output values (figure 4.1) and is by some authors (e.g. [27]) found by extrapolating two straight lines

while others (e.g. [6]) discuss the use of more advanced methods such a sigmoidal curve. However, Sanchez-Ruiz [24] believes that any reasonable function which smoothly connects the pre- and posttransitional values is an acceptable approximation to the true baseline. The method used in this work is explained by Hemminger and Sarge [10], according to whom a baseline point P may be approximated as

$$P = Q'X + Q''(1 - X) \tag{4.4}$$

where Q' and Q'' are pre- and posttransitional values. Since the activity loss appears in equation (4.4) the baseline is found by successive iteration.

4.5.1 Kinetics Modeling

Applying the above to all DSC measurement series yields data for the degree of activity loss as a function of temperature (and thereby time) to which a model for the inactivation reaction kinetics may be fitted.

The three main assumptions for the reaction kinetics model used in this work are

1. The inactivation reaction is of first order.
2. The inactivation reaction is irreversible.
3. The heat produced by a sample during a DSC scan is in fact from the inactivation reaction.

The validity of assumption (1) is discussed below while the validity of assumption (2) is shown experimentally. If the inactivation reaction is irreversible then reheating of a sample which already has been subject to temperature scanning should not show any activity loss, i.e. no peak on the DSC output. No peak is seen during the reheating scan of figure 4.2, thus assumption (2) holds true.

The heat produced by a sample during a DSC scan might be from e.g. a phase transition rather than the inactivation reaction, invalidating assumption (3).

Assumption (3) is checked by interrupting a DSC scan at a predetermined temperature which corresponds to a certain activity loss. The sample is quickly cooled and subsequently, the DSC capsule is opened and the sample is recovered. The actual activity loss of the sample is measured by an activity assay.

From a practical point view checking assumption (3) as described above is exceedingly difficult. First, the DSC capsules are not designed to be reopened after sealing, hence a special tool for this has been invented and constructed. Secondly, the very small sample (60 µL or less) must be transferred quantitatively from the capsule to a buffer prior to assaying. Any loss of sample during

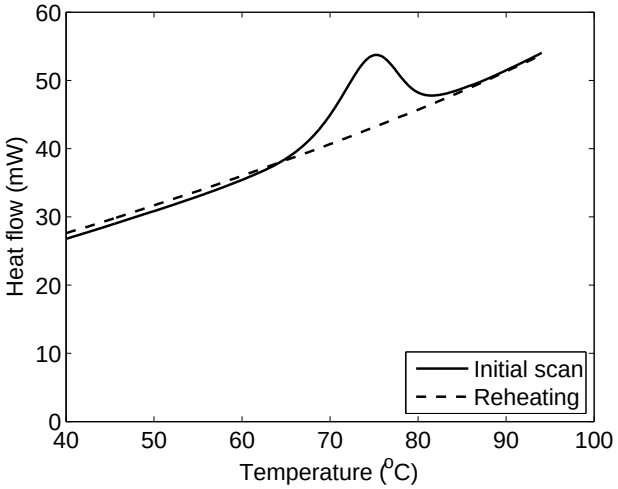

Figure 4.2: DSC output a for 10 $^{\circ C}/_{min}$ heating with subsequent reheating using the same scan rate.

this causes a lowering of the measured residual activity and consequently a too high measured activity loss.

In figure 4.3 all values are biased toward a too high measured activity loss. Note, that at theoretical activity losses (based on DSC measurements) of 0.75 and 1.00 the measured activities are below the assay activity range and the measured activity losses are consequently set to 1.00. Nevertheless, the figure displays continuous progress in the measured activity loss, rendering assumption (3) plausible.

Based on the assumptions above the reaction rate may be calculated as

$$\frac{dX}{dt} = k(1 - X) \tag{4.5}$$

This is identical to equation (4.3). The equation for the rate constant is chosen as

$$k = k^* \exp\left(\frac{-E_a}{R}\left[\frac{1}{T} - \frac{1}{T^*}\right]\right) \tag{4.6}$$

where the preexponential factor k^* may be water concentration dependent while T^* is a reference temperature in the magnitude of the measurement temperatures. In this work the reference temperature is set at 373 K.

Equations (4.5) and (4.6) may be fitted to the experimental data as described by Sanchez-Ruiz [24] and Kurganov et al. [12] by adjusting the values of the preexponential factor and the activation energy. Note that in this type of fitting the two parameters are usually strongly correlated. This correlation is, however, diminished by choosing equation (4.6) instead of equation (4.3) [22].

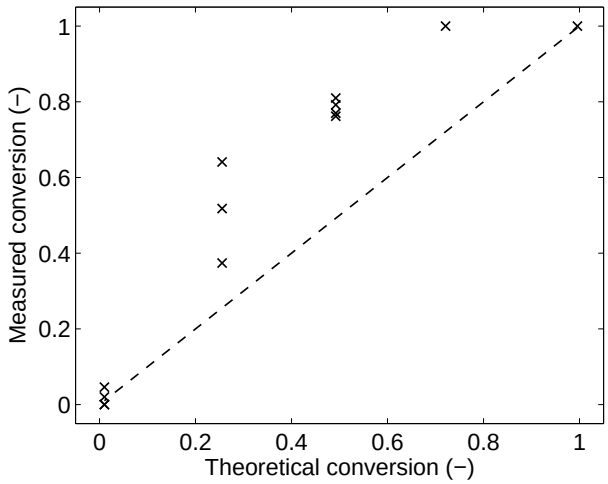

Figure 4.3: Measured and theoretical values of the enzyme activity loss during DSC experiments. The dashed line illustrates where the two values are equal.

The fitting is performed by least squares, calculating one set of the parameters, k^* and ${}^{E_a}/_R$, for each moisture content. That is, with the set of parameters found, the reaction kinetics model mimic all the three data series measured with different temperature gradients for the moisture content considered. The results for all moisture contents are given in table 4.1 along with 2σ confidence intervals for the fitting procedure.

4.5.2 Variation in Activation Energies

Table 4.1 reveals a variation in the activation energies between the individual moisture levels. The variation is within the interval ${}^{E_a}/_R \in [1.52 - 2.89] \cdot 10^4\mathrm{K}$ which is fairly narrow and it is therefore possible that the true activation energy is the same for all experiments.

Besides experimental uncertainties, a possible explanation for the variation is that the enzyme inactivation progresses slightly different than a first order reaction. As stated in assumption (1) the reaction must be of first order, otherwise the model does not fully capture the dynamics of the inactivation.

The variation in activation energies may also be explained by the so-called compensation effect which has been observed by a number of authors undertaking kinetic modeling from temperature scanning experiments (see e.g. [20, 1]). If the compensation effect occurs, the sets of preexponential factors and the activation energies obey the relation $\ln(k^*) = a \cdot {}^{\mathrm{E_a}}/_{\mathrm{R}} + b$ where a and b are constants. Garn [9] explains how the compensation effect arises from a deficiency in the

Table 4.1: Values for the preexponential factor and the activation energy at different moisture levels, including 2σ confidence intervals. *Sample prepared by Method 1. **Sample prepared by Method 2.

w	k^*, s^{-1}	E_a/R, K
0.0410*	$1.23{\cdot}10^{-3} \pm 4.05{\cdot}10^{-5}$	$1.77{\cdot}10^{4} \pm 2.62{\cdot}10^{2}$
0.0811*	$5.39{\cdot}10^{-3} \pm 4.81{\cdot}10^{-4}$	$2.12{\cdot}10^{4} \pm 1.25{\cdot}10^{2}$
0.1330*	$1.67{\cdot}10^{-2} \pm 6.28{\cdot}10^{-4}$	$2.02{\cdot}10^{4} \pm 1.11{\cdot}10^{3}$
0.1736*	$3.39{\cdot}10^{-2} \pm 1.91{\cdot}10^{-3}$	$2.04{\cdot}10^{4} \pm 1.65{\cdot}10^{3}$
0.1948*	$4.83{\cdot}10^{-2} \pm 3.52{\cdot}10^{-3}$	$2.12{\cdot}10^{4} \pm 1.28{\cdot}10^{3}$
0.2089**	$6.20{\cdot}10^{-2} \pm 6.34{\cdot}10^{-3}$	$1.85{\cdot}10^{4} \pm 1.20{\cdot}10^{3}$
0.3576**	$1.50{\cdot}10^{-1} \pm 3.33{\cdot}10^{-2}$	$1.52{\cdot}10^{4} \pm 1.41{\cdot}10^{3}$
0.4328**	$3.81{\cdot}10^{-1} \pm 1.02{\cdot}10^{-1}$	$1.94{\cdot}10^{4} \pm 1.59{\cdot}10^{3}$
0.5125**	$2.16 \pm 5.40{\cdot}10^{-1}$	$2.56{\cdot}10^{4} \pm 1.31{\cdot}10^{3}$
0.5473**	$3.02 \pm 5.43{\cdot}10^{-1}$	$2.65{\cdot}10^{4} \pm 9.14{\cdot}10^{2}$
0.5978**	$1.61 \pm 3.55{\cdot}10^{-1}$	$2.89{\cdot}10^{4} \pm 1.08{\cdot}10^{3}$
0.6278**	$1.62 \pm 3.27{\cdot}10^{-1}$	$2.28{\cdot}10^{4} \pm 9.77{\cdot}10^{2}$
0.6555**	$1.12 \pm 2.58{\cdot}10^{-1}$	$2.05{\cdot}10^{4} \pm 1.07{\cdot}10^{3}$
0.6825**	$1.74 \pm 3.60{\cdot}10^{-1}$	$2.24{\cdot}10^{4} \pm 9.68{\cdot}10^{2}$

conventional form of the Arrhenius equation when fitting kinetic data. However, this deficiency might persist though equation (4.6) is chosen over equation (4.3). In figure 4.4 the data seemingly display the compensation effect and, thus, the differences in the activation energies may only be apparent.

Based on the discussion above it seems reasonable to assume that there is one true activation energy which is valid for the model description of all data. Further, as shown below this assumption allows setting up a single equation for the reaction rate constant which is applicable at all moisture levels.

The true value of the activation energy is not known. In this case an appropriate value is found by calculating the arithmetic mean of all values found experimentally (table 4.1) which yields $E_a/R = 2.10 \cdot 10^4$ K.

Using this activation energy, the corresponding values for the preexponential factors are found by fitting the model to the experimental data. The approach is analogous to the above, only that just one parameter is adjusted. The specific values are given in table 4.2.

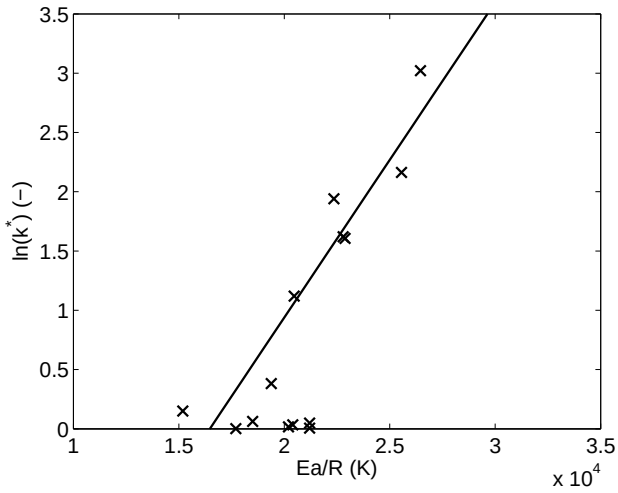

Figure 4.4: Investigation of the compensation effect. Symbols represent experimental data and a trend line is inserted.

Table 4.2: Values for the preexponential factor at different moisture levels found at a fixed value for the activation energy ($E_a/R = 2.10 \cdot 10^4$K). 2σ confidence intervals for the fitting are included. *Sample prepared by Method 1. **Sample prepared by Method 2.

w	k^*, s^{-1}
0.0410*	$8.42{\cdot}10^{-4} \pm 1.42{\cdot}10^{-5}$
0.0811*	$5.44{\cdot}10^{-3} \pm 2.15{\cdot}10^{-4}$
0.1330*	$1.67{\cdot}10^{-2} \pm 6.34{\cdot}10^{-4}$
0.1736*	$3.44{\cdot}10^{-2} \pm 1.58{\cdot}10^{-3}$
0.1948*	$4.85{\cdot}10^{-2} \pm 2.38{\cdot}10^{-3}$
0.2089**	$8.15{\cdot}10^{-2} \pm 3.10{\cdot}10^{-3}$
0.3576**	$3.69{\cdot}10^{-1} \pm 2.70{\cdot}10^{-2}$
0.4328**	$5.02{\cdot}10^{-1} \pm 2.98{\cdot}10^{-2}$
0.5125**	$9.62{\cdot}10^{-1} \pm 3.76{\cdot}10^{-2}$
0.5473**	$1.11 \pm 4.08{\cdot}10^{-2}$
0.5978**	$1.10 \pm 3.90{\cdot}10^{-2}$
0.6278**	$1.12 \pm 3.68{\cdot}10^{-2}$
0.6555**	$1.26 \pm 5.07{\cdot}10^{-2}$
0.6825**	$1.31 \pm 4.35{\cdot}10^{-2}$

4.5.3 Moisture Content Dependency

Table 4.2 indicates that the preexponential factor increases with the moisture content. To investigate the dependency between the two parameters the pre-

exponential factor is plotted versus the moisture content in figure 4.5, using logarithmic axes.

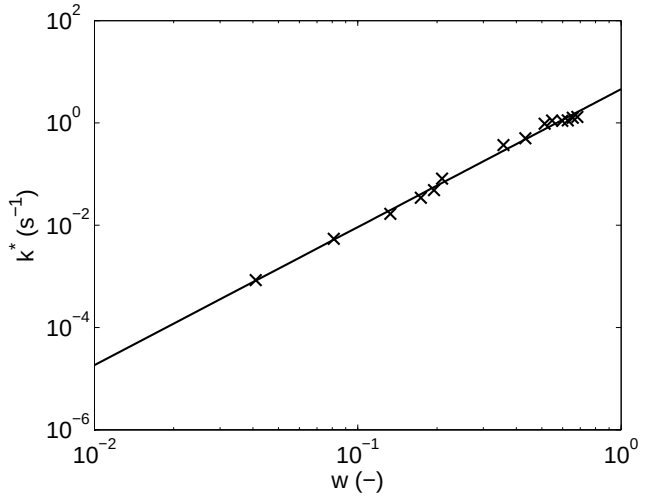

Figure 4.5: Investigation of the dependency between the preexponential factor and the moisture content. Symbols represent experimental data.

Figure 4.5 reveals a clear linear trend between the logarithms of the two parameters. This entails that eqaution (4.6) may be rewritten to include the moisture content

$$k = k_0 w^n \exp\left(\frac{-E_a}{R}\left[\frac{1}{T} - \frac{1}{T^*}\right]\right) \tag{4.7}$$

where k_0 is an preexponential factor which is independent of the moisture content while n is a contant.

The specific values of k_0 and n are readily calculated from the straight line in figure 4.5 and substituting numerical values into equation (4.7) results in

$$k = 4.58 w^{2.70} \exp\left(-2.10 \cdot 10^4 \left[\frac{1}{T\,[K]} - \frac{1}{373}\right]\right) [1/s] \tag{4.8}$$

Calculating the rate constant from this equation enables integration of equation (4.5) and the extent of enzyme activity loss during a given time interval at any temperature and moisture level may be evaluated.

Consequently, determining similar expressions for different enzyme containing formulations allow for calculation of activity loss at various conditions relevant for spray drying. Thus, the drying performance in terms of maintaining the highest residual level of enzyme activity may be compared between the formulations considered which is illustrated below.

Before this, the ability of the reaction kinetics model to describe the experimental data is addressed. Figure 4.6 shows simulated as well as experimental DSC data for $w = 0.60$ at three different temperature gradients.

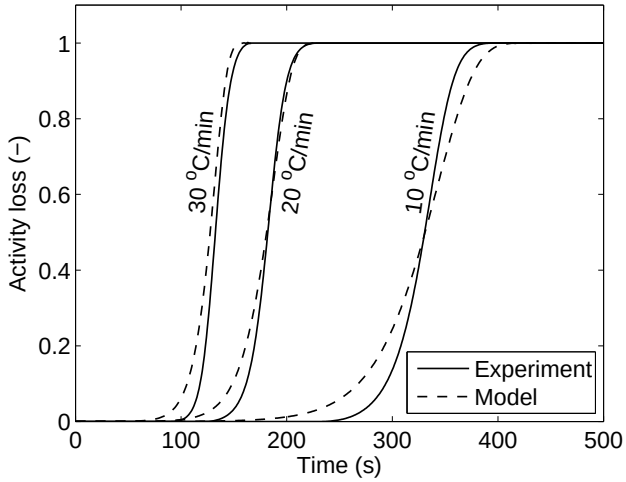

Figure 4.6: Model predictions and experimental data for the activity loss. The moisture content of all samples is $w = 0.60$.

The model predictions appear to have offsets when compared to the experimental data, especially at the lowest heating rate. The trends in the offsets are general for most of the model predictions at other moisture contents than the one shown. The disagreements between the simulations and experiments suggest that the model does not fully capture the dynamics of the inactivation reaction. As mentioned in section 4.5.2, a possible explanation for this is that the reaction is not exactly of first order which is one of the assumptions of the model, or that the inactivation takes place in multiple steps – each with its own activation energy.

Thus, implementing a more complex model might improve the capability of the model to predict the experimental data. However, a more complex model contains more parameters, is less general and does not necessarily reflect the true phenomena of the inactivation reaction. It is therefore chosen to keep the current model in order to maintain simplicity and general applicability.

Also, as validated in section 4.7 it is possible to evaluate the drying performance of enzyme containing formulations using simulations based on the current simple model which further favours keeping this model.

4.6 Performance Evaluation

Using the approach described above four different model enzyme containing formulations are investigated. The formulation ingredients cannot be given in detail as this information is commercially sensitive but they include carrier materials, enzyme stabilizers and various amounts of a soluble compound, simply referred to as *the solute*. Formulation 1 contains no solute while Formulation 3 and 4 contain, respectively, double and triple the amount of the solute in Formulation 2.

The formulations are subject to DSC experiments at different moisture levels and the data obtained is used to find the expressions for the rate constants given by equation (4.7) as explained in detail in the previous sections. The results are given in table 4.3.

Table 4.3: Reaction kinetics parameters for the four formulations considered.

Formulation	$k_0(\mathrm{s}^{-1})$	n	E_a/R (K)
1	6.79	2.82	$2.93 \cdot 10^4$
2	3.05	1.09	$2.92 \cdot 10^4$
3	5.19	1.67	$2.60 \cdot 10^4$
4	5.76	1.81	$2.56 \cdot 10^4$

When a droplet consisting of a given formulation is drying inside a spray dryer, the temperature and moisture content continuously changes. It is therefore important that a formulation performs well over a broad range of process parameters.

For this reason the enzyme activity loss is estimated at different temperatures relevant for spray drying as well as various moisture contents. The most interesting temperatures are in the interval $T \in [60; 85]^\circ$C [16], however, this is extended to $T \in [50; 100]^\circ$C.

Comparisons between the individual formulations are made by calculating the rate constants from the equations above, using the parameters of table 4.3. Subsequently, equation (4.5) is integrated over a 60 s time interval to find the enzyme activity loss. The results for the formulations and the purified enzyme concentrate are depicted in figures 4.7 through 4.9.

From the figures it is evident that Formulation 1 displays least inactivation at all parameter combinations. Note that the formulation performs better than the concentrate and is thus preferred for spray drying.

The solute is added during processing upstream from the spray dryer and the figures show that the addition of the solute should be kept at a minimum.

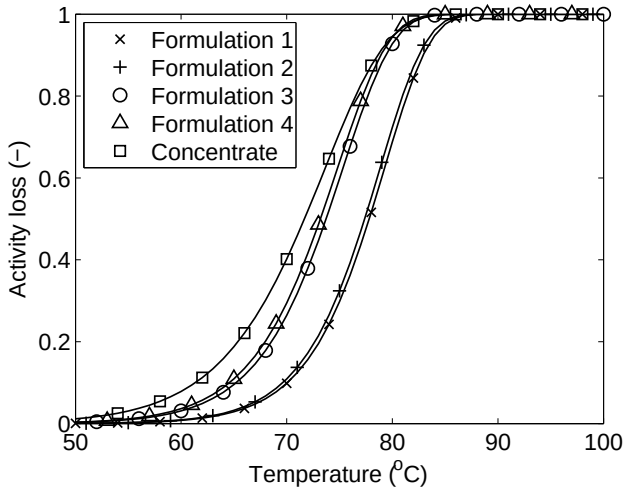

Figure 4.7: Simulations of the enzyme inactivation during a 60 s time interval at different temperatures and a moisture content of $w = 0.60$.

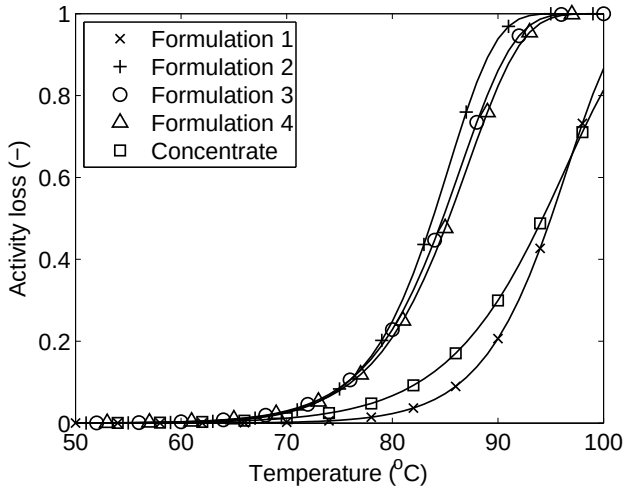

Figure 4.8: Simulations of the enzyme inactivation during a 60 s time interval at different temperatures and a moisture content of $w = 0.15$.

The formulation containing least of the solute (Formulation 2) performs better than those with elevated solute levels (Formulation 3 and 4), especially at high moisture contents.

Also, it is interesting that Formulation 3 and 4 practically perform equally well at all process parameters considered. This indicates that there is an upper level above which further addition of the solute does not increase inactivation.

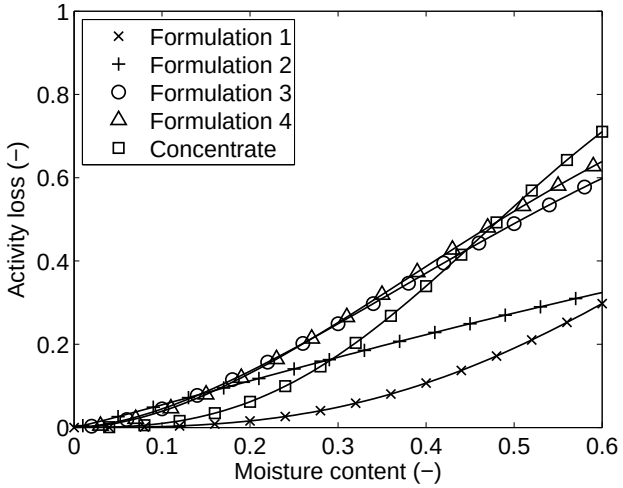

Figure 4.9: Simulations of the enzyme inactivation during a 60 s time interval at different moisture contents and a temperature of $T = 75°\mathrm{C}$.

4.7 Validation of the Method

The method for evaluation of enzyme containing formulations described above is validated by comparing the results to pilot scale spray drying experiments using a Niro Mobile Minor. This particular spray drying equipment is described in detail by several authors (see e.g. [19]).

The spray dryer is equipped with a two fluid nozzle and operated in co-current mode. The drying air inlet temperature is set at 155°C while the outlet temperature is varied by adjusting the feed rate in the interval $[2.5 - 4.5]^{\mathrm{kg}/\mathrm{h}}$. For the concentrate and each of the four formulations used above a series of consecutive experiments are conducted setting the outlet temperature at 70°C, 75°C, 80°C and 85°C.

For each individual experiment, the powder product is collected and subjected to an activity assay. By comparing the result to the activity of the initial formulation, the activity loss is found and depicted in figure 4.10.

The figure reveals that Formulation 1 performs best during spray drying. Also, if addition of the solute is necessary during upstream processing this should be kept at a minimum because Formulation 2 performs better than Formulation 3 and 4. Further, Formulation 3 and 4 practically performs equally well suggesting that there is an upper limit above which additional solute does not increase activity loss. These conclusions are the same as those drawn using the performance evaluation method described above. Thus, the validity of the method is strongly supported by the results of the spray dryer experiments.

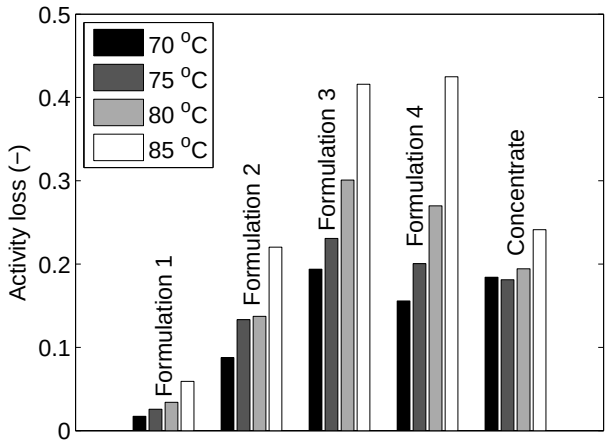

Figure 4.10: Spray drying performance of each formulation considered.

4.8 Review of the Method

The combined experimental and theoretical method for evaluation of enzyme containing formulations presented in this paper has a number of advantages and drawbacks compared to other evaluation methods such as pilot or full scale spray drying experiments. These advantages and drawbacks appear only implicitly in the above but are now elaborated.

The experimental techniques for sample preparation and DSC-analyses have been established and tested, entailing that data on additional formulations is readily obtained. A great advantage of the method is that experiments are quickly conducted, require only few man-hours – mostly for sample preparation – and data is immediately available for processing. Pilot and full scale tests of new formulations do not only involve a larger workload but also require product enzyme assay analysis to determine the residual activity.

The method described in the present work uses only very small amounts of enzymes and for this reason, numerous different formulations may be evaluated. Also, formulation design may be initiated earlier in the product development process when a new enzyme has been discovered as no large scale concentrate production is necessary.

However, no actual drying tests are performed using the method described. Thus, the method does not account for any differences in the course of drying between the individual formulations. If the formulations e.g. form significantly different particle morphologies during drying, the course of drying is not identical and the formulations preserve varying enzyme activity.

Further to this is that the calculation methods presented here in figures 4.7–4.9 do not include continuous change in moisture content and temperature of a drying droplet. These transient changes might differently influence the ability of individual formulations to maintain enzyme activity.

In theory, it is possible to account for this by coupling the equations for the inactivation reaction kinetics to a mathematical model describing the developments in droplet temperature and moisture content. Both the temperature and the moisture content are, however, difficult to predict as described in detail by Wijlhuizen et al. [29] and Sloth et al. [26].

Simulations of this kind require measurements or estimation of different parameters such as heat conductivities, heat capacities and moisture diffusion coefficients for each formulation considered. Especially, the latter requires extensive work as recently shown by Loulou et al. [14] in their elaborate study on estimation of diffusion coefficients in drying processes. Thus, figures 4.7-4.9 appear to be a reasonable basis for formulation performance evaluation as extension of the experimental work increases costs and is therefore undesirable.

4.9 Conclusion

A method to assist in the formulation design of enzyme containing particles produced by spray drying has been presented. DSC measurements have proven to be a powerful tool for obtaining the necessary data to determine the reaction kinetics and subsequently evaluate the drying performance of individual formulations by simulations. The method is fast and cheap, allowing for many different formulations to be tested early in product development process.

The method does not directly account for changes in particle temperature and moisture content or morphology formation during drying. However, the method may be used for qualitative comparison between different formulations and thereby narrow down the number of candidates. Still, the final few candidates selected must be subject to testing in a pilot or full scale spray dryer.

Notation

A	Preexponential factor (may be water concentration dependent), s^{-1}
E_a	Activation energy, J $mole^{-1}$
k	Rate constant, s^{-1}
k_0	Preexponential factor (water concentration independent), s^{-1}
k^*	Preexponential factor (water

	concentration dependent), s^{-1}
n	Constant, –
P	Point on baseline, mW
Q	DSC output, mW
R	Gas constant, J $mole^{-1}$ K^{-1}
T	Temperature, K
T^*	Reference temperature, K
w	Water mass fraction, –
X	Enzyme activity loss, –

Acknowledgments

The authors are grateful for the support of the Novozymes Bioprocess Academy and the CHEC Research Centre.

4.10 References

[1] K. B. Catherine, K. Krishnan, and K. N. Ninan. A DSC study on cure kinetics of HTPB-IPDI urethane reaction. *Journal of Thermal Analysis and Calorimetry*, 59:93–100, 2000.

[2] A. L. H. Daemen. The destruction of enzymes and bacteria during the spray-drying of milk and whey. 1. The thermoresistance of some enzymes and bacteria in milk and whey with various total solids contents. *Netherlands Milk and Dairy Journal*, 35:133–144, 1981.

[3] A. L. H. Daemen. The destruction of enzymes and bacteria during the spray-drying of milk and whey. 4. A comparison of theoretical computed results concerning the destruction of phosphatase with those obtained experimentally. *Netherlands Milk and Dairy Journal*, 38:55–70, 1984.

[4] A. L. H. Daemen and H. J. V. der Stege. The destruction of enzymes and bacteria during the spray-drying of milk and whey. 2. The effect of the drying conditions. *Netherlands Milk and Dairy Journal*, 36:211–229, 1982.

[5] A. L. H. Daemen, A. Kruk, and H. J. V. der Stege. The destruction of enzymes and bacteria during the spray-drying of milk and whey. 3. Analysis of the drying process according to the stages in which the destruction occurs. *Netherlands Milk and Dairy Journal*, 37:213–228, 1983.

[6] J. Dupuy, E. Leroy, and A. Maazouz. Determination of activation energy and preexponential factor of thermoset reaction kinetics using differential scanning calorimetry in scanning mode: Influence of baseline shape on

different calculation methods. *Journal of Applied Polymer Science*, 78: 2262–2271, 2000.

[7] M. R. Etzel, S.-Y. Suen, S. L. Halverson, and S. Budijono. Enzyme inactivation in a droplet forming a bubble during drying. *Journal of Food Engineering*, 27:17–34, 1996.

[8] W.-Y. Fu, S.-Y. Suen, and M. R. Etzel. Inactivation of lactococcus lectis ssp lactis c2 and alkaline phosphatase during spray drying. *Drying Technology*, 13(5-7):1463–1476, 1995.

[9] P. D. Garn. An examination of the kinetic compensation effect. *Journal of Thermal Analysis*, 7:475–478, 1975.

[10] W. F. Hemminger and S. M. Sarge. The baseline construction and its influence on the measurement of heat with differential scanning calorimeters. *Journal of Thermal Analysis*, 37(7):1455–1477, 1991.

[11] A. N. Kirgintsev and A. V. Luk'yanov. Water vapor pressure in a water -glycerin system at 25°C. *Russian Chemical Bulletin*, 11(83):1393–1394, 1962.

[12] B. I. Kurganov, A. E. Lyubarev, J. M. Sanchez-Ruiz, and V. L. Shnyrov. Analysis of differential scanning calorimetry data for proteins critia of validatity of one-step mechanism of irreversible protein denaturation. *Biophysical Chemistry*, 69:125–135, 1997.

[13] J. K. Liou. *An Approximate Method for Nonlinear Diffusion Applied to Enzyme Inactivation During Drying*. PhD thesis, Agricultural University of Wageningen, The Netherlands, 1982.

[14] T. Loulou, B. Adhikari, and D. Lecomte. Estimation of concentration-dependent diffusion coefficient in drying process from the space-averaged concentration versus time with experimental data. *Chemical Engineering Science*, 61:7185–7198, 2006.

[15] K. C. A. M. Luyben, J. K. Liou, and S. Bruin. Enzyme degradation during drying. *Biotechnology and Bioengineering*, 24:533–552, 1982.

[16] K. Masters. *Spray Drying Handbook*. Longman Scientific and Technical, 5th edition, 1991.

[17] G. Meerdink. *Drying of Liquid Food Droplets - Enzyme Inactivation and Multicomponent Diffusion*. PhD thesis, Landbouwuniversiteit te Wageningen, The Netherlands, 1993.

[18] A. Millqvist-Fureby, M. Malmsten, and B. Bergenståhl. Spray drying of trypsin - surface characterisation and activity preservation. *International Journal of Pharmaceutics*, 188:243–253, 1999.

[19] K. Mosén, K. Bäckström, K. Thalberg, T. Schaefer, H. G. Kristensen, and A. Axelsson. Particle formation and capture during spray drying of inhalable particles. *Pharmaceutical Development and Technology*, 9(4):409–417, 2004.

[20] R. Narayan and M. J. Antal. Thermal lag, fusion, and the compensation effect during biomass pyrolysis. *Industrial and Engineering Chemistry Research*, 35(5):1711–1721, 1996.

[21] T. Palmer. *Understanding Enzymes*. Ellis Horwood, 3rd edition, 1991.

[22] J. B. Rawlings and J. G. Ekerdt. *Chemical Reactor Analysis and Design Fundamentals*. Nob Hill Publishing, Madison, 2002.

[23] K. Samborska, D. Witrowa-Rajchert, and A. Goncalves. Spray-drying of α-amylase - the effect of process variables on enzyme inactivation. *Drying Technology*, 23:941–953, 2005.

[24] J. M. Sanchez-Ruiz. Differential scanning calorimetry of proteins. In B. B. Biswas and S. Roy, editors, *Subcellular Biochemistry - "Proteins: Structure, Function and Engineering"*, volume 24, chapter 6, pages 133–176. Plenum, New York, 1995.

[25] A. S. Selivanov. Stabilization of cellulases using spray drying. *Engineering in Life Sciences*, 5(1):78–80, 2005.

[26] J. Sloth, S. Kiil, A. D. Jensen, S. K. Andersen, K. Jørgensen, H. Schiffter, and G. Lee. Model based analysis of the drying of a single solution droplet in an ultrasonic levitator. *Chemical Engineering Science*, 61:2701–2709, 2006.

[27] K. Takahashi and J. M. Sturtevant. Thermal denaturation of streptomyces subtilisin inhibitor, subtilisin BPN' and the inhibitor-subtilisin complex. *Biochemistry*, 20:6185–6190, 1981.

[28] W. Wang. Lyophilization and development of solid protein pharmaceuticals. *International Journal of Pharmaceutics*, 203:1–60, 2000.

[29] A. E. Wijlhuizen, P. J. A. M. Kerkhof, and S. Bruin. Theoretical study of the inactivation of phosphatase during spray drying of skim-milk. *Chemical Engineering Science*, 34:651–660, 1979.

[30] S. Yamamoto, M. Agawa, H. Nakano, and Y. Sano. Enzyme inactivation during drying of a single droplet. In R. Toei and A. S. Mujumdar, editors, *Proceedings of the Fourth International Drying Symposium, Kyoto, Japan*, pages 328–335, July 1984.

Chapter 5

Spray Drying of Suspensions for Pharma and Bio Products – Drying Kinetics and Morphology

In this chapter, the drying rate and morphology formation during spray drying are investigated using an experimental approach. The purpose is to map the influence of different formulation ingredients on the drying process.

The present chapter is submitted as an article for publication in a scientific journal. The article is authored by Jakob Sloth (Technical University of Denmark), Kåre Jørgensen (Novozymes A/S), Poul Bach (Novozymes A/S), Anker D. Jensen (Technical University of Denmark), Søren Kiil (Technical University of Denmark) and Kim Dam-Johansen (Technical University of Denmark). The chapter is simply referred to as *Paper III* throughout the present work.

5.1 Abstract

An experimental investigation of the spray drying behavior of droplets containing excipients and carrier materials used in the pharmaceutical and biotechnological industries has been conducted. Specifically, rice starch suspensions with different amounts of TiO_2, maltodextrin, dextrin, NaCl and Na_2SO_4 are dried. The drying rate is measured and the morphology formation is mapped to obtain a more fundamental understanding of the drying process, which is very useful when designing product formulations. In the pilot spray dryer droplet generation is based on the JetCutter technology and the droplets are dried under well-defined temperature and flow conditions. The droplets are sampled during drying to determine the drying rate and the dried particles are collected for morphology analysis. The results show that reducing the water activity in

a suspension of insolubles by adding various amounts of inorganic salts or carbohydrates causes an increase in the droplet temperature during spray drying resulting in a rather constant the drying rate. Further, the results show that small alterations in the droplet composition may significantly change the final particle morphology. The observed morphologies are discussed in detail.

5.2 Introduction

Spray drying is commonly used in the manufacture of biotechnological and pharmaceutical products. The products are often of high value and it is therefore important that they are produced with a constant and high quality. Consequently, the choices of formulation ingredients, equipment design and process conditions become critical and preferably rely on a detailed insight into the various processes occurring during product drying.

In spray drying, a suspension or solution is fed to an atomizer and the droplets formed are mixed with a hot gas. This causes the solvent of the droplets to evaporate, leading to formation of particulates. The course of drying for a single droplet inside a spray dryer is complex, involving stages of different droplet temperatures and evaporation rates. The process is described in detail by several authors (see e.g. Nesic and Vodnik [26], Farid[13] or Sloth et al. [33]) and progresses as shown in figure 5.1. The figure is valid both for the drying of a droplet consisting of a solution or a suspension. A suspension is a mixture of solvent and primary particles, i.e. insoluble particles which normally have a size of than less 10 μm. The following briefly describes drying of a suspension droplet.

After being formed at the atomizing device the droplet is heated (stage A) and the temperature approaches the wet bulb temperature of the solvent. During stage B the surface is fully wetted by the solvent, giving rise to fast evaporation. Due to the evaporation, the size of the droplet decreases and the primary particle concentration builds up, inducing minor droplet heating because of slight solvent evaporation hindrance.

When the primary particles at the droplet surface have packed as closely as possible (stage C) a solid phase forms around the wet core of the droplet. The solid phase limits the water transport from the wet core to the surface and in the remaining part of the drying process the rate of evaporation falls while the temperature approaches the dry bulb temperature (stage D).

Throughout the entire drying process there is a strong coupling between the droplet temperature and the drying rate. If a decrease in the drying rate occurs, less heat is used for evaporation and the droplet temperature increases. A higher temperature induces accelerated drying, lowering the temperature. However, an equilibrium between temperature and drying rate is quickly obtained.

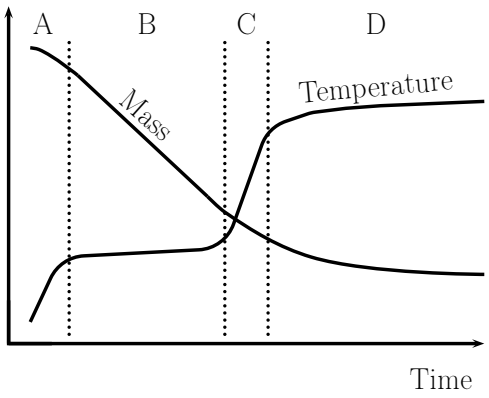

Figure 5.1: Progress of droplet drying in a spray dryer. A: Heating. B: Constant rate period. C and D: Falling rate period.

The description above is widely accepted in the literature where stage B is often referred to as the *constant rate* period and stages C and D are combined and referred to as the *falling rate* period.

5.3 Previous Studies

The development in the droplet mass shown in figure 5.1 is merely qualitative. The specific drying rate of a droplet depends on numerous variables such as composition, initial droplet size, drying air temperature, and humidity.

However, due to the complex flow field in a spray dryer, measuring the drying rate is hardly possible. Droplets released from the atomizer have different velocities and directions, and they travel through regions of varying temperatures and humidities. It is this complexity which renders the experimental investigations of drying kinetics almost impossible using a conventional industrial or pilot spray dryer.

As a consequence, authors studying droplet drying kinetics resort to purpose-built equipment. In general, equipment of this kind may be divided into two groups – *single droplet* and *in situ* drying equipment.

The former is usually performed by suspending a droplet from a filament. The stationary droplet is placed in an air stream with a constant temperature which may be well above 200 °C [11]. The drying rate is measured as a mass loss by attaching the filament to a microbalance [5, 21] or a cathetometer [29]. Alternatives include determining the deflection of a curved filament [7] or suspending the droplet from a burette and measuring the feed rate of water through the burette necessary to maintain a constant droplet diameter [27, 28]. The latter is obviously only possible for a pure liquid droplet.

The approaches described above yield precise measurements of the drying rate throughout the entire course of drying and another advantage of the suspended droplet method is that it is possible to follow the progress in temperature by inserting a small thermocouple into the droplet [5, 29, 11, 15]. Also, the particle morphology formation may be monitored using a microscope camera [15, 5, 11].

For practical reasons the authors mentioned above are compelled to conduct experiments with initial droplet sizes in the range $0.8 - 2\,\text{mm}$. This is about an order of magnitude larger than spray droplets [22] and therefore drying kinetics and resulting particle morphologies may not accurately reflect those in industrial spray drying equipment. Further, Lin and Gentry[19] note that the filament prevents the droplet from rotating freely, serves as a heat source, and may deform the droplet when a solid phase forms in the later part of the drying process.

Some of the difficulties associated with the filament are avoided when using ultrasonic levitation. Pioneering work on this technique is described by Toei et al.[36] who successfully dried non-supported droplets, held constant against gravity by the force of a standing acoustic wave. The drying rate during the constant rate period is easily measured using a camera as the droplet size changes. In contrast, the drying rate during the falling rate period is difficult to measure but enclosing the levitator in a preconditioned chamber and using a high accuracy dew point hygrometer to determine the amount of water evaporated was tested by Groenewold et al.[14]. Also, the vertical displacement of the droplet in the ultrasonic field is a function of the mass which, in theory, may be used for drying kinetics measurements [17, 41]. Droplet surface temperature measurements can be performed using by an infrared camera [35].

The droplet size is similar to that of suspended droplets and thereby about an order of magnitude larger than those in a spray dryer. If the droplets are too large (i.e. larger than 1.5mm) the acoustic waves distort the shape of the droplets [40] and therefore the experiments do not fully mimic the drying behavior in a spray dryer [1].

Despite the disadvantages mentioned for the suspended droplet and the levitation methods, single droplet drying investigations have given excellent information on drying rates and droplet temperatures. The experiments map various phenomena of droplet drying, serve as validation of modeling studies and thereby undoubtedly lead to a deeper understanding of the spray drying process.

In a fairly recent review paper Chen[6] emphasizes the importance of in situ experiments as they closely imitate the evaporation process in conventional spray drying equipment.

In the literature a few authors describe the use of in situ experiments[4, 39, 23, 42]. Generally, the experimental approach is to situate an atomizing device

at the top of a vertical drying column measuring up to 18 m [4]. The droplets dry as they fall freely down the column in a heated air stream. Droplets are sampled along the height of the tower and subsequently subjected to moisture content analysis. The analysis may be vacuum or oven drying [23, 4] or Karl Fischer titration [39].

The droplet sizes used during in situ experiments are in the same order of magnitude as that of industrial spray drying. The drying process inside the column resembles spray drying well[4, 39, 23, 42] and thus in situ experiments are well-suited both as complement to single droplet experiments and also as basis for new studies of drying kinetics and morphology.

5.4 Specific Objectives

The objective of this work is to use in situ experimental investigations to contribute to the fundamental understanding of the droplet drying process taking place inside a spray dryer. The focus is on drying of formulations containing carrier materials and excipients often used in the biotechnological and pharmaceutical industries, omitting the active ingredient typically present in very low levels. Drying of these formulations is of particular interest as the influence on the drying process of each formulation ingredient considered may be mapped without the hazards of working with active components.

Also, it is the objective of this paper to present an apparatus for in situ experimental investigations of drying droplets. Using this apparatus, the influence of formulation ingredients on the droplet drying kinetics and particle morphology formation are analyzed and discussed in detail. It is an important part of this work to connect the findings on morphology formation to the findings of other authors as this will contribute to the ongoing effort in the literature to understand morphology formation processes.

5.5 The Droplet Dryer

An experimental apparatus called the *Droplet Dryer* which can be used to investigate the drying kinetics of multi component suspensions has been constructed. The design, construction and commissioning process is described by Jørgensen[16].

The Droplet Dryer meets the following requirements:

- Droplets of an arbitrary size within the range $[200 - 1500]\mu m$ may be produced.

Table 5.1: Key specifications of the Droplet Dryer.

Tower height:	6.0 m
Inner Diameter:	0.2 m
Liquid flow rate:	$\approx 0.4\ ^{g}/_{s}$
Droplet size:	$200 - 1500\ \mu m$
Air flow rate:	$0.1\ ^{m}/_{s}$
Air temperature:	$25 - 250\ ^{\circ}C$

- The suspension feed may have a high initial solid content.
- The drying takes place under well-defined conditions.
- Sampling of the droplets during drying is possible.
- The drying air temperature may be up to 250°C.
- The dried particles may be collected for e.g. morphology analysis.

Inspiration for the design of the Droplet Dryer has been drawn from the works of Büttiker[4], Wallack et al.[39], Meerdink[23] and Zbicinski[42]. The layout of the setup is shown in figure 5.2 while key specifications are given in table 5.1.

The apparatus consists of two parts – a droplet generator and a drying tower. These are described in detail below but the main principle of the Droplet Dryer is that a suspension is fed to the droplet generator and the droplets formed are mixed with hot air and dry as they fall down the drying tower. In the particle collector at the bottom of the setup the dried particles are separated from the drying air.

5.5.1 Droplet Generator

The droplet generator chosen for the Droplet Dryer is a slightly modified version of the commercial JetCutter type S available from GeniaLab GmbH, Germany.

The principle of jet cutting is explained by Vorlop and Breford[37] and sketched in figure 5.3. A liquid jet is formed by forcing a feed through a nozzle with an orifice diameter of $[100 - 300]\ \mu m$. This jet is sliced into cylindrical pieces by a fast-rotating cutting wheel (500-15000 rpm) equipped with $24 - 240$ strings. The liquid surface tension reshapes the cylinders into spherical droplets shortly after formation. The droplet size may be altered by adjusting the jet velocity or the rotational speed of the cutting wheel. Specifically, the JetCutter installed on the Droplet Dryer is capable of producing droplets with a mean diameter in the range $[200 - 1500]\ \mu m$.

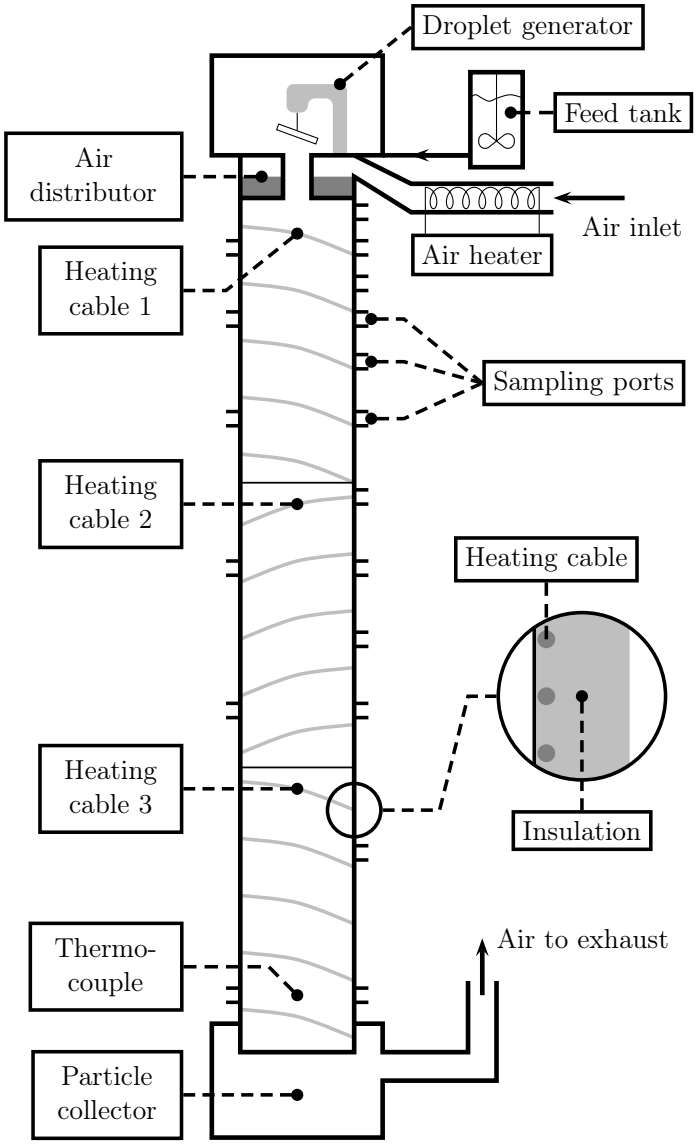

Figure 5.2: Schematic representation of the Droplet Dryer which consists of an atomizing device and a drying tower.

5.5.2 Drying Tower

The droplets generated dry as they fall through the drying tower. The tower is equipped with 12 ports at different levels, thus allowing sampling of the droplets as they dry. The sampling ports are located at distances from 100 to 5600 mm from the air distributor. More ports are located at the top of the tower as the droplets experience the most rapid evaporation here. The sampling technique is described below.

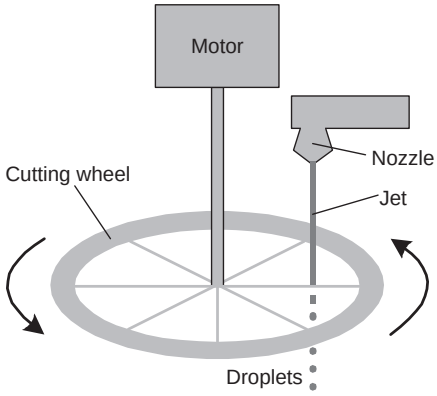

Figure 5.3: Droplet generation principle of the JetCutter.

The droplets travel in a cocurrent plug flow of hot air. Plug flow is ensured by forcing the preheated air through a sand bed of height 100 mm in the air distributor at the top of the tower. The pressure drop over the sand bed is at least 100 mmH_2O during all experiments. Although the velocity of the air stream is only 0.1 $^{m}/_{s}$, the amount of air is very large compared to the amount of moisture evaporating from the drying droplets. Thus, the relative humidity in the air is negligible.

To maintain a constant air temperature the tower is insulated and three separate sections are coiled with thermostat controlled heating cables. The temperature may be checked by a specially designed thermocouple, enabling measurements at an arbitrary sampling port without causing significant disturbance to the tower air flow field.

As mentioned above, in the particle collector at the bottom of the setup the dried particles are separated from the drying air which is exhausted to the ventilation. The particle collector is mounted directly onto the setup but is easily removed for particle recovery. The particles are used for morphology analysis by optical and scanning electron microscopy (SEM).

5.5.3 Sampling and Analysis

Droplets are caught through the ports during drying, using a special device [16] which allows sampling without drawing ambient air into the tower. A small aluminum foil container is partly filled with low vapor pressure paraffin oil and fixed into the sampling device. During sampling the droplets hit the paraffin oil, sink to the bottom because of a difference in density and evaporation ceases. The sample is subsequently subjected to Karl Fischer titration as described by Skoog et al.[32] for water mass fraction determination. Obtaining the mass

fractions from samples taken at different ports yields a measure of the drying rate, i.e. the droplet water content as a function of the distance travelled in the drying tower is known – examples are given in the next section.

The velocity of the droplets inside the drying tower may be estimated to $1.5 - 2$ $^{m}/_{s}$ (the terminal droplet velocity plus the velocity of the drying air). Sampling of droplets falling at this velocity is a difficult task. Inevitably, the experimental results are lightly scattered. From experience, particularly the measurements obtained from the top ports (ports situated less than 1000 mm from the droplet generator) display some scattering. At this point the droplets still contain a high amount of water when caught and the surface tension between the droplets and the paraffin oil retards the sinking of the droplets into the paraffin oil. Thus, evaporation is not immediately stopped during sampling which is a source of error.

Nevertheless, the trends of the results given below are always clear and thereby enable evaluation of the influence of different compounds on the drying kinetics.

5.6 Experimental Results and Discussion

Using the Droplet Dryer, several series of experiments with multi component suspension feeds have been conducted. Each series consists of four individual experiments differing only in the concentration of one component. Specifically, all experiments are conducted using suspensions containing water, 42 wt% insoluble rice starch primary particles and various amounts of a third component. The materials used in this work are given in table 5.2.

Further, unless explicitly stated below the Droplet Dryer settings are identical during the experiments, including a drying air temperature of 150 °C and an initial droplet size of approximately 275 µm.

In the following, the drying kinetics are represented as the mass fraction of water evaporated w_{evap} as a function of the distance L traveled in the drying tower. w_{evap} is found from

$$w_{evap} = 1 - \frac{m}{m_0} = 1 - \frac{w(1 - w_0)}{w_0(1 - w)} \tag{5.1}$$

where m_0 and m are, respectively, the initial and the actual mass of water in a drying droplet. However, the values of m_0 and m are immeasurable and instead w_{evap} is calculated from the latter term of equation (5.1). Here w_0 and w are, respectively, the water mass fraction of the feed and that found in the sample by Karl Fischer titration.

Table 5.2: Insolubles, carbohydrates and inorganic salts used as formulation ingredients.

	Trade name	Supplier	d_{50}[1]	Remarks
Rice starch	REMY FG	Alsiano	5.2 µm	Can gelatinize
TiO_2	Kronos 2044	Kronos	0.39 µm	–
Maltodextrin	Glucidex IT21	Roquette	Soluble	DE 20-23[2]
Dextrin	AVEDEX W80	Avebe	Soluble	DE 9.5-12.5[2]
NaCl	Suprasel	Akzo Nobel	Soluble	Food grade
Na_2SO_4	–	Sulquisa	Soluble	Pregrinded

[1]50 % fractile of the primary particle size as measured by a Malvern Mastersizer employing laser diffraction.

[2]Number of dextrose equivalents in the chain.

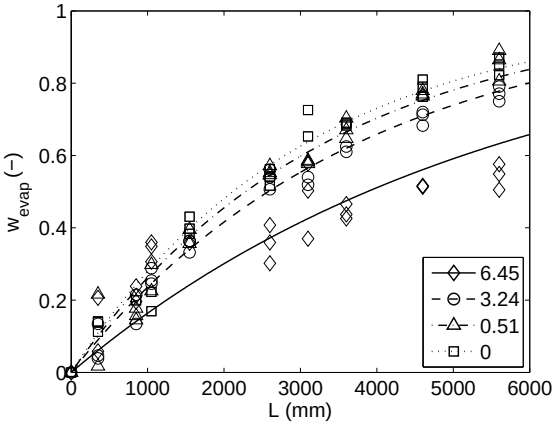

Figure 5.4: Drying curves for maltodextrin containing rice starch suspensions. The legend indicates the maltodextrin content in wt%.

5.6.1 Carbohydrates

Dextrins and maltodextrins are often used as excipients in the spray drying of proteins [24, 30]. To investigate the effect of maltodextrin on the drying kinetics and morphology formation during spray drying a series of experiments has been conducted, changing only the maltodextrin content between experiments as described above. Figures 5.4 and 5.5 show the experimental measurements and SEM pictures of the dried particles – lines are inserted in figure 5.4 to clarify the trends of the drying kinetics. Note, that one of the experiments is conducted using a feed containing only water and rice starch to serve as a reference for the other experiments. This experiment is simply referred to as the *reference experiment* throughout this paper.

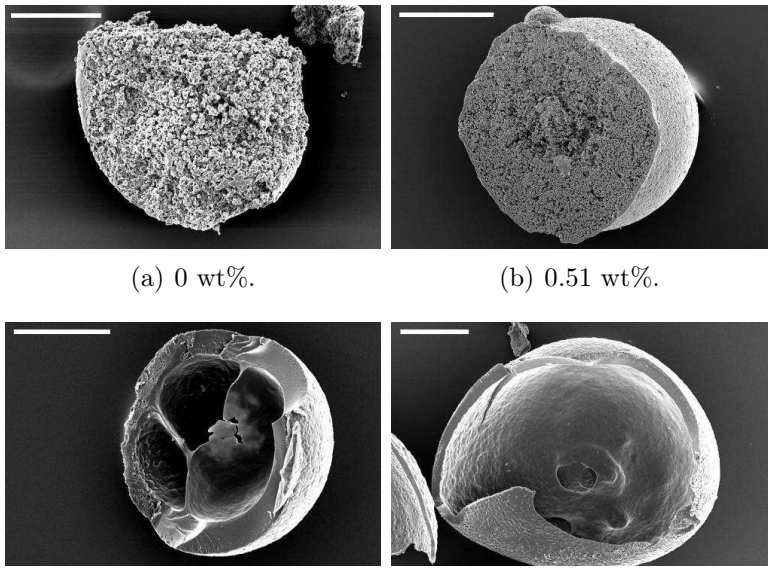

(a) 0 wt%. (b) 0.51 wt%.

(c) 3.24 wt%. (d) 6.45 wt%.

Figure 5.5: SEM pictures of dried rice starch particles containing various amounts of maltodextrin. Feed maltodextrin contents are given in the subfigure captions while all bar lengths are 100 µm.

Figure 5.4 reveals that the drying rate is only significantly affected by the addition of maltodextrin at the highest content level. Interestingly, the dried particles produced from the suspensions containing 3.24 and 6.45 wt% maltodextrin have suffered severe gelation, see figure5.5(c,d). According to Spigno and De Faveri[34] the degree of gelation for rice starch increases with temperature and moisture content indicating that the particles mentioned have experienced elevated temperatures early in the drying process. This is supported by figure 5.6 where suspensions containing only water and rice starch (≈ 24 wt%) have been dried at different air temperatures, leading to corresponding differences in the droplet temperature. For particles dried at 200 °C and 250 °C there appears to be a layer of intact primary particles around the gelatinized region. This indicates that this layer has been dry before the temperature has risen to gelatinize a wet core. Evidently, the degree of gelation increases with an increase in droplet temperature dependent on the moisture content.

Thus, figures 5.4 and 5.5 indicate that addition of maltodextrin affects the droplet temperature during drying rather than the drying kinetics. A possible explanation is that the presence of maltodextrin reduces the droplet surface water activity and thereby the surface vapor pressure. This would be expected to lower the evaporation rate. However, a temperature rise almost compensates for the water activity loss and the vapor pressure is increased which gives an

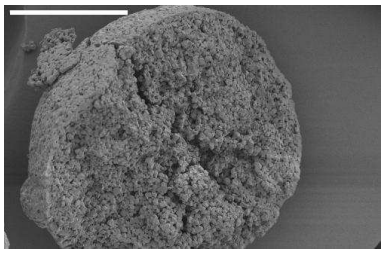

(a) 150 °C.

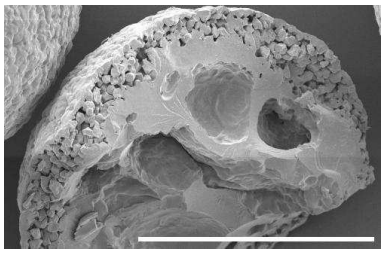

(b) 200 °C.

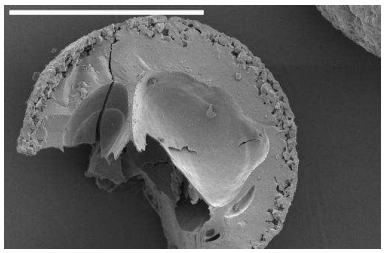

(c) 250 °C.

Figure 5.6: Dried particles from suspensions containing only water and rice starch dried at various temperatures. The bars indicates a length of 100 µm.

almost unaffected evaporation rate.

Corresponding conclusions may be drawn from a series of experiments where various amounts of dextrin have been added to the reference suspension containing water and rice starch. Figure 5.7 shows that the drying rate is only significantly influenced by the dextrin at the highest content level. Although the particles have suffered less gelation during drying, figures 5.7 and 5.8 are very similar to the results for the maltodextrin.

Morphology

The formation of the observed particle morphologies of the dried carbohydrate containing suspensions (figures 5.5 and 5.8) may be explained by the theory of Charlesworth and Marshall [5] although the theory is derived for droplets containing dissolved solids.

According to the theory, if the solid crust formed around the droplet at a distinct point in time during drying (the beginning of stage C in figure 5.1) is sufficiently porous no change in morphology occurs during the falling rate period. The water is merely transported through the pores to the surface where it evaporates. Thus, a solid and dense structure may form as is the case for several of the particles in figures 5.5 and 5.8. This course of drying is sketched in figure 5.9 (sequence a) and is also discussed by Walker Jr. and Reed[38]. Figure 5.9 shows

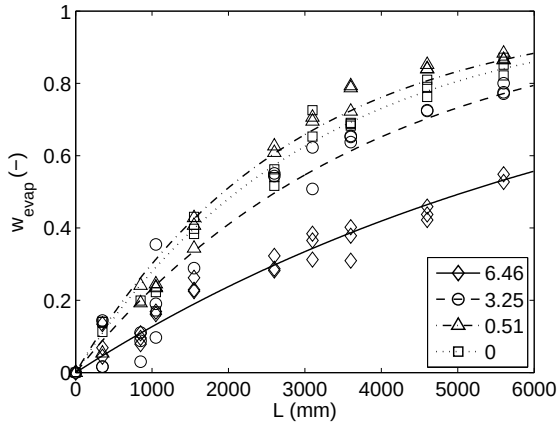

Figure 5.7: Drying curves for rice starch suspensions containing dextrin as the third component. The legend indicates the dextrin content in wt%.

the most likely sequences for formation of the particle morphologies observed throughout the present work. The figure is based on the work of several authors [5, 20, 38] and extended so that the figure is valid for the drying of materials which may gelatinize.

Contrary to the above, the crust formed around the drying droplet may become plastic and non-porous as a result of gelation. As the particle temperature increases vapor forms and a positive pressure is created inside the particle because the plastic crust is not sufficiently permeable. Consequently, a bubble forms within the particle and inflation might occur during the remaining part of the drying. This is also shown in figure 5.9 (sequence c) and leads to the formation of hollow, gelatinized particles.

A number of particles in figures 5.5 and 5.8 are hollow and it appears that especially particles dried from suspensions containing 6.45 wt% maltodextrin have experienced considerable inflation. In this case the particle diameter is significantly larger than the initial droplet size of approximately 275 µm.

Even further on the formation of hollow particles is that this process might proceed as shown in figure 5.10. As described in the introduction the droplet shrinks during the constant rate period but when the primary particles at the droplet surface have packed as closely as possible a solid phase forms around the droplet (figure 5.10a). The droplet can shrink no further and water is drawn to the surface through capillary action in the porous crust or, alternatively, a liquid/water interface is formed inside the crust. In both cases, liquid is transported from the droplet center, dragging along primary particles which are deposited inside the thickening crust. The lack of water and primary particles in the droplet center causes the formation of an internal void (figure 5.10b). The

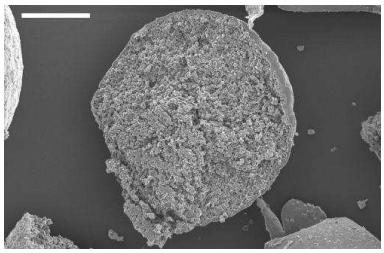

(a) 0.51 wt%.

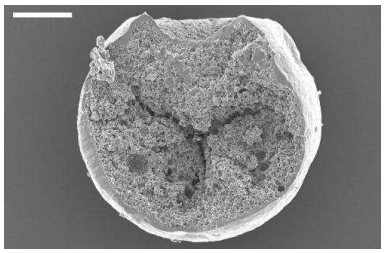

(b) 3.25 wt%.

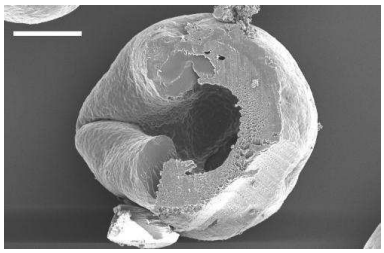

(c) 6.46 wt%.

Figure 5.8: SEM pictures of dried rice starch particles containing various amounts of dextrin. Feed dextrin contents are given in the subfigure captions while all bar lengths are 100 µm. The reference experiment is not included but shown in figure 5.5 (a).

void continues to grow while the crusts thickens until a dried hollow particle is formed (figure 5.10c). The theory is supported by Crosby and Marshall[8], Lukasiewicz[20], Walker Jr. and Reed[38] and Minoshima et al.[25] and as shown in figure 5.9 may lead to hollow gelatinized or non-gelatinized particles.

5.6.2 Inorganic Salt

The effects of reducing the water activity on the developments in drying rate and droplet temperature are further investigated by a series of experiments where various amounts of Na_2SO_4 are added to the reference suspension.

Although there is considerable scattering of the measurements from the earliest phase of the drying process, figure 5.11 illustrates that dissolved Na_2SO_4 has the same effect on the drying kinetics as the carbohydrates. Only a high initial content of the added component significantly lowers the drying rate.

Further to this is that particles produced from Na_2SO_4 containing suspension are similar in morphology to the carbohydrate containing particles – low Na_2SO_4 contents form a solid, dense morphology while high contents form hollow particles (examples are shown in figure 5.12 (a) and (b)). However, the hollow Na_2SO_4 containing particles are only slightly gelatinized. This means that on

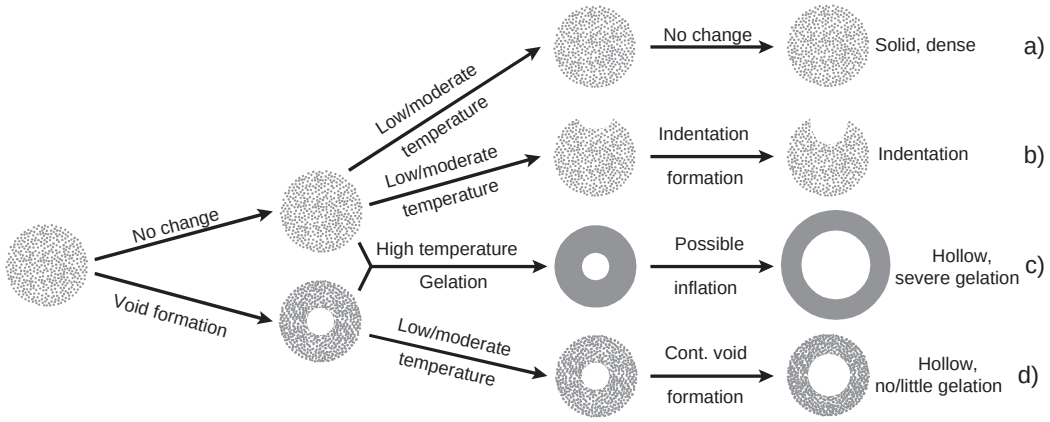

Figure 5.9: Sequences for formation of observed morphologies. The sequences are an extension of the theories outlined by Charlesworth and Marshall[5], Lukasiewicz[20] and Walker Jr. and Reed[38].

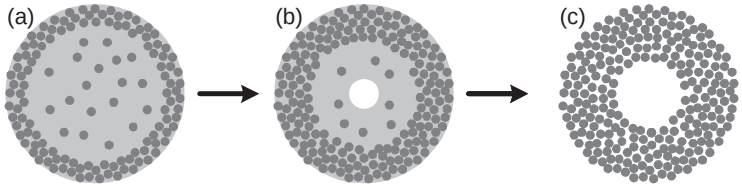

Figure 5.10: Detailed sequence for formation of hollow particles. Darker and lighter color indicate primary particles and water, respectively.

the one hand the particles have not been hot enough to gelatinize, on the other hand the temperature must have been sufficiently elevated to built an internal vapor pressure. The void may form as described above but a substantial internal pressure is necessary to avoid particle collapse. The surface of the particles appears to have poor permeability (figure 5.12 (c)) and thus provides the vapor transport resistance for internal pressure increase.

An experiment where a high amount of NaCl is added to the reference suspension produces particles (figure 5.12 (d)) very similar to those from high carbohydrate content, i.e. gelatinized, hollow particles. Thus, it appears that adding an inorganic salt instead of a carbohydrate results in a similar course of drying.

Although both the salts and the carbohydrates lower the surface water activity, the two classes of compounds could do this differently. The salts change the chemical potential while the carbohydrates might form a film with low water

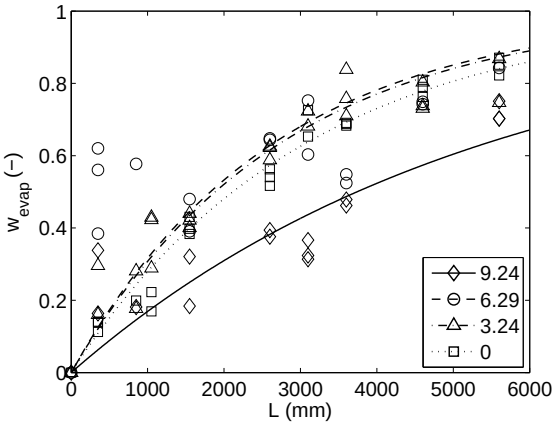

Figure 5.11: Drying curves for rice starch suspensions containing Na_2SO_4 as the third component. The legend indicates the Na_2SO_4 content in wt%.

diffusivity at the droplet surface.

Evans and Haisman[12] report that the addition of Na_2SO_4 to starch suspensions raises the gelatinization temperature significantly while the gelatinization temperature is less affected by the addition of NaCl. This may explain that only the NaCl particles are gelatinized. Further, the vapor pressure over a saturated NaCl solution is e.g. 9.1 kPa at 50 °C [2]. The same vapor pressure over a saturated Na_2SO_4 solution is obtained at 47 °C [3] while it is obtained at 44 °C for pure water [18]. Thus, it is possible that the NaCl containing droplets have experienced the highest temperatures during drying, leading to enhanced gelation.

5.6.3 Insolubles

The influence of adding insoluble TiO_2 primary particles to the reference suspension on the drying behavior is shown in figure 5.13 while the final particle morphology is given in figure 5.14 (a), (c) and (e). Clearly, the drying rate is unaffected regardless of the amount of TiO_2 added and the lack of rice starch gelation reveals that the particles have not experienced elevated temperatures. This is because TiO_2, contrary to carbohydrates and inorganic salts, does not influence the water activity being insoluble in water and does not form a film with low water diffusivity.

The primary rice starch and TiO_2 particles have average sizes of 5.2 and 0.39 μm, respectively, as given in table 5.2. The presence of the smaller TiO_2 primary particles might be expected to have an effect on the structure of the drying particle and thereby influence the internal water transport and consequently

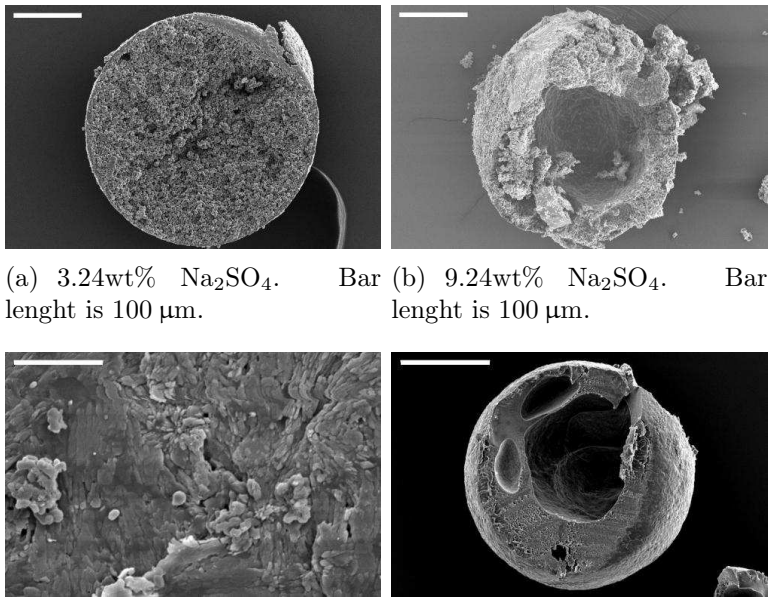

(a) 3.24wt% Na_2SO_4. Bar lenght is 100 µm.

(b) 9.24wt% Na_2SO_4. Bar lenght is 100 µm.

(c) 9.24wt% Na_2SO_4 (particle surface). Bar lenght is 10 µm.

(d) 9.36wt% NaCl. Bar lenght is 100 µm.

Figure 5.12: SEM pictures of dried rice starch particles containing various amounts of Na_2SO_4 or NaCl. Feed contents of the third component are given in the subfigure captions.

the drying kinetics during the falling rate period. However, if so, this appears to be of minor importance.

The sole effect of adding TiO_2 is that the particles formed display large indentations. This may be explained by the theory discussed by Büttiker[4], Duffie and Marshall[9, 10] and Shaw[31]. The theory is sketched in figure 5.15 as well as in figure 5.9 (sequence b) and it is assumed that the droplet does not rotate during drying. The front of the droplet is subjected to a substantial drag, increasing the transfer of heat to the droplet and the transfer of mass (i.e. evaporated liquid) from the droplet. The evaporation from the rear surface is slower, drawing liquid to the front where evaporation is quicker. The flow of liquid carries along primary particles and the rear surface is drawn inward, forming an indentation.

In the SEM pictures of figure 5.14 the TiO_2 primary particles are seemingly concentrated at the particle surfaces. This is verified by employing energy dispersive X-ray analysis (EDX) for element mapping of titanium (figures 5.14 (b), (d) and (f)).

The titanium is concentrated at the entire surface, including the indentation surface. To investigate how the surfaces may have become titanium covered, the element maps are converted into profiles using the image analysis tool available

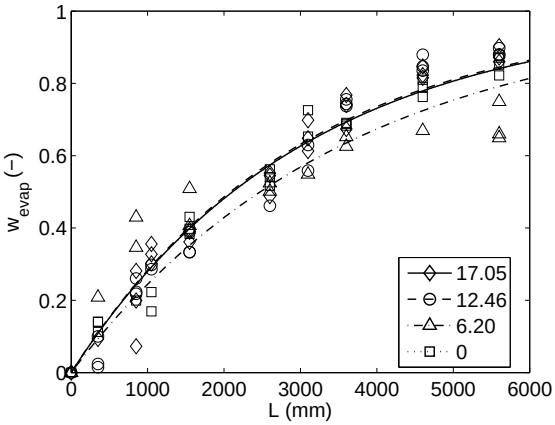

Figure 5.13: Drying curves for rice starch suspensions containing insoluble TiO_2 particles as the third component. The legend indicates the TiO_2 content in wt%.

in Matlab – a commercial computer software package. Also using Matlab, the data are smoothed by statistical data processing. The profiles of figure 5.16 are traced from a point chosen close to the particle center but precluding the indentations. The trace ends just beyond the particle surface as shown in figure 5.14. Note that analyses of this kind are merely semi-quantitative and thus, no numerical values are given in figure 5.16.

A possible explanation of the over-representation of titanium at the particle surface might be that during drying, TiO_2 primary particles are carried along with the liquid when it is transported towards the surface through the pores between the rice starch primary particles. This, however, seems unlikely considering the absence of a clear positive titanium concentration gradient in the profiles. More probable, the titanium accumulates at the surface during the constant rate period when the droplet shrinks. During shrinkage the rice starch primary particles recede but the TiO_2 deposit at the surface – possibly due to a filtering effect.

5.7 Conclusion

The droplet drying process of multi component suspensions has been investigated experimentally. The experiments were conducted using a newly constructed apparatus which is designed for in situ drying experiments so that the droplet drying process resembles that of conventional spray drying. With focus on drying of formulations containing carrier materials and excipients relevant to the biotechnological and pharmaceutical industries, the drying kinetics have been measured and the particle morphology has been analyzed.

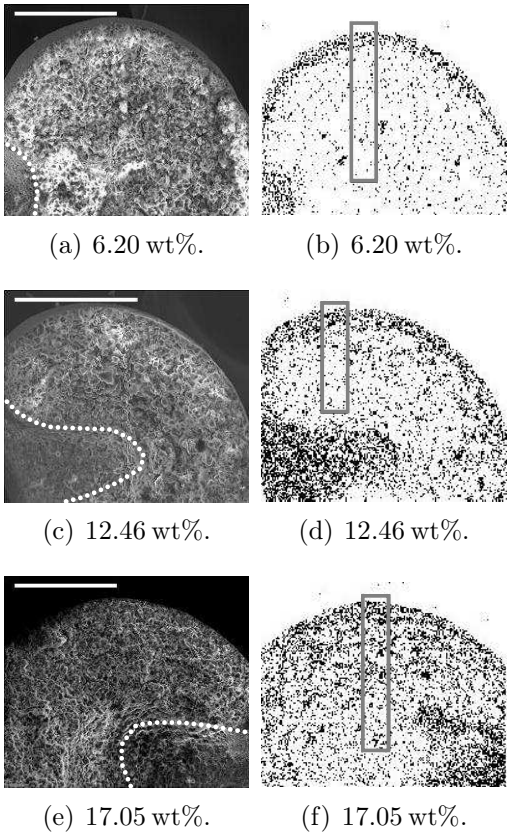

(a) 6.20 wt%. (b) 6.20 wt%.

(c) 12.46 wt%. (d) 12.46 wt%.

(e) 17.05 wt%. (f) 17.05 wt%.

Figure 5.14: SEM pictures of various TiO_2 containing particles are shown to the left where the dotted lines give the positions of the indentations. Corresponding EDX element maps of titanium are shown to the right, including areas chosen for titanium concentration profile determinations. The amount of TiO_2 in the feed suspension is given in the subfigure captions while all bar lengths are 100 µm.

The results show that adding compounds such as dextrin, maltodextrin, NaCl or Na_2SO_4 to a suspension consisting of water and insoluble rice starch primary particles causes an increase in the droplet temperature rather than a reduction of the drying rate. The compounds added are believed to change the course of droplet drying by reducing the surface water activity by either changing the chemical potential (salts) or forming a film with low water diffusivity (carbohydrates). This should be considered when altering a formulation containing temperature sensitive active ingredients.

An increased droplet temperature during drying was indicated by gelation of the rice starch.

No increase in droplet temperature nor a change in drying rate was observed when insoluble TiO_2 primary particles were added to the reference suspension of

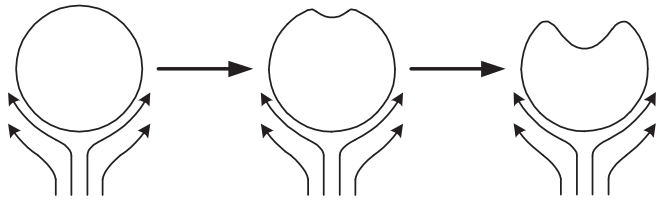

Figure 5.15: Formation of an indentation. After Büttiker[4].

water and rice starch. This is explained by the fact that an insoluble compound does not affect the chemical potential or form a film with low water diffusivity.

Observed morphologies include particles which are solid, have indentations or are hollow. Sequences for formation of the observed morphologies are given and explained in detail to contribute to the ongoing effort in the literature to understand morphology formation processes.

Acknowledgments

The authors are grateful for the support of the Novozymes Bioprocess Academy and the CHEC Research Centre.

5.8 References

[1] B. Adhikari, T. Howes, B. R. Bhandari, and V. Truong. Experimental studies and kinetics of single drop drying and their relevance in drying of sugar-rich foods: A review. *International Journal of Food Properties*, 3(3): 323–351, 2000.

[2] A. Apelblat and E. Korin. The vapour pressures of saturated aqueous solutions of sodium chloride, sodium bromide, sodium nitrate, sodium nitrite, potassium iodate, and rubidium chloride at temperatures from 227 K to 323 K. *Journal of Chemical Thermodynamics*, 30:59–71, 1998.

[3] A. Apelblat and E. Korin. The vapour pressure of water over saturated solutions of sodium sulfate, calcium bromide, ferric chloride, zinc nitrate, calcium nitrate, and lithium nitrate at temperatures from 278.15 K to 323.15 K. *Journal of Chemical Thermodynamics*, 34:1621–1637, 2002.

[4] R. Büttiker. *Erzeugung von Gleich Grossen Tropfen mit Suspendiertem und Gelöstem Feststoff und Deren Trocknung im Freien Fall*. PhD thesis, Eidgenössische Technische Hochschule Zürich, Switzerland, 1978.

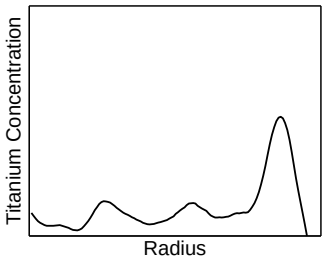

(a) 6.20 wt%.

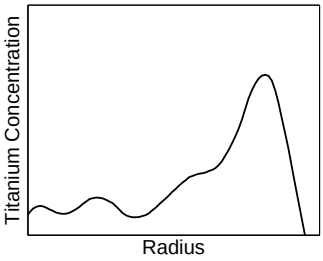

(b) 12.46 wt%.

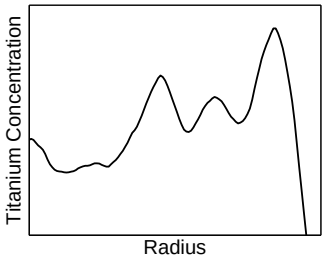

(c) 17.05 wt%.

Figure 5.16: Semi-quantitative titanium concentration profiles of the particles shown in figure 5.14. The subfigure captions give the amount of TiO_2 in the feed suspension.

[5] D. H. Charlesworth and W. R. Marshall. Evaporation from drops containing dissolved solids. *AIChE Journal*, 6(1):9–23, 1960.

[6] X. D. Chen. Heat-mass transfer and structure formation during drying of single food droplets. *Drying technology*, 22(1):179–190, 2004.

[7] H. W. Cheong, G. V. Jeffreys, and C. J. Mumford. A receding interface model for the drying of slurry droplets. *AIChE Journal*, 32(8):1334–1346, 1986.

[8] E. J. Crosby and W. R. Marshall. Effects of drying conditions on the properties of spray-dried particles. *Chemical Engineering Progress*, 54(7): 56–63, 1958.

[9] J. A. Duffie and W. R. Marshall. Factors influencing the propeties of spray-dried materials. *Chemical Engineering Progress*, 49(8):417–423, 1953.

[10] J. A. Duffie and W. R. Marshall. Factors influencing the propeties of spray-dried materials. 2. Drying studies. *Chemical Engineering Progress*, 49(9): 480–486, 1953.

[11] T. M. El-Sayed, D. A. Wallack, and C. J. King. Changes in particle morphology during drying of drops of carbohydrate solutions and food liquids - part 1: Effects of composition and drying conditions. *Industrial and Engineering Chemistry Research*, 29(10):2346–2354, 1990.

[12] I. D. Evans and D. R. Haisman. The effect of solutes on the gelatinization temperature range of potato starch. *Starch*, 34(7):224–231, 1982.

[13] M. Farid. A new approach to modelling of single droplet drying. *Chemical Engineering Science*, 58:2985–2993, 2003.

[14] C. Groenewold, C. Möser, H. Groenewold, and E. Tsotsas. Determination of single-particle drying kinetics in an acoustic levitator. *Chemical Engineering Journal*, 86:217–222, 2002.

[15] J. P. Hecht and J. King. Spray drying: Influence of developing drop morphology on drying rates and retention of volatile substances. 1. Single-drop experiments. *Industrial and Engineering Chemistry Research*, 39(6):1756–1765, 2000.

[16] K. Jørgensen. *Drying Rate and Morphology of Slurry Droplets*. PhD thesis, Technical University of Denmark, 2005.

[17] O. Kastner, G. Brenn, D. Rensink, and C. Tropea. The acoustic tube levitator - a novel device for determining the droplet kinetics of single droplets. *Chemical Engineering Technology*, 24(4):335–339, 2001.

[18] D. R. Lide, editor. *CRC Handbook of Chemistry and Physics*. Internet Version - http:/www.hbcpnetbase.com, Taylor and Francis, Boca Raton, FL, United States, 87th edition, 2007.

[19] J.-C. Lin and J. W. Gentry. Spray drying drop morphology: Experimental study. *Aerosol Science and Technology*, 37:15–32, 2003.

[20] S. J. Lukasiewicz. Spray-drying ceramic powders. *Journal of the American Ceramic Society*, 72(4):617–624, 1989.

[21] A. N. Malakhovskii. Drying kinetics of single drops by ferrite suspensions. *Soviet Powder Metallurgy and Metal Ceramics*, 19(3):76–78, 1980.

[22] K. Masters. *Spray Drying Handbook*. Longman Scientific and Technical, 5th edition, 1991.

[23] G. Meerdink. *Drying of Liquid Food Droplets - Enzyme Inactivation and Multicomponent Diffusion*. PhD thesis, Landbouwuniversiteit te Wageningen, The Netherlands, 1993.

[24] A. Millqvist-Fureby, M. Malmsten, and B. Bergenståhl. Spray drying of trypsin - surface characterisation and activity preservation. *International Journal of Pharmaceutics*, 188:243–253, 1999.

[25] H. Minoshima, K. Matsushima, H. Liang, and K. Shinohara. Basic model of spray drying granulation. *Journal of Chemical Engineering of Japan*, 34 (4):472–478, 2001.

[26] S. Nesic and J. Vodnik. Kinetics of droplet evaporation. *Chemical Engeering Science*, 46:527–537, 1991.

[27] W. E. Ranz and W. R. Marshall. Evaporation from drops - part 1. *Chemical Engineering Progress*, 48:141–146, 1952.

[28] W. E. Ranz and W. R. Marshall. Evaporation from drops - part 2. *Chemical Engineering Progress*, 48:173–180, 1952.

[29] Y. Sano and R. B. Keey. The drying of a spherical particle containing colloidal material into a hollow sphere. *Chemical Engineering Science*, 37 (6):881–889, 1982.

[30] A. S. Selivanov. Stabilization of cellulases using spray drying. *Engineering in Life Sciences*, 5(1):78–80, 2005.

[31] F. V. Shaw. Spray drying: A traditional process for advanced applications. *Ceramic Bulletin*, 69(9):1484–1489, 1990.

[32] D. A. Skoog, D. M. West, and F. J. Holler. *Fundamentals of Analytical Chemistry*. Saunders College Publishing, Orlando, FL, United States, 7 edition, 1996.

[33] J. Sloth, S. Kiil, A. D. Jensen, S. K. Andersen, K. Jørgensen, H. Schiffter, and G. Lee. Model based analysis of the drying of a single solution droplet in an ultrasonic levitator. *Chemical Engineering Science*, 61:2701–2709, 2006.

[34] G. Spigno and D. M. De Faveri. Gelatinization kinetics of rice starch studied by non-isothermal technique: Influence of extraction method, water concentration and heating rate. *Journal of Food Engineering*, 62:337–334, 2004.

[35] R. Toei and T. Furuta. Drying of a droplet in a non-supported state. *AIChE Symposium Series*, 78:111–117, 1982.

[36] R. Toei, M. Okazaki, and T. Furuta. Drying mechanisms of a non-supported droplet. In A. S. Mujumdar, editor, *Proceedings of the First International Drying Symposium*, pages 53–58, Princeton, United States, 1978. Science Press.

[37] K.-D. Vorlop and J. Breford. Verfahren und Vorrichtung zur Herstellung von Teilchen aus einem flüssige Medium. German Patent DE 4424998 A1, 1994.

[38] W. J. Walker Jr. and J. S. Reed. Influence of slurry parameters on the characteristics of spray-dried granules. *Journal of the American Ceramic Society*, 82(7):1711–1719, 1999.

[39] D. A. Wallack, T. M. El-Sayed, and C. J. King. Changes in particle morphology during drying of drops of carbohydrate solutions and food liquids - part 2: Effects on drying rate. *Industrial and Engineering Chemistry Research*, 29(10):2354–2357, 1990.

[40] A. L. Yarin, G. Brenn, O. Kastner, D. Rensink, and C. Tropea. Evaporation of acoustically levitated droplets. *Journal of Fluid Mechanics*, 339:151–204, 1999.

[41] A. L. Yarin, G. Brenn, O. Kastner, and C. Tropea. Drying of acoustically levitated droplets of liquid-solid suspensions: Evaporation and crust formation. *Physics of Fluids*, 14(7):2289–2298, 2002.

[42] I. Zbicinski. Development and experimental verification af momentum, heat and mass transfer model in spray drying. *Chemical Engineering Journal*, 58:123–133, 1995.

Chapter 6

A Combined Model of Drying and Inactivation

In chapters 3-5 the subjects of drying kinetics, enzyme inactivation and particle morphology formation have been treated somewhat separately. In this chapter, particularly the investigations of the drying kinetics and the enzyme inactivation are combined but in connection to this, elements of the morphology formation studies are discussed.

The purpose of the present chapter is to use and extend the work in the previous chapters in such a way that suggestions for improving operation of industrial spray dryers during production of enzyme containing particles may be put forward.

A model for the drying of a water droplet containing primary particles and dissolved material is presented. The model is based on the work of Abuaf and Staub [1] but various parts of the work presented in chapter 3 about the drying of a droplet containing dissolved solids are included. The new model is coupled to the enzyme inactivation model presented in chapter 4, enabling estimation of the enzyme activity loss during industrial scale spray drying. The influence of different process parameters on the severity of the activity loss is investigated. Finally, suggestions for improved spray dryer operation are presented.

The theoretical investigations of the drying rates and activity losses in the following are conducted using the four enzyme containing formulations also used in chapter 4.

In connection with the enzyme formulations a small digression must be made before commencing the model recapitulation. The specific compositions of the formulations are commercially sensitive and cannot be given in detail as mentioned in chapter 4. However, in the following it is important to distinguish between the different components of the formulations. Beside water, each formulation consists of four components which are referred to as the *carrier*, the

stabilizer, the *solute* and the *enzyme*. The carrier is insoluble in water while the stabilizer, the solute and the enzyme are soluble. A few further details on the formulations are given in table 6.1 and in the following the four formulations are simply referred to as *Formulation 1-4*.

Table 6.1: Enzyme containing formulations investigated both in the present chapter and in chapter 4. The amount of solute added to each formulation varies and the enzyme concentrate is included as a reference.

Formulation	Enzyme	Carrier	Stabilizer	Solute
1	Yes	Yes	Yes	No
2	Yes	Yes	Yes	1 unit
3	Yes	Yes	Yes	2 units
4	Yes	Yes	Yes	3 units
Concentrate	Yes	No	No	No

6.1 Model for Drying of Enzyme Containing Suspension Droplets

The model for simulating the drying rate of an enzyme containing particle is based on the work of Abuaf and Staub [1] as mentioned above. The model presented by Abuaf and Staub [1] is only valid for the drying of droplets consisting of a suspension of solvent and primary particles but not dissolved material. However, the objective of the modeling in this chapter is to describe the drying of the four different enzyme containing formulations. Droplets formed from feeds of these formulations consist of water and both insoluble primary particles and dissolved material. Therefore, the model of Abuaf and Staub [1] is extended so that it describes the drying of multi component droplets and the inactivation of enzyme.

The complete model divides the course of drying into two periods – the constant rate period and the falling rate period. A general description of the drying of a single droplet is given in section 2.2.1 on page 26 but the specific course of drying assumed by the model is shown in figure 6.1.

A) The first phase of drying (the constant rate period) starts when the droplet has been formed at the atomizing device in the spray dryer. Evaporation occurs and the liquid water mass decreases.

B) As the water evaporates the droplet continuously shrinks while the solid mass (dissolved and undissolved), obviously, remains constant.

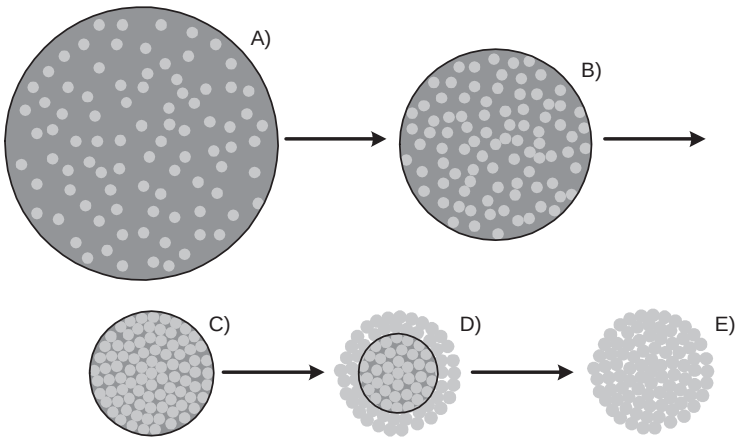

Figure 6.1: Course of drying for which the model is valid. Solid material is shown by a lighter color whereas the liquid solution is shown by a darker color. The black line indicates the position of the gas/liquid interface.

C) At a critical liquid to solid volume ratio the primary particles inside the droplet touch each other and the droplet can shrink no further. This marks the beginning of the second phase of drying (the falling rate period).

D) In the second phase of drying, the droplet (which is actually now a particle) is a porous sphere with a dry outer crust and a wet core at the center. The wet core shrinks due to evaporation and water vapor is transported by diffusion through the pores of the crust to the particle surface. As the wet core recedes into the particle the dissolved material precipitates at the interface between the crust and the core, partly filling the pores of the crust.

E) The particle is dry when the wet core has evaporated entirely.

The kinetic model describing the course of drying calculates both the droplet moisture content and the droplet temperature. However, an additional feature of the model is that it calculates the enzyme activity loss during drying. The mathematical equations for these calculations are given below but first the assumptions leading to the equations are stated and explained in detail.

6.1.1 Model Assumptions

The model is based on a number of assumptions which serve to simplify the calculations of the drying rate and enzyme activity loss. The most important

assumptions of the model include:

1. The course of drying follows that given in figure 6.1 and the final particle morphology is as shown in figure 6.1 E.
2. All formulations follow the same course of drying.
3. The droplet/particle remains spherical throughout the course of drying and evaporation occurs at the same rate from the entire core/droplet surface.
4. The primary particles are small compared to the total droplet diameter, i.e. the size difference is about two orders of magnitude.
5. When forced together the primary particles pack randomly into a dense structure.
6. A component with high solubility precipitates in the particles pores during the falling rate period whereas a component with low solubility precipitates during the constant rate period.
7. The distributions of the primary particles and dissolved compounds are uniform in the droplet. That is, there are no concentration gradients in the radial direction.
8. The temperature distribution is uniform in the entire droplet during the constant rate period and in the wet core during the falling rate period.
9. The water vapor pressure at the gas/liquid interface may be found from a desorption isotherm.
10. During the falling rate period there are no capillary forces which draw liquid from the wet core through the crust to the surface.
11. There is no accumulation of water vapor in the crust or in the immediate vicinity (i.e. in the film layer) of the droplet/particle.
12. Though the crust is considered to be *dry* the crust may contain a small fraction of water. In fact, there is assumed to be equilibrium between the amount of water vapor in the pores and the amount of water in the solid material of the crust.

In chapter 5 as well as in section 2.2.2 particle morphology formation is investigated in detail. Chapter 5 explains how small changes in the feed composition may drastically change the final particle morphology. Thus, it is difficult to predict if assumption 1 holds true. Many of the particles shown in chapter 5 are hollow but these particles are dried at an elevated temperature (150°C) and

as explained in section 2.2.2 lower drying temperatures are more likely to form non-hollow particles. This renders assumption 1 plausible because the temperatures used in the model simulations (in section 6.2) are in the range $70 - 85°C$. Furthermore, it appears reasonable to assume that a shrinking core surrounded by a dry crust exists in the falling rate period. The existence of a wet core during drying of suspension droplets is indicated by the results shown in figure 5.6 on page 112.

Assumption 2 is made to ensure that the comparisons of drying rates and activity losses between each formulation are done using the same conditions. Investigating the influence of the individual formulations on the course of drying is outside the scope of this chapter.

Assumption 3 is closely related to assumption 1. During the constant rate period the droplet is obviously spherical because of the effect of the water surface tension but the sphericity during the falling rate period depends on the morphology formation. If the particle collapses, displays blow holes, craters, cavities, fractures or the like, the sphericity is lost. However, the enzyme containing formulations treated in this chapter are dried at low and moderate temperatures (as explained above) and according to section 2.2.2 it is therefore likely that the particle remains spherical during the falling rate period.

In the enzyme containing formulations treated in this chapter, the carrier is insoluble in water and thereby constitutes the primary particles. The average size of the primary particles is about 5 µm (no reference is given because the nature of the carrier is commercially sensitive) while the initial droplet size during industrial spray drying of the enzyme in question is about 150 µm. Thus, the droplet size is about 30 times larger than the primary particle size, rendering assumption 4 reasonable.

The packing of particles is difficult to predict but the subject is investigated by German [4]. Assumption 5 is made to provide for a theoretical estimate of the porosity marking the transition between the constant and the falling rate period. The specific value is given later.

Estimates have been conducted to verify assumption 6. First, there are three dissolved components in each of the four formulations – the solute and the stabilizer which have high solubilities and the enzyme which in comparison has a low solubility. The estimate calculations show that almost all of the enzyme precipitates during drying at the end of the constant rate period. Evidently, the solution present in the pores of the particle at the beginning of the falling rate period is saturated with enzyme. This is, however, neglected and it is assumed that all enzyme precipitates during the constant rate period.

Further, the estimates show that the stabilizer and the solute do not precipitate during the constant rate period when using formulation 1 and 2. The solute is very close to precipitation in Formulation 3 while the solute in Formulation

4 reaches saturation prior to the falling rate period. It is, however, assumed that the solute does not precipitate and that the liquid of the droplet is supersaturated until the falling rate period commences. It is chosen to assume this because the course of drying would otherwise vary between the individual formulations and thereby conflict with assumption 2.

Assumption 7 states that there are no concentration gradients inside the droplet. Thus, the assumption contradicts the conclusions drawn in chapter 3 where it is shown that concentration gradients develop near the surface of a drying droplet which contains dissolved solids (see e.g. figure 3.15 on page 74). The high surface concentration slows the drying and the present model might therefore underestimate the total drying time. However, the assumption mentioned is imposed on the model because it greatly simplifies the mathematical equations for the drying rate simulations and ease the model parameter estimation. The latter especially concerns the diffusion coefficients of the dissolved compounds in water. These are difficult to determine as described in chapter 3 and they are needed if assumption 7 is discarded.

In sections 3.1.2 and 3.5.2 the Biot number is discussed in detail. This number may be used to estimate whether the temperature distribution inside a drying droplet is uniform and may thereby be used to evaluate assumption 8. It is calculated that the drying droplets investigated in this chapter have a maximum Biot number of approximately 0.1 which as found in chapter 3 gives a droplet temperature distribution that is very close to uniform.

All of assumptions 9, 10, 11 and 12 appear reasonable but assumption 12 requires further explanation. As the wet core recedes into the droplet the newly formed crust cannot completely dry because water vapor is present in the pores. Assumption 12 simply states that there is a well-defined equilibrium between the vapor in the pores and the water in the crust.

The assumptions stated and discussed above greatly simplifies the model. Indeed, the model may not describe all phenomena of the drying process with high accuracy. Nevertheless, the model provides for basic calculations of both the drying rate and the enzyme activity loss.

6.1.2 Model Equations

Based on the course of drying shown in figure 6.1 and the assumptions given in the previous section mathematical equations for the drying rate and the enzyme activity loss may be set up. As mentioned above the drying rate is calculated separately for the constant rate period and for the falling rate period. Also, the activity loss is calculated subsequent to the drying. This is described further in section 6.1.4 where the strategy for solving the equations is explained.

The equations given contain a number of parameters which may be constant or

a function of e.g. temperature or moisture concentration. Values and functions assigned to these parameters are given in a separate section below.

Constant Rate Period

During the constant rate period, the rate of evaporation is modeled to be controlled by the gas phase mass transfer resistance. Thus, the droplet is surrounded by a film layer through which evaporated water is transported to the ambient air. The driving force of this transport is a difference in water vapor mole fractions between the droplet surface and the bulk phase. Also, solids (dissolved and primary particles) do obviously not evaporate and the decrease in droplet mass may by calculated as

$$\frac{\mathrm{d}m_d}{\mathrm{d}t} = \frac{\mathrm{d}m_w}{\mathrm{d}t} = -k_m 4\pi r_d^2 \frac{M_w P_{tot}}{R_g T_{av}} \left(y_{v,sur} - y_{v,\infty}\right) \tag{6.1}$$

where m_d is the total droplet mass and m_w is the mass of water in the droplet. The film layer mass transfer coefficient is k_m while $y_{v,sur}$ and $y_{v,\infty}$ are, respectively, the water vapor mole fractions at the droplet surface and in the bulk phase. Finally, T_{av} is the average temperature in the film layer. The equation is analogue to equation (3.8) of the model for drying of solution droplets.

Note that there is a list of symbols on page 150 which, however, applies to this chapter only.

The droplet size decreases during constant rate period drying, necessitating calculations of the droplet radius as a function of time

$$\frac{\mathrm{d}m_w}{\mathrm{d}t} = 4\pi r_d^2 \rho_w \frac{\mathrm{d}r_d}{\mathrm{d}t} \tag{6.2}$$

where r_d is the droplet radius and ρ_w is the water density.

Further, it is necessary to calculate the droplet temperature as it affects the rate of enzyme activity loss along with several model parameters. It is assumed that the droplet temperature distribution is uniform, leading to the following energy balance for the droplet

$$\underbrace{(m_s C_{p,s} + m_w C_{p,w} + m_z C_{p,z})\frac{\mathrm{d}T_d}{\mathrm{d}t}}_{\text{Heating}} = \underbrace{h 4\pi r_d^2 (T_\infty - T_d)}_{\text{Transferred}} + \underbrace{\lambda \frac{\mathrm{d}m_w}{\mathrm{d}t}}_{\text{Evaporation}} \tag{6.3}$$

Here, $C_{p,s}$, $C_{p,w}$ and $C_{p,z}$ are, respectively, the heat capacity of solids, water and dissolved material. The heat transfer coefficient between the droplet and the bulk phase is denoted h whereas λ is the heat of evaporation of water. The equation is analogous to equation (3.14) which is a boundary condition for the heat balance in the model for drying of solution droplets described in chapter 3.

Thus, equation (6.3) states that heat transferred to the droplet from the bulk phase is used either for evaporation or droplet heating.

As shown during the parameter estimation on page 134 the relative velocity between the droplet and the drying gas greatly influences the transport of water vapor from the droplet surface to the bulk phase. The relative velocity v between the droplet and the drying gas may be calculated by a force balance equation. The equation states that the acceleration force is equal to the sum of the gravity, buoyancy and drag forces [21]

$$\frac{\mathrm{d}v}{\mathrm{d}t} = \left(1 - \frac{\rho_g}{\rho_d}\right) g - \frac{C_D \rho_g v^2 \pi r_d^2}{2 m_d} \tag{6.4}$$

C_D is the droplet drag coefficient.

The four ordinary differential equations (6.1)-(6.4) allow for determination of the development in droplet mass (i.e. the drying rate) and the droplet temperature throughout the constant rate period. However, one additional algebraic equation is needed to find the point in time where the transition between the constant and the falling rate period occurs. The transition occurs when the primary particles have packed as closely as possible – a specific porosity is reached. The value of this porosity is given later but the porosity ε of the drying droplet is tracked as follows

$$\varepsilon = 1 - \frac{1}{1 + \frac{\rho_s m_l}{\rho_l m_s}} \tag{6.5}$$

where m_l is the mass of the liquid phase (water and dissolved solids). The latter term of (6.5) is simply the solid volume fraction of the droplet.

Falling Rate Period

As explained earlier, the drying in the falling rate period proceeds as the drying of a particle. The particle has pores which are filled with water that starts to evaporate. The wet core interface recedes into the droplet and the crust thickens, providing an increasing resistance to mass transfer. The radius of the receding wet core r_i can be found by

$$\frac{\mathrm{d}r_i}{\mathrm{d}t} = \frac{r_p}{3 m_{w,e}^{1/3} m_w^{2/3}} \frac{\mathrm{d}m_w}{\mathrm{d}t} \tag{6.6}$$

r_p and $m_{w,e}$ are, respectively, the particle radius and the mass of water at the beginning of the falling rate period.

Again, it is noted that there is a list of symbols on page 150.

The transport of vapor from the particle surface to the bulk phase is calculated from an expression similar to (6.1)

$$\frac{\mathrm{d}m_w}{\mathrm{d}t} = -k_m 4\pi r_p^2 \frac{M_w P_{tot}}{R_g T_{av}} \left(y_{v,o} - y_{v,\infty}\right) \tag{6.7}$$

where $y_{v,o}$ is the water vapor fraction at the particle surface.

Also, the change in liquid water mass may be calculated from equation (6.8) which considers a Stephan type diffusion through the crust

$$\frac{\mathrm{d}m_w}{\mathrm{d}t} = -\frac{4\pi}{\frac{1}{r_p}-\frac{1}{r_i}}\frac{M_w\mathcal{D}_{v,eff}P_{tot}}{T_{av,c}R_g}\ln\left\{\frac{1-y_i}{1-y_{v,o}}\right\} \tag{6.8}$$

where $\mathcal{D}_{v,eff}$ is the effective diffusion coefficient of water vapor through the crust.

Both equation (6.7) and equation (6.8) have the two unknown quantities m_w and $y_{v,o}$. To eliminate $y_{v,o}$ equation (6.7) is substituted into equation (6.8)

$$\frac{\mathrm{d}m_w}{\mathrm{d}t} = -\frac{4\pi}{\frac{1}{r_p}-\frac{1}{r_i}}\frac{M_w\mathcal{D}_{v,eff}P_{tot}}{T_{av,c}R_g}\ln\left\{\frac{1-y_i}{1-y_{v,\infty}+\frac{R_gT_{av}}{k_m4\pi r_p^2M_wP_{tot}}\frac{\mathrm{d}m_w}{\mathrm{d}t}}\right\} \tag{6.9}$$

Next, an equation for the wet core temperature T_i may be set up analogously to equation (6.3). That is, the equation is an energy balance which states that heat transferred to the wet core is either used for heating or evaporation

$$\underbrace{\frac{T_\infty - T_i}{\frac{1}{4\pi r_p^2 h}+\frac{r_p-r_i}{4\pi r_p r_i k_{h,c}}}}_{\text{Transferred}} = \underbrace{-\lambda\frac{\mathrm{d}m_w}{\mathrm{d}t}}_{\text{Evaporation}} + \underbrace{(m_{s,i}C_{p,s}+m_{w,i}C_{p,w}+m_{z,i}C_{p,z})\frac{\mathrm{d}T_i}{\mathrm{d}t}}_{\text{Heating}} \tag{6.10}$$

The term for the amount of heat transferred to the wet core is quite different from the corresponding term of equation (6.3). The term in the equation above includes both transport resistance in the film layer surrounding the particle and transport resistance in the porous crust. The thermal conductivity coefficient is denoted $k_{h,c}$ while $m_{x,i}$ is the mass of compound x in the wet core. Sensible heating of the crust is neglected.

During the model parameter estimation below it is necessary to know the particle surface temperature T_o. This quantity is found from the heat transport through the film layer and crust

$$T_o = T_\infty - \frac{\frac{1}{hr_p^2}}{\frac{1}{hr_p^2}-\frac{r_p-r_i}{r_pr_ik_{h,c}}}\cdot(T_\infty - T_i) \tag{6.11}$$

Also, as stated in assumption 12 there is equilibrium between the amount of water vapor in the pores and the amount of water in the solid material of the crust. Thus, to find the amount of water in the solid material, it is necessary to first calculate vapor content in the pores of the crust. However, the vapor content is dependent on the position in the crust – at the interface between the crust and the wet core the vapor pressure of water is found from a desorption

isotherm but it is much lower at the particle surface. From assumption 11 the following may be derived accounting for one-way diffusion through the crust

$$y_v = 1 - (1 - y_i) \left(\frac{1 - y_s}{1 - y_i} \right)^{\left(\frac{1/r_i - 1/r}{1/r_i - 1/r_s} \right)} \tag{6.12}$$

where the $r \in [r_i, r_p]$ and y_v is the fraction of vapor in the pores corresponding to the position r. The particle surface vapor fraction $y_{v,o}$ may be calculated from equation (6.7) when the derivative of the mass of water has been determined from equation (6.9). The relation between the vapor fraction and the crust water content is found in section 6.1.3.

Finally, the relative velocity between the particle and the drying gas is found equivalently to equation (6.4)

$$\frac{\mathrm{d}v}{\mathrm{d}t} = \left(1 - \frac{\rho_g}{\rho_d} \right) g - \frac{C_D \rho_g v^2 \pi r_p^2}{2 m_d} \tag{6.13}$$

Combined equations (6.6), (6.9), (6.10), (6.11) and (6.13) allow for calculations of the drying rate (particle mass change) and temperature development during the falling rate period.

Enzyme Inactivation

The model for the drying given above determines the droplet moisture content and temperature as a function of time. Thus, the equations for the enzyme inactivation may be used as stated in chapter 4 where the equations also are explained in detail.

$$\frac{\mathrm{d}X}{\mathrm{d}t} = k \left(1 - X \right) \tag{6.14}$$

where X is the fraction of enzyme activity lost while k is given by

$$k = k_0 w_w^n \exp \left(\frac{-E_a}{R_g} \left[\frac{1}{T} - \frac{1}{T^*} \right] \right) \tag{6.15}$$

6.1.3 Parameter Estimation

The equations constituting the model for the drying process, including the enzyme activity loss, contain a number of parameters which are treated in this section. Key parameters are discussed below while other parameters are given in table 6.2.

Table 6.2: Parameters of the combined model for simulations of drying kinetics and enzyme inactivation. Examples of specific values are given at 25°C and 1 atm for parameters which are functions of the temperature and the ambient pressure. Key parameters are given in the text.

Parameter	Meaning	Value	Remarks	References
$\mathcal{D}_v$	Diffusion coefficient of water vapor in air	$2.501 \cdot 10^{-5}$ $^{m^2}/_{s}$	Function of T, P_{tot}. Calculated using correlation from reference.	[17]
μ_g	Air viscosity	$1.847 \cdot 10^{-5}$ Pa s	Function of T. Calculated using correlation from reference.	[6]
ρ_g	Air density	1.185 $^{kg}/_{m^3}$	Using the ideal gas law. ($\rho_g = {}^{P_{tot}M_g}/_{R_gT}$)	–
M_g	Air molar mass	0.02898 $^{kg}/_{mole}$	–	[10]
$C_{p,g}$	Air heat capacity	1007 $^{J}/_{kg\ K}$	–	[10]
λ	Heat of evaporation for water	2444 $^{J}/_{g}$	Function of T. Calculated using correlation from reference.	[22]
$P_{v,sat}$	Saturated water vapor pressure	0.0313 atm	Function of T. Using the Antoine equation	[3]
T_{av}	Film layer temperature	–	Arithmetical mean between droplet surface and bulk phase temperatures. ($T_{av} = {}^1/_2(T_\infty + T_d)$)	–

continued on next page

continued from previous page

Parameter	Meaning	Value	Remarks	References
$C_{p,s}$	Heat capacity of solids	1650 $^{\mathrm{J}}/_{\mathrm{Kg\ K}}$	Nature of compound commercially sensitive – no reference given.	–
$C_{p,w}$	Heat capacity of water	4154 $^{\mathrm{J}}/_{\mathrm{kg\ K}}$	Function of T. Calculated using quadratic polynomial from reference.	[22]
$C_{p,z}$	Heat capacity of dissolved material	1650 $^{\mathrm{J}}/_{\mathrm{Kg\ K}}$	Nature of compound commercially sensitive – no reference given.	–
$k_{h,g}$	Air heat conductivity	$5.88 \cdot 10^{-2}$ $^{\mathrm{J}}/_{\mathrm{s\ m\ K}}$	Function of T. Polynomial fitted to data of reference.	[19]
ε_e	Porosity marking end of constant rate period	0.38	Based on assumption 5.	[9, 16]
$T_{av,c}$	Crust temperature	–	Arithmetical mean between wet core and particle surface temperatures. ($T_{av,c} = {}^1\!/_2(T_i + T_o)$)	–
$k_{h,c}$	Crust thermal conductivity	–	$k_{h,c} = (1-\varepsilon)\, k_{h,s}$ where $k_{h,s}$ is the thermal conductivity of the solids. $k_{h,s} = 0.30$ $^{\mathrm{J}}/_{\mathrm{s\,m\,K}}$.	[1, 18]

Film Layer Mass Transfer Coefficient

The first parameter addressed is the mass transfer coefficient k_m in the film layer between the droplet surface and the bulk phase used in equation (6.1). The mass transfer coefficient is estimated from the Sherwood number Sh, using the correlation given by Renksizbulut and Yuen [20]

$$Sh = \frac{2k_m r_d}{\mathcal{D}_v} = \frac{2 + 0.6\,(Sc)^{1/3}\,(Re)^{1/2}}{(1 + B_T)^{0.7}} \tag{6.16}$$

where Sc and Re are, respectively, the Schmidt and Reynolds numbers

$$Sc = \frac{\mu_g}{\rho_g \mathcal{D}_v} \tag{6.17}$$

$$Re = \frac{2\rho_g v r_d}{\mu_g} \tag{6.18}$$

and B_T is the Spalding number which accounts for the blowing effect caused by water evaporating from the surface

$$B_T = \frac{C_{p,g}\,(T_\infty - T_d)}{\lambda} \tag{6.19}$$

Film Layer Heat Transfer Coefficient

The heat transfer coefficient h in the film layer between the droplet surface and the bulk phase used in equation (6.3) is determined equivalently to the mass transfer coefficient. According to Renksizbulut and Yuen [20] the following correlation for the Nusselts number may be used

$$Nu = \frac{2hr_d}{k_{h,g}} = \frac{2 + 0.6\,(Pr)^{1/3}\,(Re)^{1/2}}{(1 + B_T)^{0.7}} \tag{6.20}$$

where $k_{h,g}$ is the air heat conductivity while Pr is the Prandtl number

$$Pr = \frac{C_{p,g}\mu_g}{k_{h,g}} \tag{6.21}$$

Drag Coefficient

For calculations of the droplet velocity in equation (6.4) the drag coefficient is needed. The following is valid for all Reynolds numbers [8]

$$C_D = \frac{24}{Re} + 3.3643 Re^{-0.3471} + \frac{0.4607 Re}{Re + 2682.5} \tag{6.22}$$

Parameters in the Falling Rate Period

The correlations for the mass and heat transfer coefficients and the drag coefficient given above only apply in the constant rate period. The correlations also apply in the falling rate period if the variables in the equations are substituted with the corresponding variables of the falling rate period, e.g. r_d must be substituted with r_p in equation (6.18). These substitutions are, however, trivial and correlations for the three parameters mentioned during the falling rate period are not given. Still there is the effective diffusion coefficient which is only needed for simulations of the falling rate period.

Effective Diffusion Coefficient

The effective diffusion coefficient $\mathcal{D}_{v,eff}$ is included in equation (6.9) to account for the retarding effect which the crust has on the water vapor diffusion from the wet core to the particle surface. Abuaf and Staub [1] use the following expression for the effective diffusion coefficient

$$\mathcal{D}_{v,eff} = \mathcal{D}_v \varepsilon^b \tag{6.23}$$

where $b = 1$. This value is based on the assumption that the capillary channels of the crust are straight – the tortuosity τ equals 1. However, according to Wakao and Smith [23] there is an approximately inverse relationship between the porosity and the tortuosity, i.e. $\varepsilon/\tau = \varepsilon^2$. The value of $b = 2$ in equation (6.23) is used in this work.

Interface Water Vapor Pressure and Crust Water Content

The last parameters to be determined are the water vapor pressure at the liquid/gas interface and the crust moisture content. The former applies both in the constant and falling rate periods whereas the latter applies in the falling rate period only. Both parameters are found from desorption isotherms.

The isotherms were found experimentally using a Hiden Analytical Ltd. IGAsorp moisture sorption analyzer. The equipment is only briefly described here because the experiments are not pivotal but details are given by Kringelum [7]. A sample of a few milligrammes of a powder was placed inside a preconditioned chamber. A constant temperature of 25°C was imposed along with a well-defined relative humidity. The experiment was initiated at $RH = 0\,\%$ and the humidity was increased in steps of 10 %. When equilibrium between the humidity and powder moisture content was attained at a given humidity, the amount of water absorbed by the sample was determined by weighing. After the measurement at the maximum relative humidity of 90 % was obtained, a series

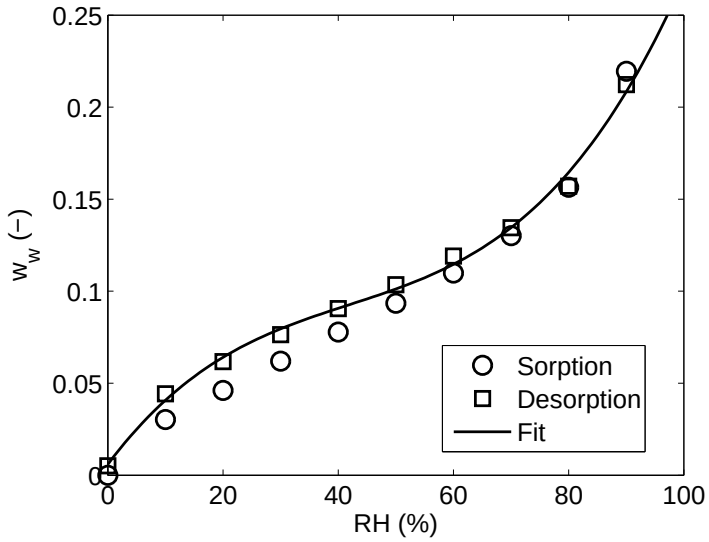

Figure 6.2: Sorption and desorption of moisture in a sample of enzyme powder at different relative humidities. A polynomial fit to the desorption data is included.

of measurements using stepwise decreasing humidities was conducted, giving the desorption isotherm.

An example of a data set obtained for freeze dried powder of the enzyme is shown in figure 6.2 along with a cubic polynomial fitted to the desorption curve. The desorption data is chosen because it is assumed to resemble drying better than the sorption data. The polynomial is given by

$$w_{w,e} = 6.00 \cdot 10^{-7} RH^3 - 7.54 \cdot 10^{-5} RH^2 + 4.18 \cdot 10^{-3} RH + 5.91 \cdot 10^{-3} \quad (6.24)$$

where $w_{w,e}$ is the equilibrium moisture content in the enzyme.

The individual components in a given formulation each have a specific desorption curve. These were determined experimentally as described above or found in the work of Kringelum [7] and polynomials were fitted to find an expression equivalent to (6.24) for each formulation compound, i.e. the solute, the stabilizer, and the carrier. To find the relative humidity at the liquid/gas interface the four polynomials are solved simultaneously with a relation that couples the total droplet (or wet core) water content to the equilibrium moisture content of each formulation compound

$$w_w = \frac{\sum_x w_{w,x} m_x}{m_{tot}} \quad (6.25)$$

where $w_{w,x}$ is the equilibrium moisture mass fraction of component x. Equation (6.25) is taken from the work of Dalton and Hancock [2].

In order to determine the enzyme activity loss in the particle crust during drying from (6.14), it is necessary to calculate the moisture content of the crust. As stated in assumption 12 there is equilibrium between the water content of the crust and the amount of vapor in the pores. The latter is readily calculated from equation (6.12) when the relative humidity at the wet core interface has been found as described above. The crust moisture content is then determined from the desorption polynomials and equation (6.25).

Determination of the relations for calculating the amount of water present in the crust completes the estimation of key parameters. A model capable of simulating the drying rate and enzyme activity loss during drying of a single droplet consisting of an enzyme containing suspension is now set up. However, before any results are presented the strategy for solving the model equations is briefly explained.

6.1.4 Solution Strategy

The model may be solved in subsequent parts. First, initial conditions are set (these are given in section 6.2), then the developments in droplet mass and temperature during the constant rate period are calculated. After this, the drying during the falling rate period is simulated followed by some intermediate calculations needed for determination of the enzyme activity loss during the entire course of drying which is done next. Finally, a few post processing calculations are conducted. Each of the steps mentioned are briefly explained in this section. All the equations of the model – differential and algebraic – are solved using the standard tools available in MATLAB.

Setting the initial conditions and solving the model for the constant rate period is straightforward. The four ordinary differential equations (6.1)-(6.4) are simply solved using the built-in MATLAB differential equation solver. Parameters which are dependent on e.g. the droplet temperature are calculated during the simulations along with the water vapor mass fraction at the liquid/gas interface which is found from the desorption isotherms. The calculations of constant rate period drying are terminated when the porosity has decreased to a prespecified value (ε_e).

The results from the constant rate period are used as initial conditions for the falling rate period. Here, equations (6.6), (6.9), (6.10) and (6.13) are solved in MATLAB. However, at the beginning of the falling rate period the shrinking core radius is equal to the particle radius ($r_i = r_p$), leading to a discontinuity in equation (6.9). To resolve this, the initial shrinking core radius is manually set to a value slightly smaller than the particle radius.

Furthermore, determination of the heat transfer coefficient needed in equation (6.10) requires calculation of the particle surface temperature by equation (6.11)

which again requires calculation of the heat transfer coefficient. Therefore, equation (6.11) is solved by successive iteration. Also, the time derivative of m_w appears on both the left and the right hand sides of equation (6.9) and is therefore solved for by Newton-Raphson iteration. The simulations of the falling rate period drying are terminated when the wet core radius has decreased to zero ($r_i = 0$).

Next, the vapor fraction y_v is calculated at different positions in the crust as a function of time during the falling rate period using equation (6.12) and subsequently the moisture contents at these positions are determined from the desorption polynomials and equation (6.25). These values are needed for the final part of the simulation which is to find the enzyme activity loss.

The enzyme activity loss is found from equations (6.14) and (6.15). The activity loss may be calculated subsequent to the drying process simulations because the activity loss is decoupled from the rest of the model. That is, the activity loss does not influence the drying process in terms of drying rate and temperature development.

Using the approach explained above, the crust moisture content is calculated at different radial positions, entailing that the activity loss is also determined at different positions. To find the overall activity loss in the particle at a given point in time, the following relation is used

$$X_{tot}(t) = \frac{3}{r_p^3} \int_0^{r_p} r^2 X(r,t) \mathrm{d}r \tag{6.26}$$

6.2 Results and Discussion

The model and the parameters presented above are now used to simulate the drying of droplets consisting of enzyme containing formulations. The focus is on industrial applications and therefore relevant process parameters are determined based on the work of Masters [11, 12]. In the following, the influence of varying the process parameters on the total drying time and the enzyme inactivation is investigated. During the investigations a series of simulations is carried out and the results are compared to the results of the so-called *reference simulation* which is conducted using the initial conditions and process parameters given in table 6.3. However, before the effect of altering process variables is investigated the drying behavior of a single droplet is analyzed, using the reference simulation.

Drying Behavior

The reference simulation shows that most of the drying takes place in the constant rate period (figure 6.3) though the time span of this period is very small

Table 6.3: Initial conditions and process parameters for the reference simulation.

Initial conditions	Process parameters
$T_d = 25°C$	$RH = 20\,\%$
$r_d = 75\,\mu m$	$T_\infty = 80°C$
$v = 15\,{}^{m}/_{s}$	$P_{tot} = 1\,atm$
$w_z = 0.11$	$F^1 = 4$
$w_s = 0.38$	

[1]Formulation as used in chapter 4 and given in table 6.1

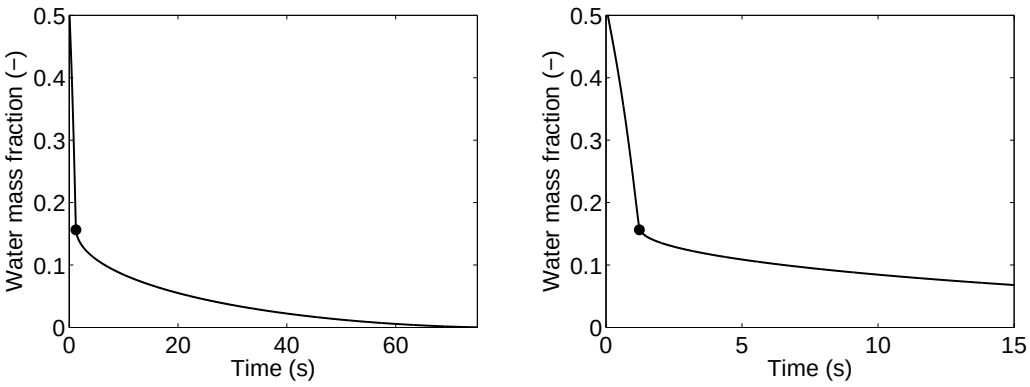

(a) Entire course of drying.

(b) First part of drying.

Figure 6.3: Droplet water content during drying of a single droplet. The dot marks the transition between the constant rate period and the falling rate period. The results are from the reference simulation.

compared to the total drying time. The drying rate is significantly lowered when the particle enters the falling rate period. Thus, the crust poses a large resistance to mass (vapor) transfer which is consistent with the findings of chapter 3 where it is concluded that the drying rate during the falling rate period is controlled by internal mass transport. Figure 6.3 does not include the moisture in the crust which is in equilibrium with the water vapor in the pores. The amount of moisture in the crust is shown in figure 6.8 and discussed below.

The lowering of the drying rate in the falling rate period causes an increase in the particle temperature (figure 6.4). This is in agreement with the description of the process of single droplet drying in section 2.2 and also with the conclusions of chapter 3. Furthermore, in chapter 3 it is found that there is only a very small temperature gradient in the radial direction of a drying droplet. Indeed,

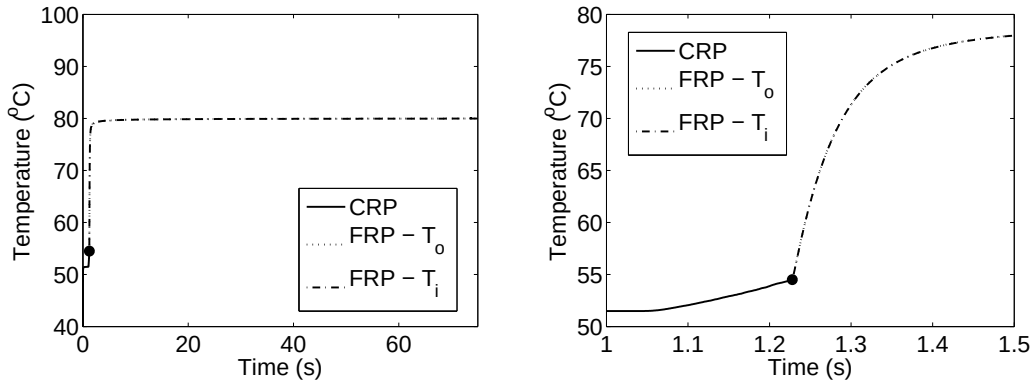

(a) Entire course of drying.

(b) Transition between constant and falling rate period.

Figure 6.4: Temperatures during drying of a single droplet – the lines for the wet core temperature (T_i) and the surface temperature (T_o) overlap. The dot marks the transition between the constant rate period (CRP) and the falling rate period (FRP). The results are from the reference simulation.

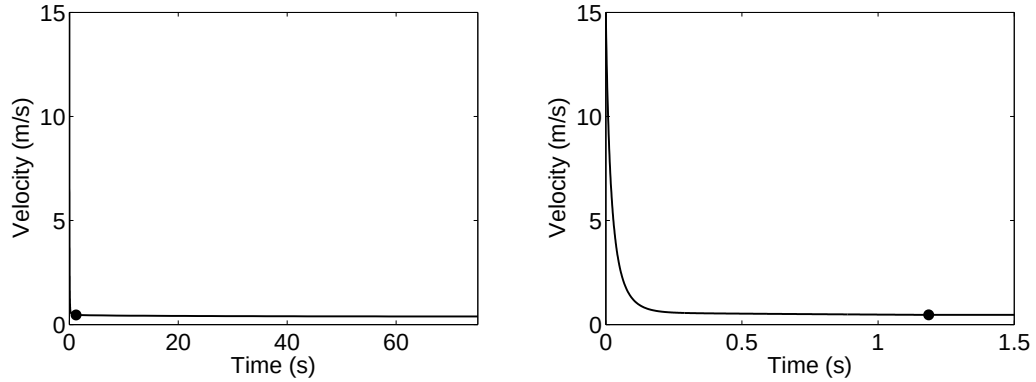

(a) Entire course of drying.

(b) First part of drying.

Figure 6.5: Droplet velocity during drying. The dot marks the transition between the constant rate period and the falling rate period. The results are from the reference simulation.

the reference simulation shows that the wet core temperature lags a maximum of 0.3°C behind the surface temperature during the falling rate period. As expected the droplet temperature in the constant rate period attains a value of 51.5°C which is close to the wet bulb temperature of 49.5°C [13] (the wet bulb temperature is described in section 2.2). Interestingly, the temperature increases slightly at the end of the constant rate period due to evaporation

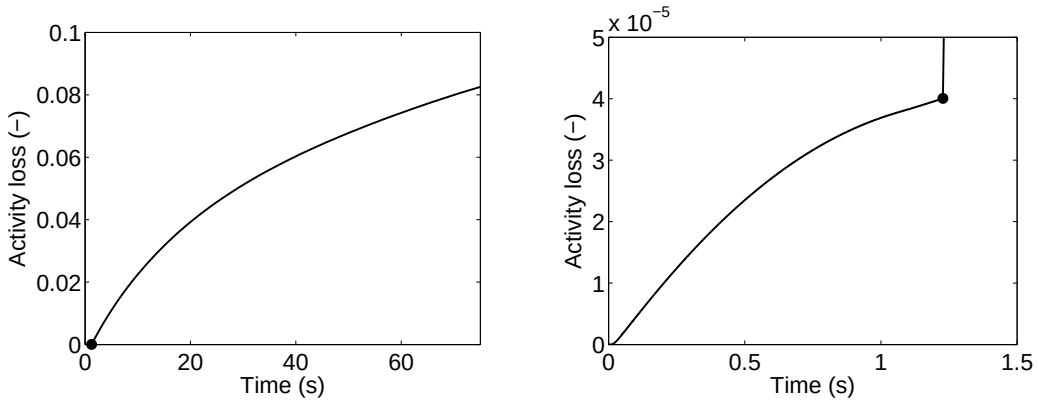

(a) Entire course of drying. (b) First part of drying.

Figure 6.6: Activity loss during drying. The dot marks the transition between the constant rate period and the falling rate period. The results are from the reference simulation.

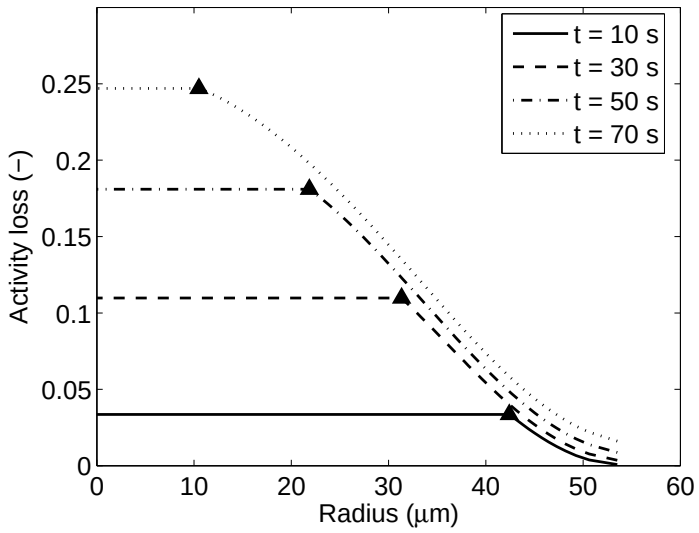

Figure 6.7: Enzyme activity loss inside a particle at different time points during the falling rate period. The abscissa indicates the position in the particle from the particle center (at $r = 0$) to the particle surface (at $r \approx 55$ µm). The triangles show the position of the interface between the wet core and the crust.

hindrance. As the solid mass fraction in the droplet builds up, the relative humidity at the droplet surface decreases which retards the drying and slightly increases the temperature.

Overall, the model calculated developments in droplet water content and tem-

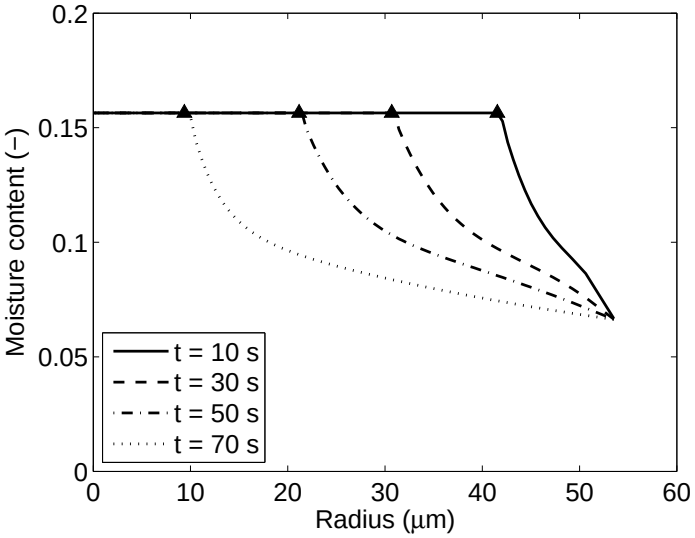

Figure 6.8: Moisture content inside a particle at different points in time during the falling rate period. The abscissa indicates the position in the particle from the particle center (at $r = 0$) to the particle surface (at $r \approx 55\,\mu\text{m}$). The triangles show the position of the interface between the wet core and the crust. The moisture content of the crust is that in equilibrium with the water vapor in the pores.

perature are consistent with the findings of chapter 3 and section 2.2.

Also, as concluded in chapter 3 the drying rate during the constant rate period is limited by mass and heat transfer in the film layer between the droplet surface and the surroundings. Thus, the droplet velocity might be expected to have a significant influence on the course of drying as a high velocity evidently increases the rate of mass and heat transfer in the film layer. However, as shown in figure 6.5 the droplet quickly decelerates from the initial velocity of $15\,{}^{\text{m}}/_{\text{s}}$ to the terminal velocity. Throughout the remaining part of the drying, the droplet experiences further – but only slight – deceleration because of mass loss.

As shown in chapter 4 the enzyme inactivation during drying of a single droplet is highly dependent on the droplet temperature and moisture content. The reference simulation shows (figure 6.6) that the enzyme inactivation takes place almost entirely during the falling rate period although the droplet has the highest water concentration in the constant rate period. This is explained by the fact that the droplet temperature remains low in the constant rate period. Furthermore, the constant rate period only constitutes a small part of the total drying time. The elevated temperature in the falling rate period speeds up the inactivation reaction but as drying progresses the rate of inactivation falls because the particle water content decreases.

Simulations of drying of enzyme containing droplets conducted by Meerdink [14], Wijlhuizen et al. [24] and Yamamoto et al. [25] also show that the enzyme inactivation primarily takes place in the falling rate period even though both the experimental and theoretical approaches taken are fundamentally different from those of this thesis. The references mentioned are discussed in detail in section 2.3.4 of the literature survey.

The inactivation in the falling rate period is further investigated in figure 6.7 where the activity loss is shown as a function of the radial coordinate inside the particle at different points in time. Apparently, the activity loss occurs primarily is the wet core whereas only minor activity loss is suffered in the particle crust. The moisture content is much higher in the wet core compared to the crust where only water in equilibrium with vapor is present – figure 6.8. Thus, unfortunate combinations of moisture content and temperature occur in the wet core as the temperature increases in the beginning of the falling rate period. This is supported by figure 5.6 on page 112 which shows that rice starch has gelatinized as a consequence of water being trapped inside a wet core of a particle which experiences a rising temperature.

The conclusion that the inactivation predominantly occurs in the particle center seemingly contradicts the findings of Millqvist-Fureby et al. [15]. As described in sections 2.3.2 and 2.3.3 of the literature survey, Millqvist-Fureby et al. [15] showed that the enzyme in a dried particle was overrepresented at the surface and that addition of a surface active component expelled the enzyme from the surface during drying, leading to improved activity preservation. This renders significant inactivation at the surface probable. However, Millqvist-Fureby et al. [15] used feed formulations with a very low initial total solid content (i.e. 10 wt%), entailing that the constant rate period during drying was prolonged. In section 5.6.3 it was shown that some components deposit at the droplet surface as the droplet shrinks during the constant rate period – this might also be the case for enzymes. Enzymes located at a liquid/gas interface are prone to aggregation (see section 2.3 for details) which could explain the activity losses observed by Millqvist-Fureby et al. [15]. Contrary to the model formulations used by Millqvist-Fureby et al. [15], the commercial formulations treated in this chapter have high initial solid contents and a very short constant rate period. Only small amounts of enzyme accumulate at the surface, rending figure 6.7 reasonable. Thus, the findings of Millqvist-Fureby et al. [15] do not necessarily contradict the findings of this chapter.

Influence of Process Parameters

Next, the model presented above is used to evaluate the influence of different process parameters and initial conditions on the drying time and enzyme activity loss. As mentioned previously the focus is on industrial applications. A

series of simulations is conducted, changing a single parameter or initial condition in each simulation compared to the reference simulation. The results of the simulation series are given in table 6.4 along with the results from the reference simulation.

Table 6.4: Total drying time and activity loss for a series of simulations where one process parameter or initial condition is changed compared to the reference simulation.

Change	Activity loss (%)	Drying time (s)
None[1]	8.34	77.64
$r_d = 50\ \mu m$	4.59	34.67
$r_d = 100\ \mu m$	12.80	137.63
$v = 5\ ^m/_s$	8.34	77.67
$v = 25\ ^m/_s$	8.34	77.63
$RH = 10\ \%$	6.49	68.71
$RH = 30\ \%$	10.99	89.94
$T_\infty = 70°C$	1.91	134.14
$T_\infty = 75°C$	4.10	102.33
$T_\infty = 85°C$	15.78	58.33
$F^2 = 1$	0.78	77.64
$F^2 = 2$	10.49	77.64
$F^2 = 3$	9.28	77.64

[1]Reference simulation. Process parameters and initial conditions are given in table 6.3.
[2]Formulation – as given in table 6.1.

First, the effect of altering the initial droplet size is investigated. Evidently, a reduction in the droplet size leads to a shorter drying time and a lowered enzyme activity loss. As the initial droplet size is increased the drying time is prolonged, simply because more water has to be removed. This also leads to an increased activity loss as more water is trapped in the wet core. To minimize the activity loss it is suggested to carry out the spray drying process with a small initial droplet size. However, often it is not possible to alter the initial droplet size because the final product must have a specific particle size.

The initial droplet velocity has no significant influence on the drying time nor on the activity loss. As shown in figure 6.5 the droplet decelerates very rapidly and thus, the initial velocity only affects an infinitesimal part of the total drying time. Further, the initial velocity of a droplet in an industrial spray dryer is very difficult to control (see section 2.1.1 for details on industrial scale droplet generation). Therefore, this parameter is of little interest in industrial applications.

The driving force of drying in the falling rate period is the difference in vapor mole fractions between the wet core interface and the bulk phase (in the constant

rate period the driving force is the difference in vapor mole fractions between the droplet surface and the bulk phase). Thus, decreasing the relative humidity in the bulk phase leads to faster drying and thereby less activity loss. However, from a practical point of view it may be difficult to reduce the humidity inside the spray dryer because the humidity is correlated to the amount of water evaporated. Lowering the humidity means lowering the spray dryer throughput capacity. Nevertheless, this is an option which may be considered.

Obviously, an increased bulk phase temperature leads to faster drying. The faster drying may be expected to limit the activity loss but apparently the elevated temperature has a substantial negative effect on the activity loss. The reduced drying rate caused by lowering the drying temperature is likely to entail that the particles are not completely dry when they exit the drying chamber. Thus, choosing the drying air temperature is a trade-off between acceptable enzyme activity loss and acceptable level of residual moisture content. However, an additional advantage of lowering the drying chamber air temperature is that it results in a higher spray dryer throughput because the temperature is often lowered by increasing the suspension feed rate.

From table 6.4 it is evident that Formulation 1 should be chosen for spray drying which is in agreement with the conclusion drawn in chapter 4. The formulation performs significantly better than the other formulations which essentially suffer the same activity losses. The same trend is found at a bulk phase temperature of $T_\infty = 70°\text{C}$ where Formulations $1-4$ experience activity losses of, respectively, 0.12 %, 1.82 %, 2.07 % and 1.91 %.

Model Performance

The modeling and simulation work above has provided results which may be used to obtain a better understanding of the single droplet drying process, including enzyme inactivation. Also, the simulations may be used to evaluate the effect of altering process variables and thereby improve spray dryer operation.

However, as discussed in section 6.1.1 the model contains a number of assumptions which simplify the mathematical equations of the model and allow for carrying out the simulations. Further, elements of the modeling and simulation work are associated with considerable uncertainties which might lead to deviations between the results of the simulations and results obtained during actual spray drying. The most important of these issues are addressed below and suggestions for model improvements are made.

First, the influence of the choice of formulation on the course of drying is not considered. As shown in chapter 5 even small formulation changes may alter the particle morphology, signifying different courses of drying. In chapter 5 small formulation variations appeared to change the development in droplet/particle temperature considerably which is particularly important for temperature-sensitive

materials. However, incorporating the effect of the choice of formulation on the course of drying includes modeling different sequences of particle morphology formation (as shown in e.g. figure 5.9) which is a comprehensive task.

Furthermore, the work above contains substantial simplifications regarding modeling of the dissolved material inside the droplet. Especially, the model lacks consideration of a concentration gradient inside the droplet which in chapter 3 is shown to influence the droplet drying process. The assumption does, however, simplify the mathematical equations appreciably but it is suggested to incorporate more of the work of chapter 3 into the present model if better simulation results are to be attained.

Also, a number of the model parameters (section 6.1.3) are associated with some uncertainty. The parameters influence the simulation results differently and a sensitivity analysis of important model parameters has been conducted. It is found that in particular the effective diffusion coefficient of water vapor in the particle crust ($\mathcal{D}_{v,eff}$) affects the results for the total drying time and enzyme activity loss. For example, decreasing $\mathcal{D}_{v,eff}$ by 10 % increases the calculated results for the total drying time from 77.64 s to 86.05 s and the enzyme activity loss from 8.34 % to 9.24%. Thus, intensive work to find a precise correlation for this parameter might lead to improved simulation results.

Finally, it is noted that the model has not been experimentally validated. Although many parts of the model is set up based on the findings of the previous chapters of the present work and the work of other authors, the simulation results are not completely reliable until an extensive experimental model validation has been conducted. Though the part of the model concerning the drying rate to a certain extent has been validated by Jørgensen [5], the full model presented in this chapter would be ideally validated using the Droplet Dryer experimental setup (described in chapter 5), measuring both the droplet moisture content and the residual enzyme activity as a function of the drying time. This, however, requires reconstruction of the Droplet Dryer as this piece of equipment is not designed for drying of hazardous active components.

6.3 Summary

A mathematical model which couples drying kinetics and enzyme inactivation during drying of a single droplet has been presented. The model is based on the work of the previous chapters and the work of other authors, primarily Abuaf and Staub [1]. The model is set up using a number of assumptions which simplifies the mathematical equations. The model is valid for the drying of a droplet consisting of water, insolubles and dissolved compounds, including enzymes. The course of drying is divided into two parts – the constant and the falling rate period. In the latter evaporation is assumed to occur from a

shrinking wet core surrounded by a thickening crust through which water vapor diffuses to the particle surface.

Using the model, a number of simulations of the developments in droplet water content and enzyme activity has been conducted. The results show that most of the water in the droplet evaporates during the constant rate period although this phase only constitutes a small part of the total drying time. It has been shown that the droplet temperature is close to the wet bulb temperature during the constant rate period and rapidly approaches the air dry bulb temperature in the beginning of the falling rate period. The developments in drying rate and droplet temperature are concluded to be consistent with those found in chapter 3. Additionally, it is concluded that the transport phenomena controlling the drying process are the same in the present model as in the model put forward in chapter 3.

Furthermore, it is found that the enzyme suffers most of the inactivation during the falling rate period due to the elevated temperatures prevailing in this phase. Also, during the falling rate period most of the inactivation occurs in the shrinking wet core because of unfortunate combinations of water content and temperature in this part of the droplet. On the contrary, inactivation is low in the crust surrounding the wet core.

Based on a series of simulations, a number of suggestions is put forward for improving spray dryer operation during drying of enzyme containing suspensions. First, it is suggested to use an initial droplet size which is as small as possible. Further, the relative humidity inside the drying chamber should be maintained at a minimum to shorten the drying time and thereby limit the enzyme activity loss. The air temperature in the spray dryer should also be low as the simulations have shown that the prolonged drying time caused by a low temperature affects the inactivation less than an elevated temperature.

It is suggested to carefully investigate the impact of the formulation chosen on the activity loss during spray drying. The simulations have confirmed that even simple formulation changes may significantly reduce the activity loss. Finally, it is noted that the choice of spray drying process parameters is a trade-off between acceptable activity loss and other requirements of the final product.

6.4 References

[1] N. Abuaf and F. W. Staub. Drying of liquid-solid slurry droplets. In A. S. Mujumdar, editor, *Drying '86 Volume 1. Proceedings of the Fifth International Symposium on Drying*, pages 277–284, Berlin, Germany, 1983. Springer-Verlag.

[2] C. R. Dalton and B. C. Hancock. Processing and storage effects on water

vapor sorption by some model pharmaceutical solid dosage formulations. *International Journal of Pharmaceutics*, 156(2):143–151, 1997.

[3] J. A. Dean. *Lange's Handbook of Chemistry*. McGraw-Hill, 15th edition, 1999.

[4] R. M. German. *Particle Packing Characteristics*. Metal Powder Industries Federation, Princeton, NJ, United States, 1989.

[5] K. Jørgensen. *Drying Rate and Morphology of Slurry Droplets*. PhD thesis, Technical University of Denmark, 2005.

[6] K. Kadoya, N. Matsunaga, and A. Nagashima. Viscosity and thermal conductivity of dry air in the gaseous phase. *Journal of Physical and Chemical Reference Data*, 14(4):947–970, 1985.

[7] J. Kringelum. Measurement and modelling of water sorption kinetics of enzyme granules. Master's thesis, Department of Chemical Engineering, Technical University of Denmark, 2002.

[8] D. Kunii and O. Levenspiel. *Fluidization Engineering*. Butterworth-Heinemann, Massachusetts, United States, 2nd edition, 1991.

[9] H. Liang, K. Shinohara, H. Minoshima, and K. Matsushima. Analysis of constant rate period of spray drying of slurry. *Chemical Engineering Science*, 56:2205–2213, 2001.

[10] D. R. Lide, editor. *CRC Handbook of Chemistry and Physics*. Internet Version - http:/www.hbcpnetbase.com, Taylor and Francis, Boca Raton, FL, United States, 87th edition, 2007.

[11] K. Masters. *Spray Drying Handbook*. Longman Scientific and Technical, 5th edition, 1991.

[12] K. Masters. *Spray Drying in Practice*. Gershof Grafisk ApS, 2002.

[13] W. L. McCabe, J. C. Smith, and P. Harriott. *Unit Operations of Chemical Engineering*. McGraw-Hill, 6th edition, 2001.

[14] G. Meerdink. *Drying of Liquid Food Droplets - Enzyme Inactivation and Multicomponent Diffusion*. PhD thesis, Landbouwuniversiteit te Wageningen, The Netherlands, 1993.

[15] A. Millqvist-Fureby, M. Malmsten, and B. Bergenståhl. Spray drying of trypsin - surface characterisation and activity preservation. *International Journal of Pharmaceutics*, 188:243–253, 1999.

[16] H. Minoshima, K. Matsushima, H. Liang, and K. Shinohara. Estimation of diameter of granule prepared by spray drying of slurry with fast and easy evaporation. *Journal Chemical Engineering of Japan*, 35(9):880–885, 2002.

[17] H. R. Pruppacher, J. D. Klett, and D. E. Haman. *Microphysics of clouds and precipitation*. Kluwer Academic Publishers, 2 edition, 1996.

[18] M. Räderer. *Drying of viscous, shrinking products: Modelling and experimental validation*. PhD thesis, Technical University of Munich, Germany, 2001.

[19] K. Raznjevic. *Handbook of Thermodynamic Tables and Charts*. Hemisphere Publishing Corporation, 1st edition, 1976.

[20] M. Renksizbulut and M. Yuen. Experimental study of droplet evaporation in a high-temperature air stream. *Transactions of the ASME*, 105:384–388, 1983.

[21] M. Rhodes. *Introduction to Particle Technology*. John Wiley & Sons, 1999.

[22] J. M. Smith, H. C. van Ness, and M. M. Abbott. *Chemical Engineering Thermodynamics*. McGrawHill, 6 edition, 2001.

[23] N. Wakao and J. M. Smith. Diffusion in catalys pellets. *Chemical Engineering Science*, 17:825–834, 1962.

[24] A. E. Wijlhuizen, P. J. A. M. Kerkhof, and S. Bruin. Theoretical study of the inactivation of phosphatase during spray drying of skim-milk. *Chemical Engineering Science*, 34:651–660, 1979.

[25] S. Yamamoto, M. Agawa, H. Nakano, and Y. Sano. Enzyme inactivation during drying of a single droplet. In R. Toei and A. S. Mujumdar, editors, *Proceedings of the Fourth International Drying Symposium, Kyoto, Japan*, pages 328–335, July 1984.

Chapter 7

Conclusion

The drying kinetics, enzyme inactivation and morphology formation during spray drying of enzyme containing formulations have been investigated. The focus has been on obtaining a fundamental understanding of the topics mentioned while suggestions for improved spray dryer operation on an industrial scale have been put forward.

A model has been developed for the drying of a single solution droplet into a solid, dense particle to achieve a more fundamental understanding of the droplet drying process. The model describes mass and heat transfer to the surface and inside the droplet. Model predictions of the drying behavior are compared to data for the drying of aqueous solutions of maltodextrin and trehalose from experiments conducted using an ultrasonic levitator.

The model provides for evaluation of the influence of different process parameters on the drying process. More importantly, the following was found about the drying process. The simulations show two rather distinct phases of drying where a period of fast drying is followed by a period with a sigficantly lower drying rate. In the literature the two periods are often referred to as the constant rate period and the falling rate period. Also, in agreement with the literature the simulated droplet temperature is close to the wet bulb temperature in the constant rate period but rapidly approaches the temperature of the surroundings in the beginning of the falling rate period. The model shows that even though the Biot number is slightly above the critical value of 0.1 a uniform temperature distribution in the radial direction inside the droplet can be assumed. Finally, it is concluded that the drying rate during the constant rate period is limited by mass and heat transfer between the droplet surface and the bulk phase. In the falling rate period the drying rate is found to be limited by the internal droplet mass transport.

The development in drying kinetics during droplet drying has been further investigated by conducting series of experiments, using the so-called *Droplet Dryer*

pilot spray dryer apparatus. The Droplet Dryer is designed for in situ drying experiments where droplets are dried under well-defined flow and temperature conditions.

Based on the experimental results, it is concluded that adding water activity reducing compounds (Na_2SO_4, NaCl, dextrin or maltodextrin) to a suspension of water and insoluble rice starch particles causes an increase in the droplet temperature during drying rather than a reduction of the drying rate. This should be considered when designing a formulation which contains temperature-sensitive active components such as enzymes.

Adding insoluble TiO_2 particles to the suspension of water and rice starch particles is found not to affect the drying rate nor the droplet temperature. This is explained by the fact that the TiO_2 does not reduce the water activity.

Also, the series of experiments carried out were used for analyses of particle morphology. Sequences for formation of the observed morphologies are given and explained in detail. The most important conclusion is that even small alterations in the feed formulation may lead to significant changes in the final particle morphology.

Furthermore, a method for evaluation of the performance of enzyme containing formulations in terms of preserving the highest enzyme activity during spray drying has been developed. The method is fast and cheap and allows for many different formulations to be tested. Hence, the method may be used in industry to aid in the formulation development process.

The method is based on a combination of differential scanning calorimeter experiments and modeling of the thermal enzyme inactivation reaction which occurs during the spray drying process. Relevant kinetic parameters are determined from the differential scanning calorimeter experiments and the activity loss is calculated from the reaction model at moisture contents and temperatures relevant for spray drying. After conducting experiments and calculations of the severity of the inactivation reaction for four different enzyme containing formulations, it is concluded that a simple change in formulation significantly improves activity preservation during drying. Thus, using the method to evaluate the performance of different formulations may be valuable in the industry. Also, an important result of the work developing the method is that a model which calculates the rate of inactivation as a function of temperature and moisture content has been set up and validated.

The model for inactivation is used in the final part of the thesis where it is combined with a model which calculates the droplet temperature and moisture content during drying. The combined model is valid for the drying of a droplet consisting of insolubles, water and dissolved compounds, including enzymes. In the constant rate period water evaporates from the droplet surface whereas the evaporation occurs from a shrinking wet core during the falling rate period.

The wet core is surrounded by a thickening crust through which the water vapor diffuses to the particle surface.

Simulation results obtained by using the combined model show that the enzyme experiences most inactivation during the falling rate period due to the high temperatures attained in this period. Further, it is concluded that only little inactivation occurs in the particle crust while the enzyme in the wet core suffers significant inactivation because of unfortunate combinations of temperature and moisture content in this part of the particle.

Based on the model simulations the following advice is given for limiting the activity loss when spray drying enzyme containing formulations on an industrial scale. The initial droplet size should be as small as possible and the relative humidity should be kept at a minimum. Moreover, the temperature inside the spray dryer should also be kept low. Finally, it is suggested to carefully investigate the impact of the spray drying on the activity loss. Simulations have confirmed that simple formulation changes may lead to significantly improved activity preservation. However, the choices of process parameters and formulation design are trade-offs between activity loss and other product requirements.

7.1 Suggestions for Further Work

In the present work the drying rate, enzyme inactivation and morphology development during spray drying of enzyme containing formulations are investigated. To complement the work of this thesis, it is suggested to carry out the following work.

First, the Droplet Dryer has proven to a be valuable setup for investigating the drying rate and morphology formation during drying of droplets under conditions which resemble those of spray drying. It is suggested to redesign and rebuild this apparatus so that it may be used for drying of formulations which contain active compounds such as enzymes. This will first and foremost provide for measurements of the enzyme inactivation as a function of the drying time. These measurements may initially be used for validation of the model of chapter 6 which combines drying rate and enzyme inactivation calculations.

Also, the influence of adding enzymes to a given formulation on the drying kinetics and morphology formation may be evaluated if the Droplet Dryer is rebuilt. The knowledge obtained by these experiments may be used to extend the model presented. Ideally, a model should be set up which accounts for the influence of the varying formulation ingredients on the course of drying for a single droplet, including prediction of the morphology formation. A model of this kind will calculate quantitative results for the activity loss during spray drying and provide for prediction of final particle properties.